THE QUADRATURE DISCRETIZATION METHOD AND ITS APPLICATIONS

By

Heli Chen

B. Sc. (Mechanics), Peking University, 1987

M. Sc. (Mechanical Engineering), University of Calgary, 1993

A THESIS SUBMITTED IN PARTIAL FULFILLMENT OF

THE REQUIREMENTS FOR THE DEGREE OF

DOCTOR OF PHILOSOPHY

in

THE FACULTY OF GRADUATE STUDIES

(Department of Mathematics)

We accept this thesis as conforming

to the required standard

THE UNIVERSITY OF BRITISH COLUMBIA

October 1998

Department of ___Mathematics___

The University of British Columbia
Vancouver, Canada

Date ___Oct. 12, 1998___

DE-6 (2/88)

Abstract

A discretization method referred to as the quadrature discretization method is introduced and studied in this thesis. The quadrature discretization method is a spectral method based on a grid of points that coincide with the points of a quadrature. The quadrature is based on a set of nonclassical polynomials orthogonal with respect to some weight function over some interval. The method is flexible with respect to the choice of the weight function and quadrature points so that the optimum accuracy and convergence in the solution of differential equations and/or partial differential equations can be obtained. The properties of the quadrature discretization method are studied and compared with classical spectral methods as well as finite difference methods. Several analytic model problems in one and three dimension are studied. The quadrature discretization method competes well with classical spectral methods and is far more superior than the finite difference method. In some cases it provides significant improvement in the accuracy and convergence of the solution of the problem over other methods.

The main objective of the quadrature discretization method is to determine the weight function that defines the polynomial basis set and hence the grid points that provide optimum convergence in a given application. The quadrature discretization method is applied to a large class of time dependent Fokker-Planck equations. Several weight functions are used and the results are compared with several other methods. The weight functions that have often provided rapid convergence of the eigenvalues and eigenfunctions of the Fokker-Planck operator are the steady solutions at infinite time.

The quadrature discretization method is also employed in the solution of Schrödinger equations. The weight functions that are used are related to the ground state wave

functions if known, or some approximate form. The eigenvalues and eigenfunctions of four different potential functions discussed extensively in the literature are calculated and compared with the published values. The eigen-problem of a two-dimensional Schrödinger equation with the Henon-Heiles potential is also calculated with the quadrature discretization method. The rate of convergence of the eigenvalues and eigenfunctions of the Schrödinger equations is very rapid with this approach.

Table of Contents

List of Tables

vii

List of Figures

Acknowledgement

I wish to express my sincere thanks to my research supervisor, Dr. B. Shizgal. It has been a pleasure to have worked with him, and his support, direction and assistance will always be greatly appreciated.

This thesis is dedicated to my families and Michael.

Chapter 1

Introduction

Differential equations are widely used in almost all areas of science, engineering for modeling and forecasting. However, most of them can hardly be solved in closed form. Therefore, accurate and efficient numerical algorithms are required to provide solutions to many different types of differential equations. The major numerical techniques widely used include finite difference method (FD), finite element method (FEM), and spectral methods.

The main objective of these numerical methods is to approximate derivatives by algebraic expressions involving the solution evaluated on a grid. Ordinary differential equations (ODE) are thus reduced to algebraic equations and partial differential equations (PDE) (PDE) are reduced to systems of ODEs. In this section, we shall confine our discussion to linear differential equations.

A differential equation can be written as

$$Lu = -f(x) \tag{1.0.1}$$

where $u(x)$ is the solution of the equation, and L is the linear differential operator. Discretizing the variable x on a grid with N points, Eq. (1.0.1) can be approximated by algebraic equations

$$\mathbf{L_N}\mathbf{u}_N = -\mathbf{f}, \tag{1.0.2}$$

with $\mathbf{L_N}$, the matrix representative of the differential operator L, and $\mathbf{u}_N$, the approximate solution at the grid points. With different numerical techniques, the choice of the

gridding and construction of the derivative and differential matrix may vary.

Similarly, a time-dependent partial differential equation can be written in general as

$$\partial u(x,t)/\partial t = Lu + f(x), \tag{1.0.3}$$

where t is the temporal variable, x is the spatial variable, $f(x)$ is a source function, $u(x,t)$ is the solution and L is the differential operator which contains all the spatial derivatives of u. The steady solution of Eq. (1.0.3) is Eq. (1.0.1). Eq. (1.0.3) must be coupled with an initial condition $u(x,0)$ and suitable boundary conditions. For simplicity, we only consider one spatial dimension in this chapter. Similar statements can be applied to the higher dimensions. By discretizing the spatial variable x, the partial differential equation, Eq. (1.0.3) can be approximated by a system of first order ODEs,

$$\frac{\partial \mathbf{u}_N}{\partial t} = \mathbf{L}_N + \mathbf{f}_N. \tag{1.0.4}$$

We shall often confine the discussion of time discretizations to Eq. (1.0.3) with $f(x) = 0$, i.e., we consider

$$\frac{\partial \mathbf{u}_N}{\partial t} = \mathbf{L}_N \mathbf{u}_N. \tag{1.0.5}$$

There are several ways to solve the ODE system Eq. (1.0.5). The solution of this time dependent PDE can be evaluated by an eigenfunction expansion. The formal solution (with $f(x) = 0$) is then of the form

$$u(x,t) = \sum_{n=0}^{\infty} c_n e^{\lambda_n t} \phi_n(x), \tag{1.0.6}$$

where λ_n and $\phi_n(x)$ are the eigenvalues and eigenfunctions of the eigenvalue problem

$$L\phi_n(x) = \lambda_n \phi_n(x), \tag{1.0.7}$$

the coefficients c_n are determined from the initial condition, $u(x,0)$, and are given by

$$c_n = \int u(x,0)\phi_n(x)dx. \tag{1.0.8}$$

The convergence and accuracy of the eigenvalues and eigenfunctions of the matrix $\mathbf{L}_N$ determine the convergence and accuracy of the solution. The convergence as well as the rate of the convergence of the eigenvalues and eigenfunctions depend on the choice of the numerical methods and spatial gridding used to construct the differential discretization matrix representation in the spatial variable.

The second method is to discretize the ODE system Eq. (1.0.5) in time, and thus integrate the ODE system numerically. This approach is applicable for both linear and nonlinear problems. In most applications, the temporal discretization uses conventional finite difference methods, including implicit, explicit and semi-implicit or implicit-explicit schemes. Among the factors which influence the choice of a time-discretization are the accuracy, stability, storage requirements and work demands of the methods. The explicit scheme is easy to implement and relatively less costly, but has a strong stability restriction which is determined by the eigenvalue spectrum of the differential operator L. The popular explicit schemes are the Adams-Bashforth methods which includes the simple first order forward Euler (FE) method. The implicit scheme provides the best stability but involves a matrix inverse and is expensive, especially for nonlinear problems. It is the best choice for stiff (large condition number) linear problems which encounter instability while using an explicit scheme. A related set of implicit methods are the Adams-Moulton methods which include the first order backward Euler (BE) and the second order Crank-Nicolson (CN) method. Implicit-explicit schemes become popular for the time integration of nonlinear problems. The idea of these type of schemes is to an apply implicit scheme for the linear term and an explicit scheme for the nonlinear term of the problem. Another popular class of temporal discretization methods are the Runge-Kutta Methods. Some standard references in these temporal discretization methods are the books by Gear (1971) [1], Lambert (1973) [2], Shampine and Gordon (1976) [3], Dekker (1984) [4], Butcher (1987) [5], and Hairer (1989) [6].

The basic idea above is to discretize the differential operator L in physical space, *i.e.* approximate the differential operator directly by discretization. Most finite difference and collocation methods use this idea. Another popular approach is to approximate the solution in transform space. It involves expansion of the solution by a finite sum. For example, the solution $u(x)$ of Eq. (1.0.1) can be expanded in a set of orthogonal basis functions $\psi_k(x)$ $(k = 1, 2, ..., N)$, that is

$$u(x) = \sum_{k=1}^{k=N} c_k \psi_k(x).$$ (1.0.9)

The transform coefficients c_k are constant and can be solved by an algebraic equation

$$Ac = b$$ (1.0.10)

where c is the coefficient vector of c_k, and A and b are the transform matrix and vector determined by minimizing the residual function $R(x; c_k) \equiv Lu + f$ or its related functionals. The methods used in this approach include finite element methods, tau and Galerkin spectral methods.

Finite difference methods for solving differential equations consist of replacing each of the derivatives in the differential operator by an appropriate difference-quotient approximation (such as $du(x)/dx \approx [u(x+h) - u(x-h)]/2h$, where h is a small grid spacing). The difference quotient is generally chosen such that a certain order of truncation error is maintained. The method approximates derivatives of a function by local arguments and is designed to be exact for polynomials of low order. The matrix representative of the derivative operator is generally banded. The FD algorithm is easy to program and implement, but relatively low in accuracy. A higher order of accuracy for the finite difference method is possible and has strong restriction to the stability of the solution.

The FEM is frequently used to solve partial differential equations that occur in engineering applications, especially, in the areas of solid mechanics, elasticity, and computational fluid dynamics [7–17]. The idea of the finite element method is to divide the

interval in x into a number of sub-interval and approximate the solution by a sum of basis functions which are piecewise polynomials of low fixed degree. The differential matrix derived is sparse because only a handful of basis functions are non zero in a given sub-interval. Since the approximate solutions are piecewise polynomials, the pieces or the sub-intervals can be easily chosen to fit the geometry of the problem. The FEM is therefore very useful in solving problems with complex geometry in multi-dimensional problems. The FEM is closely related to the finite difference method. The discretization of the differential equation are difference equations, but derived by a different approach. In some cases (especially in one-dimensional cases), they can be equivalent. The disvantage of the FEM is the relatively low accuracy because each basis function is a polynomial of low degree.

Spectral methods involve the expansion of the solution by a finite sum

$$u(x) \approx u_N(x) = \sum_{k=0}^{N} a_k \phi_k(x) \qquad (1.0.11)$$

in a set of orthogonal basis functions (trial functions), $\phi_k(x)$. When this series is substituted into Eq. (1.0.1), we can define a residual function

$$R(x; a_0, a_1, ..., a_N) \equiv Lu_N + f. \qquad (1.0.12)$$

The spectral method is constructed using test functions to minimize the residual i.e. the coefficients in the series expansion are chosen so that the residual is orthogonal to the space spanned by the basis of test functions, $\psi_k(x)$:

$$\int R(x; a_0, a_1, ..., a_N)\psi_k(x)dx = 0. \qquad (1.0.13)$$

This is analogous to techniques used in the FEM. The choice of the test functions distinguishes between the spectral Galerkin, tau and collocation (also referred to as pseudospectral) methods [18,19]. In the Galerkin approach, the test functions are the same as

the trial functions and individually satisfy the boundary condition. Spectral tau methods are similar to Galerkin methods, but none of the test functions need to satisfy the boundary conditions. Hence a supplementary set of equations is required to apply the boundary condition. In the collocation method, the test functions are shifted Dirac delta functions centered at so-called collocation points. For many problems, especially nonlinear ones, the collocation (or pseudospectral) method is the easiest to implement, and the most efficient [19–23]. Spectral methods use global basis functions which are polynomials (or trigonometric polynomials) of high degree and generate solutions with high accuracy. Pseudospectral method can be viewed as the limit of FD methods when the order of accuracy tends to infinity [24]. Unlike low order FD method and FEM which result in large, sparse matrices; the differential matrix representative by the spectral method is usually full.

There are numerous numerical schemes available in the numerical computation. Most of them belong to the three methods discussed above, or schemes which are a combination of several techniques. The geometry of the domain and required level of accuracy are the key factors in selecting among these approaches. The FEM is particularly well suited to problems in very complex geometries, whereas spectral methods can offer superior accuracies and cost efficiencies, mainly in simple geometries. Although sometimes a mapping of a complicated physical domain onto a simple computational domain is possible, the mapping must be smooth to preserve the high-order accuracy and exponential convergence rates associated with the spectral method. Finite difference methods perform well over a broad range of accuracy requirements and (moderately complex) domains. For years, many numerical analysts have been working on the spectral domain decomposition or spectral element methods [25–32]. The techniques can apply to problems with complicated domain and provide superior accuracy and convergence over the FEM.

The advantage of spectral methods is that they are more accurate than the FD method

and the FEM so that far fewer grid points are required. A principal disadvantage is that in solving time dependent problems in finite boundaries, they are often subject to tight stability restrictions when an explicit temporal discretization methods is used.

For a specific problem, a particular numerical scheme may be selected to meet stability and convergence requirements, as well as the physical and geometric aspects of the problem.

In the context of solving time-dependent PDEs, spectral methods have notable advantages over other numerical methods. First, the error between the numerical solution and exact solution decays exponentially versus number of grid points N. This high accuracy allows one to treat problems with very much fewer grid points which would otherwise require an enormous number of mesh points by other numerical methods. For multi-dimensional problems, the use of relatively coarse grids that suffice for most accuracy requirements offer superior efficiency in time and memory. Besides this potentially high accuracy, spectral methods are also powerful for many cases in which solutions and variable coefficients are nonsmooth or even discontinuous [19,22,33,34].

Spectral methods and pseudospectral methods based on the expansion of the solution in orthogonal polynomials have been successfully applied in many areas such as simulations of turbulence flow [18,19,35], computational fluid dynamics [18–20,29,36–41], weather prediction [19,42,43], kinetic theory [44–47], and quantum mechanics [48–51], etc.

It has been demonstrated numerically that the condition number, i.e. the ratio of the largest to the smallest eigenvalue of the spectral approximation matrix is large. It is known that finite difference and finite element methods have an $O(N^2)$ condition number. For spectral methods, the largest eigenvalue of the first derivative operator grows as $O(N^2)$, and of the second derivative operator grows as $O(N^4)$, as N increases, leading to

poorly conditioned matrices [18,19,29,36,39,52–58]. This effect upon the numerical computations of the eigenvalues of the derivative operator is caused by the round off error depending on machine precision of the computer. One cause of the roundoff error in using the spectral differentiation matrix is attributed to inaccurate computation of certain matrix elements, particularly certain large elements in the upper and lower right corner of the matrix [52,53,56]. Methods for reducing the error of Chebyshev pseudospectral approximation of derivative matrix are discussed by several researchers [52,53,55,56,59]. Several researchers [29,60] also point out that the poor condition of the derivative matrices is related to the minimum spacing of the grid points. The large condition number of the spectral derivative matrix is not necessarily a problem in the accuracy of the solution of differential equations. However, the large condition number of the derivative matrix brings stringent stability restrictions to solve time dependent PDEs by temporal discretization, since in actual computations, the stability limit depends on the precision of the numerical solution of eigenvalues. On the other hand, the differential matrices by a spectral method are usually dense. Direct inversion of these matrices is usually expensive for large matrices. Iterative schemes are sometimes a practical necessity. Therefore, reduction of the condition number of spectral differential matrices is necessary for stability of iterative methods and time integration. There have been numerous studies on the preconditioning of spectral matrices. The idea of preconditioning with second-order finite difference methods is described by Orszag [25]. Some other preconditioners based on the FD [61,62], the FEM [31,63,64], and the spectral methods [65,66] have been proposed and successfully tested in the literature. Besides preconditioning techniques, algorithms for direct improvement of the condition number of derivative matrices are also discussed by Heinrichs [57], and Kosloff and Tal-Ezer [60].

Most spectral and pseudospectral methods currently used are restricted to traditional or "classical" basis functions such as trigonometric functions and polynomial solutions

of Sturm-Liouville eigenvalue problems. The details of these polynomials are described in most texts on spectral methods [18,19,29,36,38,39]. The choice of basis functions is dictated by the weight function, $w(x)$ and the domain of the problem considered. For example, for $[-1,1]$ and $w(x) = 1$, $w(x) = (1-x)^\alpha (1+x)^\beta$ and $w(x) = \frac{1}{\sqrt{1-x^2}}$, one has the "classical" Legendre, Jacobi, and Chebyshev polynomials, respectively. Laguerre and Hermite polynomials are used for $w(x) = e^{-x}$ on $[0, \infty]$ and for $w(x) = e^{-x^2}$ on $[-\infty, \infty]$, respectively. When the basis set is chosen, the associated grid points in a pseudospectral method are fixed, and adaptive gridding techniques are difficult but possible [40,67]. In many cases, the choice of grid points is essential to the convergence of the eigenvalues and eigenfunctions of the differentiation matrix. For some physical problems, spectral solution with classical polynomials may result in poor convergence or even inaccurate results. Therefore more flexibility in choice of grid points is desired.

Many problems of physics and engineering lead naturally to the solution of a partial differential equations in an unbounded domain. The condition at infinity given by a certain asymptotic behavior of the solution can be obtained by asymptotic analysis at infinity. However, for numerical approximation, it is not easy to interpret the behavior at infinity. Most numerical methods such as finite difference, finite element methods and spectral methods with trigonometric functions and Jacobi-type polynomials as basis functions can only apply to the problem with finite domain. One of the most widely used techniques is to restrict the computation to a finite domain by truncating the domain and imposing "artificial boundary" conditions. Another treatment consists of mapping the unbounded domain into a bounded one and using the standard discretization techniques mentioned above. The more attractive technique is to use basis functions defined on an unbounded domain such as Hermite polynomials (or Gaussian-type polynomials) on $(-\infty, \infty)$ and Laguerre polynomials on $(0, \infty)$. For those polynomials, the collocation points spread all over the infinite domain with increasing N, and there is no restriction

on the size of the domain is required and thus no artificial boundary cutoff is needed. As to the approximation by spectral methods, some results and a comparison with these techniques can be found in the papers by several workers [29,67–69]. Although use of Hermite and Laguerre polynomials bring some promising results for solving unbounded boundary problems, the direct spectral approach may not produce good approximation. Scaling and shifting factors may be necessary in practical applications of the classical spectral methods. On the other hand, many physics problem have some special charac-teristics and need special treatment when solving these models. For example, the solution of the optical bistability model for laser physics is usually characterized by two stable states. Use of the Hermite spectral method may result in slow convergence and/or poor accuracy. Thus, it is necessary to find some nonclassical basis functions that can relate to the physics of the problem very well and generate good convergence and accuracy of the solution. Recently, Shizgal and coworkers started using nonclassical polynomials on an infinite domain to solve some physics related problems [43,45–47,51,70–72]. They received very encouraging results. Another reason for using those physics related basis functions is that they have very attractive properties from the numerical point of view. There is evidence that the condition number of the first and second Hermite differen-tiation matrices are $O(\sqrt{N})$ and $O(N)$, respectively [29,68,73]. Numerical results from our work also showed that the condition number for a second differentiation matrix can be improved to be between $O(N)$ and $O(N^2)$ depending on the physical problem and polynomial basis set chosen. This is better than second order finite difference which is $O(N^2)$, and far better than $O(N^4)$, for example, by Chebyshev spectral method.

For these reasons, it is necessary to have a spectral method which is not restricted to the "classical" orthogonal basis functions and associated points.

The purpose of this thesis is to study a fast, and accurate spectral method, namely, the quadrature discretization method (QDM), and apply the method to solve several

differential equations, notably, the Fokker-Planck equation (FPE) and the Schrödinger equations (SE).

In this thesis we introduce the quadrature discretization method (QDM), which allows nonclassical polynomials as basis functions in a spectral approximation. The idea of the QDM is initially introduced by Shizgal in solving eigenvalues of Lorentz Fokker-Planck equation [74]. A set of nonclassical polynomials called "speed" polynomials based on weight function $x^2 \exp(-x^2)$ was used in this work. The method was later developed further by Shizgal and Blackmore by using speed and some other weight functions [71,72,75]. Their generation of polynomials was based on a recursion subject to round-off errors and hence their approach was limited to a small set of weight functions. In this thesis, by introducing the Stieltjie's procedure, it is easy to construct accurately a set of nonclassical polynomials defined by any weight function. For a specific problem, a specific weight function may be chosen to optimize the accuracy and convergence of the solution. The details of the QDM is described in Chapter 2.

Another main interest of this thesis is to solve differential equations in an unbounded domain. Two types of second order differential equations in an unbounded domain are discussed and solved numerically by the QDM.

The first type of equation is the Fokker-Planck equation (FPE) of the form:

$$\frac{\partial P(x,t)}{\partial t} = \frac{\partial A(x)P(x,t)}{\partial x} + \frac{\partial^2 B(x)P(x,t)}{\partial^2 x}, \qquad (1.0.14)$$

with homogeneous boundary conditions at infinity. $P(x,t)$ is related to some probability density function of a system. $A(x)$ and $B(x)$ are referred to as the drift and diffusion coefficients and depend on the particular application considered.

The FPE was introduced by *Fokker* and *Planck* to describe the Brownian motion of particles [76,77]. For the past several decades, there has been an ongoing interest by numerous researchers in the description of nonequilibrium phenomena modeled with a

FPE. This interest continues unabated to the present date [78]- [91]. The basis for many of these models is Brownian diffusion in a potential characterized by Gaussian white noises. This leads to a time dependent linear FPE with drift and diffusion coefficients which can be nonlinear functions of the independent variable of interest. The theoretical basis for this approach has been provided in several standard references [92–94].

The traditional method for the solution of the FPE is a spectral method which usually involves the expansion of the probability density function (PDF) in a suitable basis set, and the reduction of the differential equation to a set of algebraic equations for the expansion coefficients. An alternate approach involves the discretization of the PDF on a grid of points. This discrete approach in the solution of differential and/or integral equations has been used by researchers in other fields, notably neutron transport [95], radiative transfer [96], and computational fluid dynamics [18,36]. Fourier series or Chebyshev polynomials are almost exclusively chosen as basis functions in the application of the pseudospectral approach. Other popular discretization schemes are based on the finite-difference technique such as those proposed by Chang and Cooper [97], Larsen *et al* [98] and Epperlein [99] primarily for the solution of a nonlinear FPE that arises in plasma physics. Park and Petrosian [100] have recently provided a detailed comparison of several different methods to the solution of FPEs applied to astrophysical problems.

Another type of equation to be studied in this thesis is the Schrödinger equation (SE) that arises in quantum mechanics and molecular physics. The equation has the form

$$\left[-\frac{d^2}{dy^2} + V(y) \right] \psi(y) = E\psi(y) \tag{1.0.15}$$

with V(y) as the potential. There have been numerous studies on the solution of the SE with different methods for several potential function V(y) [101]- [133]. The methods include variational and spectral techniques with Gaussian-type basis functions [29,101–111], perturbative approach [112–117], Pade approximation [118–122], FD methods [123–125],

and some other methods [126–131]. A very similar approach to the QDM for the solution of the SE referred to as the Discrete Variable Representation (DVR) was developed by Light and co-workers [132], and has been used by several other researchers [133]. The QDM and DVR differ in the use of polynomial basis functions. The QDM uses nonclassical polynomials and the DRV uses classical polynomial, majorly the Hermite (or scaled Hermite) polynomials. Hermite functions are the exact eigenfunctions of the quantum mechanical harmonic oscillator which has one well in the potential. This close connection with the physics makes them a nature choice of basis functions for the quantum mechanical problems. However for many problems with more than one well in potential Hermite polynomials are barely a good approximation of the solutions, as we will show later in this thesis. Therefore, new polynomial sets suitable to the physical nature of the solution are needed to improve the accuracy and convergence.

The purpose of this thesis is to study the quadrature discretization method and apply it to solve second order partial differential equations with unbounded boundaries. It is shown in this thesis that the QDM is easy to implement. The method provides high accuracy and rapid convergence, and is very efficient in solving high dimensional PDEs. Unlike most spectral methods and FD methods, it is possible for the QDM discretization to preserve the symmetry for the self-joint joint differential operator. Furthermore, the flexibility of the QDM in choosing weight function provides one the opportunity to achieve the best solution with the least computation work.

In Chapter 2, the basic ideas of the QDM are introduced. The QDM is tested and compared with other numerical methods. The applications of the QDM to the FPEs and SEs as well as the implementations and the results are presented in Chapter 3 and Chapter 4, respectively. Finally, a summary of the completed research and suggestions for the future work are given in Chapter 5.

Chapter 2

The Quadrature Discretization Method (QDM)

The QDM, originally introduced by Shizgal *et al* as discrete ordinate method [71, 72], is a numerical method for the efficient solution of integral and differential equations. The QDM can be used to solve a large class of differential and integral equations [71,72] and has also been applied to fluid dynamics problems [40]. The QDM is a spectral method based on the discretization of the solution on a grid of points (collocation points) that coincide with the points of a quadrature. The quadrature is based on a set of nonclassical polynomials orthogonal with respect to a specified weight function.

In this chapter, the fundamentals of the QDM are introduced and discussed. It differs from traditional spectral methods in that it is based on nonclassical polynomials. In the next section, several aspects of classical polynomials and spectral/pseudospectral methods are discussed. The numerical solution of differential equations is based on the approximate representation of the first derivative operator by a finite derivative matrix of dimension equal to the number of grid points. Higher order derivatives are represented by powers of the derivative matrix. The QDM is based on the use of nonclassical polynomials which are generated by a method developed by Gautschi [134]. Several model problems are studied with the QDM, and the results are compared with those for the classical pseudospectral method and the finite difference method. In the comparison of exact and approximate solutions, we introduce the errors E_1 (average error), E_2 (standard error) and E^∞ (maximum error) defined by

$$E_1 = \frac{1}{N} \sum_{i=1}^{N} |u_i^a - u_i^e|, \tag{2.0.1}$$

$$E_2 = \sqrt{\frac{1}{N} \sum_{i=1}^{N} (u_i^a - u_i^e)^2}, \tag{2.0.2}$$

and

$$E^\infty = max\{|u_i^a - u_i^e|, \quad i = 1, 2, ..., N\}, \tag{2.0.3}$$

where u_i^a is the approximate solution and u_i^e is the exact solution.

2.1 Classical polynomials and the pseudospectral method

Classical polynomials referred to in this thesis are the polynomials used by most researchers in the application of spectral methods. They include Chebyshev, Legendre, Jacobi, Laguerre and Hermite polynomials as well as their related polynomials. The details of these polynomials are discussed in most standard references on orthogonal polynomials and spectral methods [18,39,36,135]. Here we only give a brief summary of these polynomials and some of their properties.

Classical polynomials used in spectral methods are related to the polynomial solutions of eigenvalue problems of Sturm-Liouville equation

$$-(a(x)u_n(x)')' + b(x)u_n(x) = \lambda_n w(x)u_n(x) \tag{2.1.1}$$

in some interval I. λ_n are the eigenvalues and $u_n(x)$ are the corresponding eigenfunctions. The coefficients $a(x)$, $b(x)$ and $w(x)$ are real-valued functions, and $w(x)$ is referred to as the weight function. With particular choices for these coefficients, several classical polynomial sets are obtained. For Jacobi polynomials,

$$a(x) = (1 - x)^{\alpha+1}(1 + x)^{\beta+1}, \quad b(x) = 0, \quad w(x) = (1 - x)^\alpha (1 + x)^\beta, \tag{2.1.2}$$

for $\forall x \in (-1, 1)$, and $\alpha > -1$, $\beta > -1$. Legendre and Chebyshev polynomials are Jacobi polynomials with $\alpha = \beta = 0$ and $\alpha = \beta = -\frac{1}{2}$ respectively. For Laguerre polynomials, we have the coefficients

$$a(x) = x^{\alpha+1}e^{-x}, \quad b(x) = 0, \quad w(x) = x^{\alpha}e^{-x}, \tag{2.1.3}$$

for $\forall x \in (0, \infty)$, $\alpha > -1$, whereas for Hermite polynomials, these are given by,

$$a(x) = w(x) = e^{-x^2}, \quad b(x) = 0, \tag{2.1.4}$$

for $\forall x \in (-\infty, \infty)$. The polynomials satisfy a three recurrence relation [39]

$$u_{n+1}(x) = (\rho_n x + \sigma_n)u_n(x) + \tau_n u_{n-1}, \tag{2.1.5}$$

where $u_0(x)$ and $u_1(x)$ are the first two polynomials in a given set. The recurrence relations for Legendre, Chebyshev and Hermite polynomials are as follows:

Legendre

$$L_{n+1}(x) = \frac{2n+1}{n+1}xL_n(x) - \frac{n}{n+1}L_{n-1}(x), \tag{2.1.6}$$

with $L_0(x) = 1$, $L_1(x) = x$;

Chebyshev

$$T_{n+1}(x) = 2xT_n(x) - T_{n-1}(x), \tag{2.1.7}$$

with $T_0(x) = 1$, $T_1(x) = x$;

Hermite

$$H_{n+1}(x) = 2xH_n(x) - 2nH_{n-1}, \tag{2.1.8}$$

with $H_0(x) = 1$, $H_1(x) = 2x$;

If the zeros of the Nth order polynomial are $\{x_i, i = 1, 2, .., N\}$, a Gauss quadrature formula, for an arbitrary smooth function $f(x)$, gives

$$\int_I f(x)w(x)dx \approx \sum_{j=1}^{N} f(x_j)w_j, \tag{2.1.9}$$

where $w_j = \int_I l_j(x)w(x)dx$, are the weights, and x_j are the quadrature points of the integration formula. If $f(x)$ is a polynomial of degree $2N - 1$ or less, Eq. (2.1.9) is exact [39,136]. The function $l_j(x)$ is the interpolating polynomial uniquely defined by the condition

$$l_j(x_i) = \begin{cases} 0, & \text{if } i \neq j \\ 1, & \text{if } i = j \end{cases} \qquad (2.1.10)$$

The quadrature points and weights for the classical polynomials and related Gauss-type quadrature formula can be found in standard references in spectral methods [18,19].

The classical pseudospectral method is based on the discretization of a smooth function $f(x)$ on a grid of these quadrature points $\{x_i, i = 0, 1, 2, ..., N\}$. Derivatives of the function are approximated by the analytic derivatives of the interpolating polynomial $l_j(x)$. The first derivative can be represented in a matrix form as

$$(D_N f)(x_i) = \sum_{j=0}^{N} (D_N)_{ij} f(x_j), \quad (i = 0, 1, 2, ..., N), \qquad (2.1.11)$$

where D_N is the derivative matrix with the entries $(D_N)_{ij} = l'_j(x_i)$. Higher order derivative matrices can be obtained by multiplying D_N by itself a suitable number of times. The spectral derivative matrix is usually full. The explicit expression of the derivative matrices based on the quadrature points is described in the references by Canuto [18], Peyret [137,138], and Funaro [39,68].

The advantage of the spectral method is its spectral accuracy, that is, errors for numerical approximation decrease exponentially with increasing number of grid points. Consider a second order differential equation

$$\frac{d^2 u}{dx^2} = \sin(\pi x) \qquad (2.1.12)$$

with homogeneous Dirichlet boundary condition $u(-1) = u(1) = 0$. The problem has an analytic solution $u(x) = -\pi^2 \sin(\pi x)$. We solve the problem with a Legendre spectral

N	Legendre			FD		
	E_1	E_2	E^∞	E_1	E_2	E^∞
4	4.09(-02)	5.01(-02)	6.13(-02)	1.56(-01)	1.91(-01)	2.34(-01)
8	2.40(-04)	2.83(-04)	4.46(-04)	3.66(-02)	4.01(-02)	5.30(-02)
16	1.50(-11)	1.72(-11)	2.91(-11)	8.68(-03)	9.46(-03)	1.30(-02)
32	2.73(-14)	3.23(-14)	6.03(-14)	2.11(-03)	2.31(-03)	3.22(-03)
64	1.21(-14)	1.52(-14)	4.36(-14)	5.19(-04)	5.73(-04)	8.04(-04)
128				1.29(-04)	1.43(-04)	2.01(-04)
256						5.01(-05)
512						1.26(-05)

Table 2.1: Errors for the numerical approximation of $u'' = \sin(\pi x)$ with a Legendre spectral method and a finite difference method.

method and a 2nd order central difference method. Table 2.1 gives the errors of the numerical solutions of Eq. (2.1.12) with both methods.

It can be seen from the results that for the Legendre method, the error decays very fast. The maximum error decays to $O(10^{-14})$ within 32 points. Increasing N beyond this point would not reduce the errors significantly, and the errors remain close to machine accuracy.

For the FD method, the error decays at a much slower rate. With 128 grid points, the error is $O(10^{-4})$ and with 512 grid points, it is $O(10^{-5})$. This indicates that to obtain 4 decimal places accuracy for the solution of Eq. (2.1.12), the FD method requires more than 100 grid points, while for the Legendre spectral method, approximately 8 points are needed. As a matter of fact, the error for the FD method decays at the rate of $O(N^{-2})$. For the Legendre spectral method the errors decay at an exponential rate as the number of grid points N increases. To show this point, we plot the logarithm of the errors versus $log_{10}(N)$ in Fig. 2.1. The exponential accuracy of the spectral method makes it very attractive for solving multi-dimensional problems since much coarser grids are needed in comparison with the finite difference method.
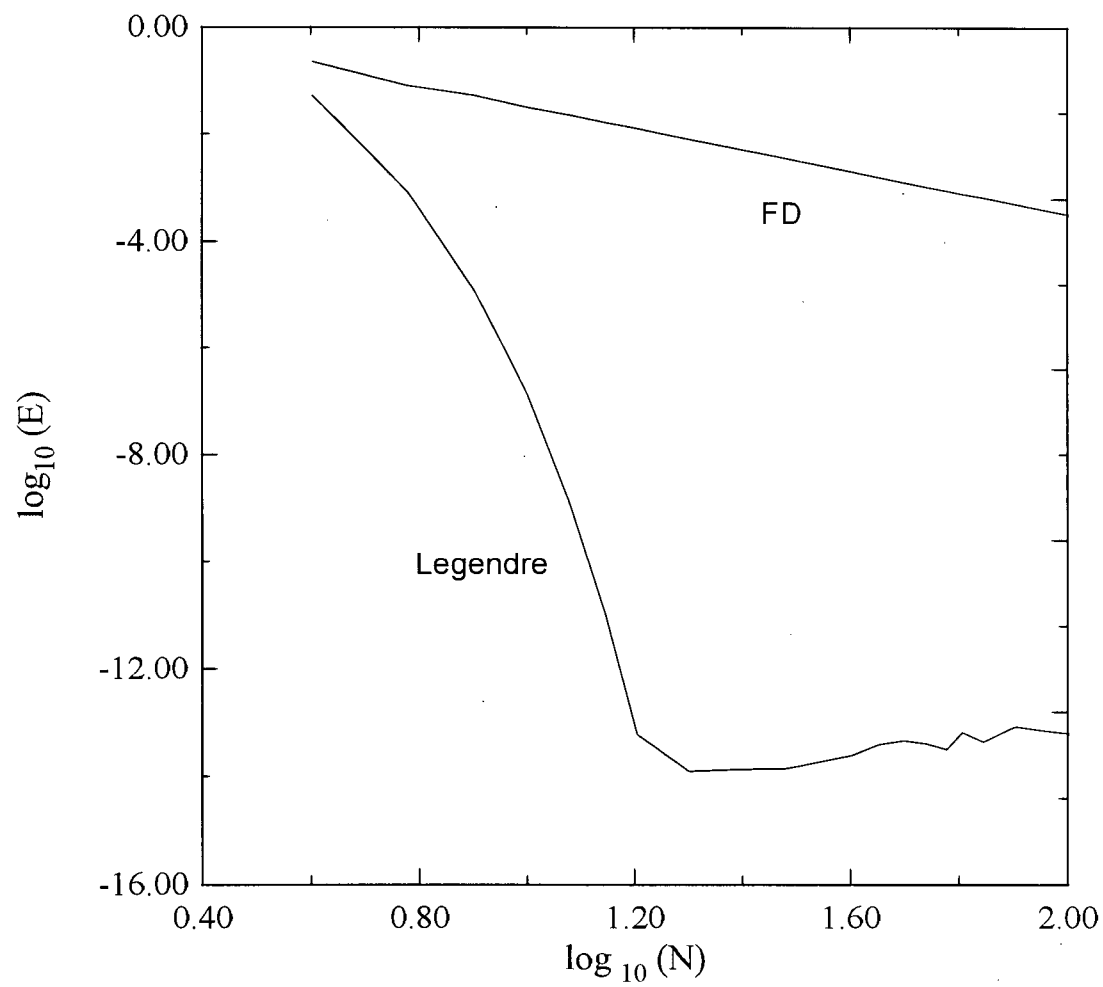
Figure 2.1: Maximum error E^∞ in variation with N for the solution of $u'' = \sin(\pi x)$.

As mentioned in Chapter 1, spectral derivative matrices based on classical polynomials have some drawbacks. The main disadvantage of the spectral discretization is the large value of the largest eigenvalue of the differentiation matrix, which can result in an instability when iteration and/or explicit time integration methods are applied. The largest eigenvalue of the derivative matrices with Chebyshev and Legendre collocation methods grows very fast as number of grid points N increases.

Consider the eigenvalue problem of the advection operator

$$\frac{d\phi_n(x)}{dx} = \lambda_n \phi_n(x) \quad \text{on (-1,1)} \tag{2.1.13}$$

subject to the boundary condition

$$\phi_n(1) = 0 \tag{2.1.14}$$

The eigenvalues are computed with Chebyshev and Legendre collocation methods. The boundary condition is imposed by removing the last row and column of the derivative matrix D_N. The resulting $(N-1) \times (N-1)$ is diagonalized numerically. Figs. 2.2 and 2.3 show the eigenvalues of the first derivative matrix with N=8, 16, 32, 64. Although most of the eigenvalues converge to a curve in the left half-plane between $-iN$ and iN, a few spurious eigenvalues diverge at a much faster rate. The modulus of the largest eigenvalue $|\lambda_N|$ in relation with the number of grid points N is plotted in Fig. 2.4. The largest eigenvalue grows like $O(N^2)$ as $N \to \infty$. For the Legendre method, $|\lambda_N| \approx 0.080N^2$, and for the Chebyshev method, $|\lambda_N| \approx 0.089N^2$.

For the second derivative matrix, we consider the eigenvalue problem of the diffusion operator

$$\frac{d^2\phi_n(x)}{dx^2} = \lambda_n \phi_n(x) \quad \text{on (-1,1)} \tag{2.1.15}$$

with the boundary conditions of Dirichlet type: $\phi_n(1) = \phi_n(-1) = 0$. The problem has the analytical solution, $\lambda_n = -(n\pi/2)^2$ and $\phi_n(x) = sin\sqrt{\lambda_n}x$, $n = 0, 1, 2, ...$
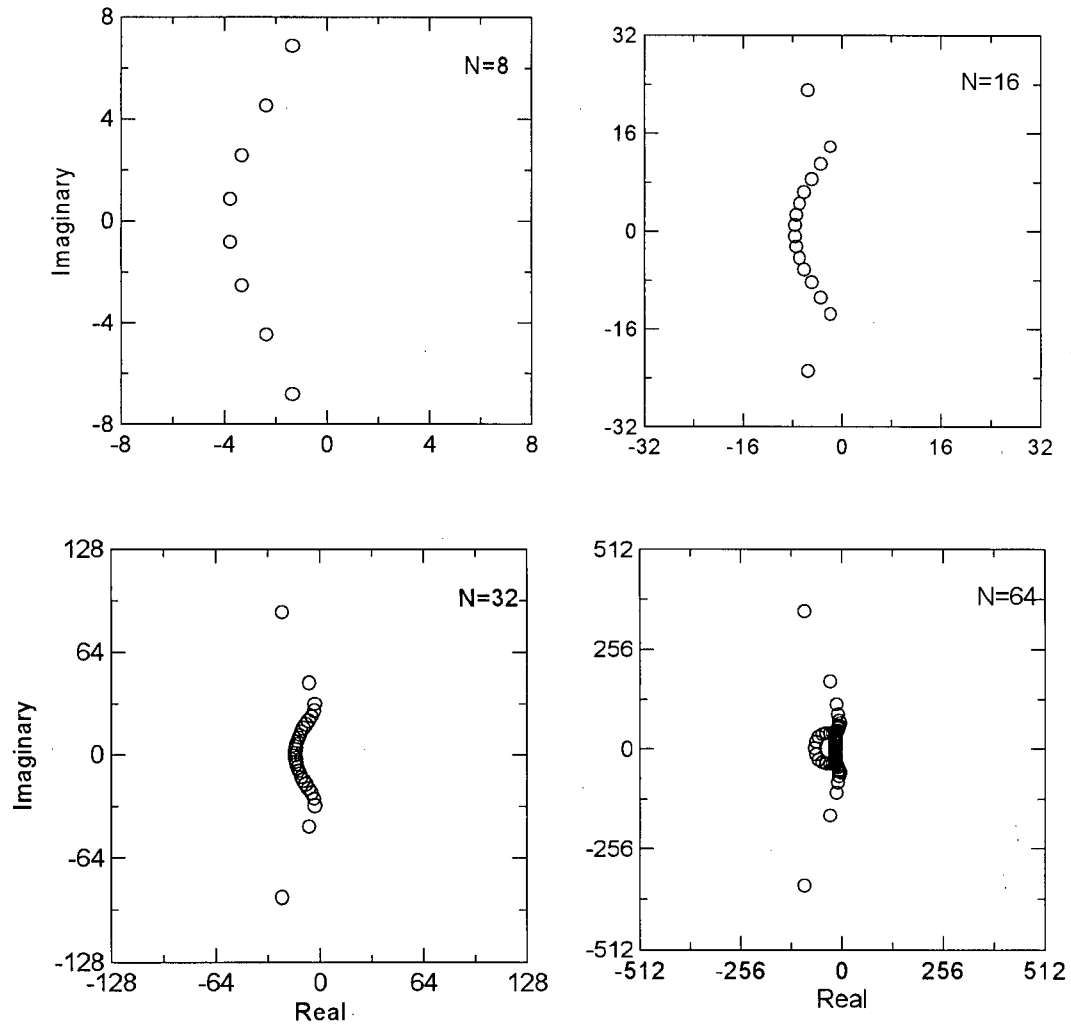
Figure 2.2: Eigenvalues of the 1st derivative matrix with Chebyshev discretization with N=8, 16, 32, 64.
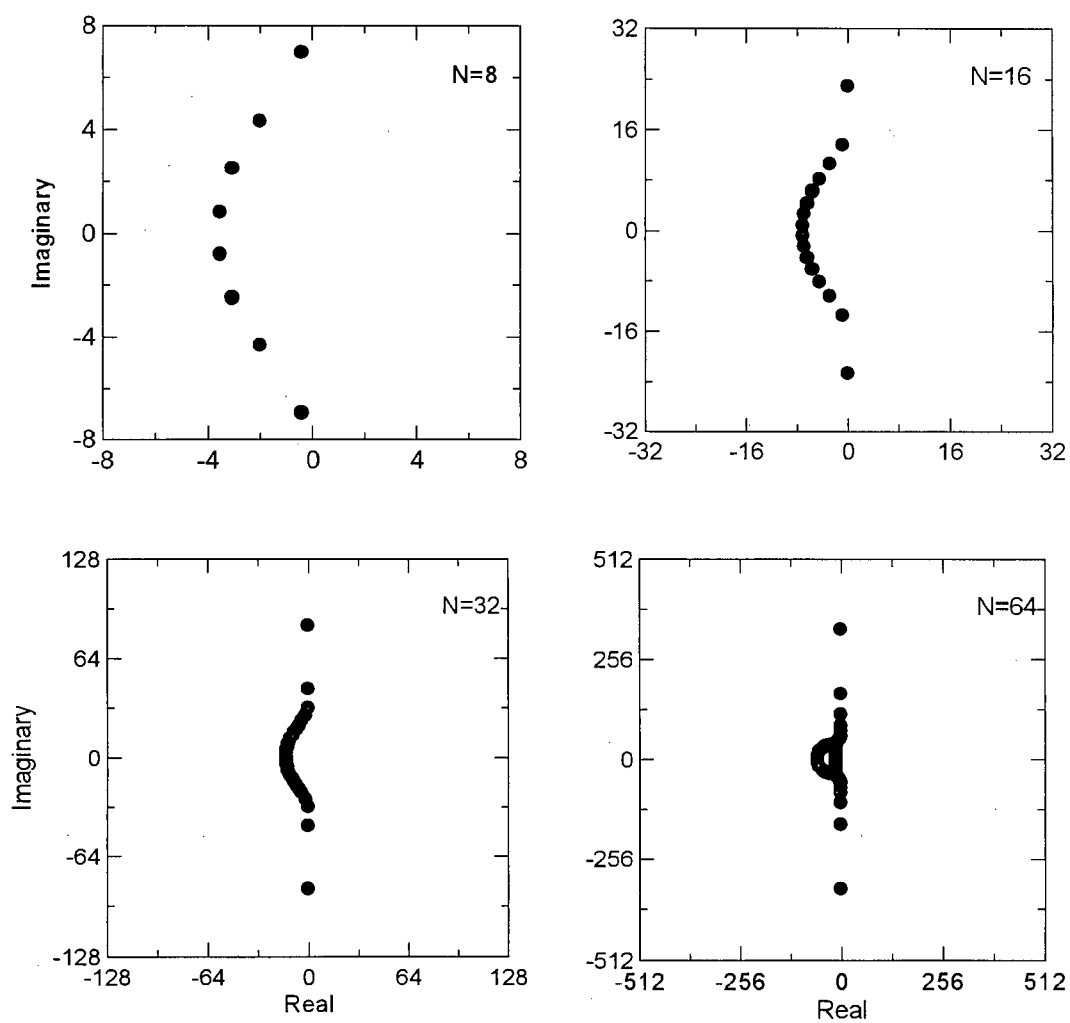
Figure 2.3: Eigenvalues of the 1st derivative matrix with Legendre discretization with $N=8, 16, 32, 64$.
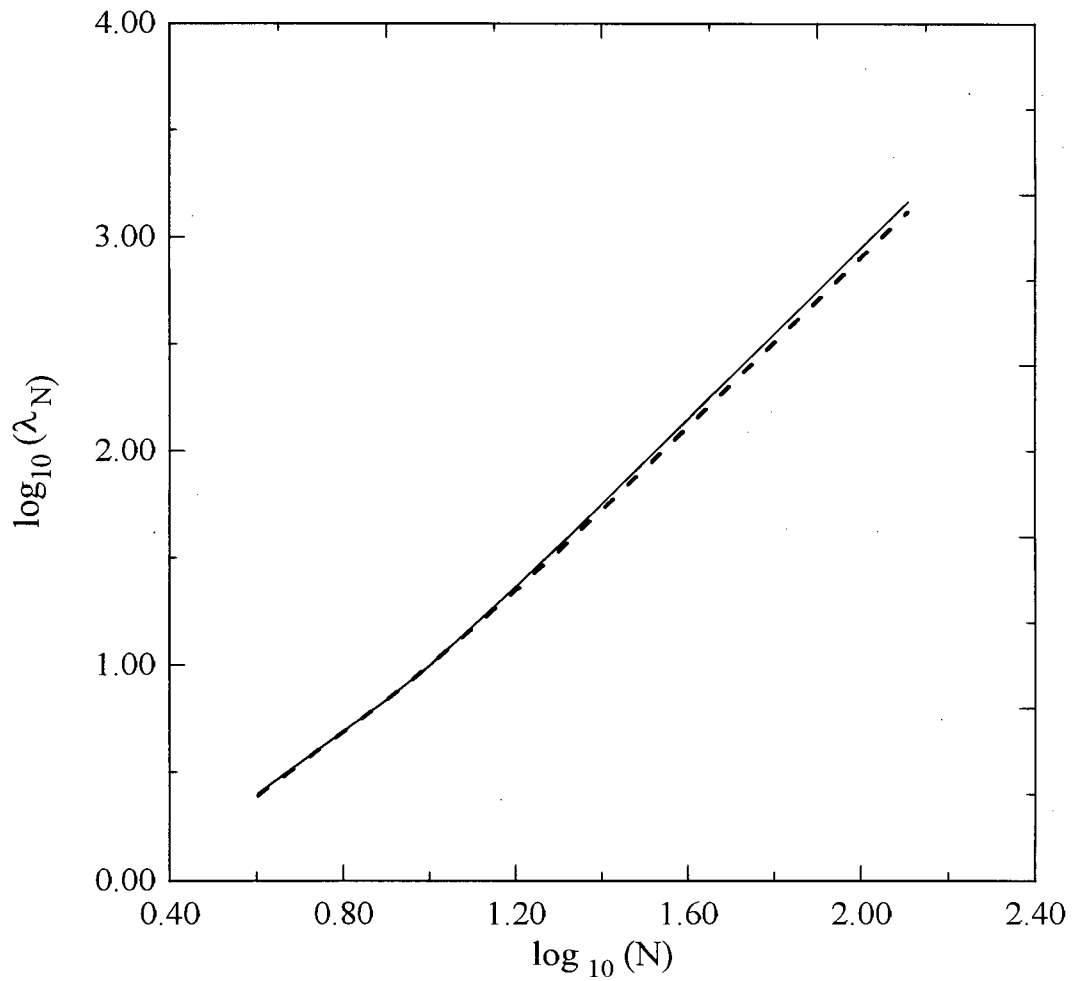
Figure 2.4: Eigenvalues of 1st derivative matrix with Chebyshev and Legendre discretization. The solid line is for Chebyshev. The dashed line is for Legendre.

The largest eigenvalues calculated with Chebyshev and Legendre collocation methods are given in Fig. 2.5. The boundary conditions are imposed by removing the first and last rows and columns of the derivative matrix D_N. The resulting $(N-2) \times (N-2)$ is diagonalized numerically. The largest eigenvalue grows like $O(N^4)$ as $N \to \infty$, and $|\lambda_n| = 0.026N^4$ and $|\lambda_n| = 0.047N^4$ for the Legendre and Chebyshev method, respectively.

Several researchers showed that the effect upon the numerical computation of the eigenvalues of the derivative matrix is caused by round off error [52,53,55,56,59]. This property of the derivative matrix does not play a role in the solution of a differential equation. As seen in Fig. 2.1, the error of the solution of the differential equation Eq. (2.1.12) decreases at a very fast rate with N increasing. However, for the time-dependent differential equation, the large value of the largest eigenvalue causes an instability in the time integration when explicit time-stepping techniques are applied. For the first order explicit Euler method, for example, the time step Δt to ensure the stability of the time integration may be $O(N^{-4})$ for a 2nd order time-dependent differential equation. To reduce the order of growth rate of the largest eigenvalue, preconditioning of the derivative matrix is usually used. The topic of the preconditioning is out of the scope of this thesis. Methods for preconditioning can be found in many references [66,139–141].

Another way to improve the condition of the spectral derivative matrix is to use mapping techniques. Several researchers suggested that [29,60] the growth rate of the largest eigenvalue is related to the minimum spacing Δx_{min} between the adjacent grid points. The largest eigenvalue (in modulus) of the first derivative matrix is of the order of $1/\Delta x_{min}$, and for the second derivative matrix it is of the order of $1/\Delta^2 x_{min}$. Most classical points in finite domains, for example, Chebyshev and Legendre points, have minimum spacing of $O(1/N^2)$ such that the 1st and 2nd derivative matrices grow like $O(N^2)$ and $O(N^4)$, respectively. Kosloff and Tal-Ezer proposed a modified Chebyshev method to improve this condition [60]. They mapped the Chebyshev points in [-1,1]
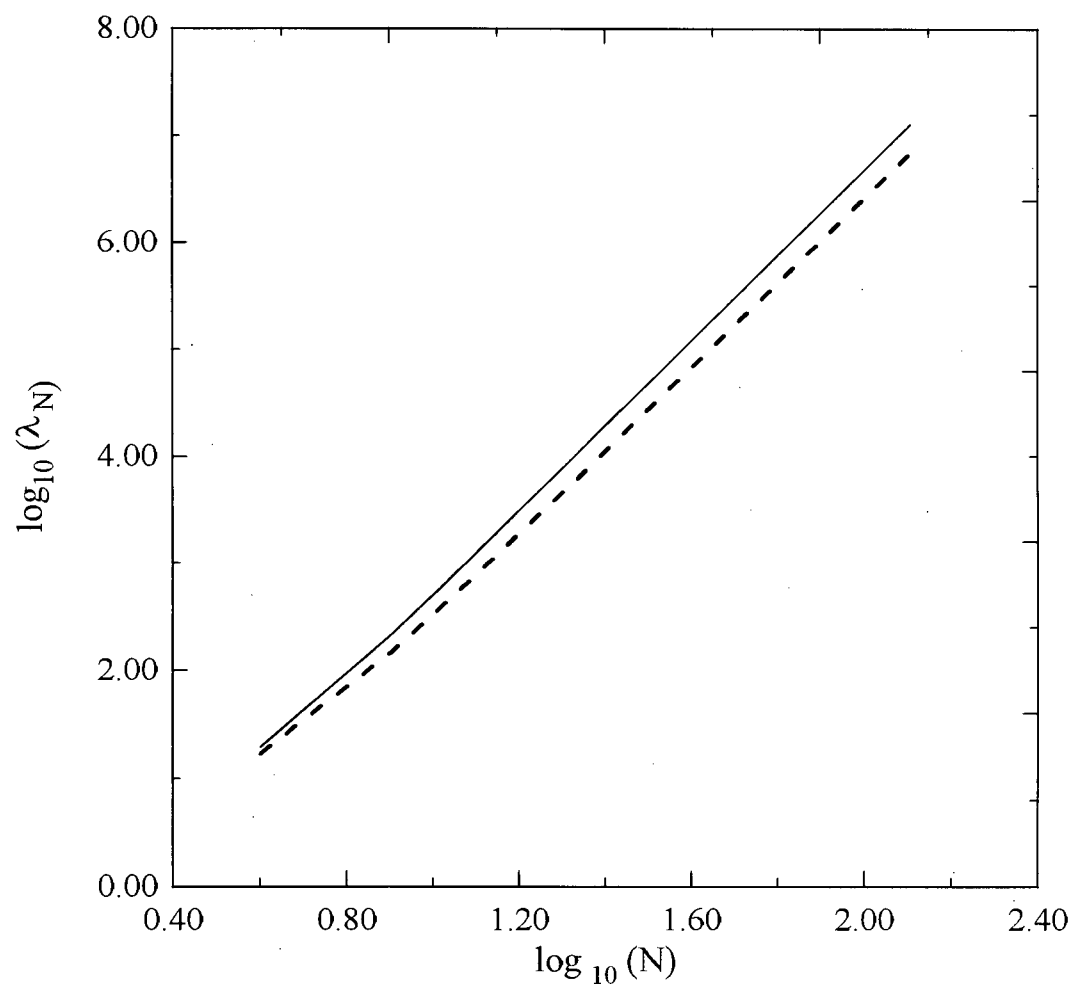
Figure 2.5: Eigenvalues of the 2nd derivative matrix with Chebyshev and Legendre discretization. The solid line is for Chebyshev. The dashed line is for Legendre.

to a new set of grid points in [-1,1] which has minimum spacing of $O(1/N)$ such that the largest eigenvalues of 1st and 2nd derivative matrices improve to $O(N)$ and $O(N^2)$, respectively. Their algorithm is similar to those of the Fourier method but it provides accurate solutions for nonperiodic problems. The detailed description of the method can be found in their paper [60]. Fig. 2.6 give the largest eigenvalues related to the modified Chebyshev approximation versus the number of grid points N.

Classical Chebyshev and Legendre polynomials are defined in a finite domain (-1,1). For a problem in an arbitrary finite domain (a,b), one can either map the domain into (-1,1) by using change of variable, or use scaled Chebyshev and Legendre polynomials. For problems with unbounded domain, one needs to truncate artificially the infinite domain into a finite domain in order to apply the Chebyshev or Legendre spectral method. The accuracy and convergence of the solution are directly related to the domain truncation. For a certain number of grid points, the larger the domain, the coarser the grid, and the slower the convergence. If the domain is too small, the error caused by domain truncation may exceed the accuracy requirement.

The Hermite points for the infinite domain naturally spread over the whole domain with increasing N and no artificial boundary cutoff is involved. As shown in several literatures [29,68,73], Hermite points have another advantage that the minimum spacing is $O(1/\sqrt{N})$ such that the largest eigenvalues of the first and second derivative matrices are $O(\sqrt{N})$ and $O(N)$ as $N \to \infty$. This property of Hermite polynomials and their close connection to the physics usually make them the natural candidate for solving problems in an infinite domain. However, it may not be always the best choice as we will see later in the thesis. The largest eigenvalues of the derivative matrix for the Hermite points versus number of grid points N is plotted on a logarithm scale in Figure 2.7. Numerical fitting shows that the largest eigenvalue satisfies $\lambda_N \approx 0.28 N^{0.7}$ for the first derivative matrix and $\lambda_N \approx 0.38 N^{1.27}$ for the second derivative matrix. These orders are slightly
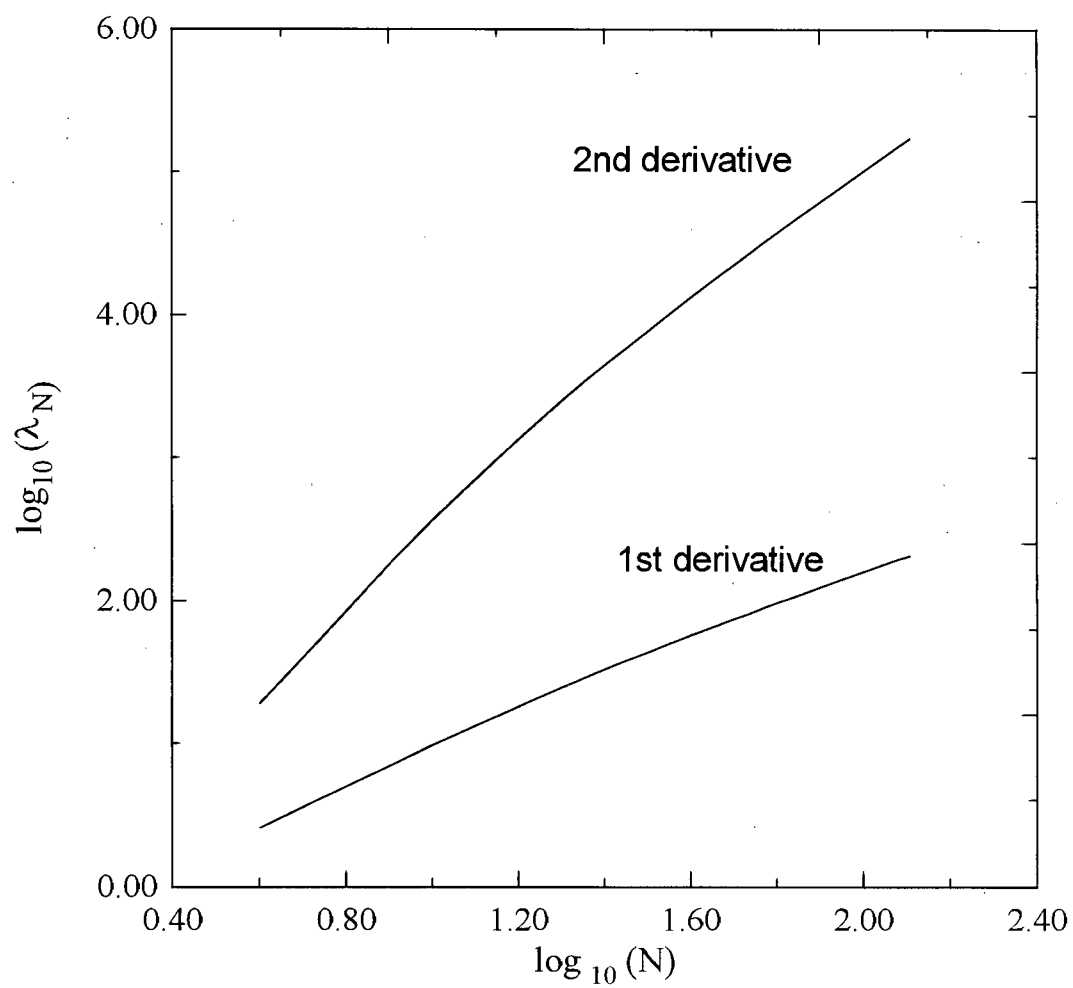
Figure 2.6: Largest eigenvalues of the 1st and 2nd derivative matrices calculated by the Kosloff modified Chebyshev method.

larger than the asymptotic results.

2.2 The quadrature discretization method

2.2.1 Construction of derivative matrices

Consider a set of polynomials, $F_n(x)$, orthogonal with respect to a weight function $w(x)$, that is,

$$\int w(x) F_n(x) F_m(x) dx = \delta_{nm}. \tag{2.2.1}$$

There are as many quadrature rules as there are sets of orthogonal polynomials. The familiar quadratures are those based on the classical polynomials discussed in the last section. Theoretically, a set of orthogonal polynomials can be constructed for any interval and any weight function. The major development of the QDM is to generate, with the method introduced by Gautschi [134], new sets of points and weights from nonclassical polynomials chosen to maximize the rate of convergence of the solution of a specific differential equation.

The QDM is based on the discrete representation of a function $f(x)$ by its values at the set of N quadrature points x_i, that is, $f(x_i)$. We expand $f(x)$ in the $\{F_n\}$ orthogonal basis set,

$$f(x) = \sum_{n=1}^{N} a_n F_n(x), \tag{2.2.2}$$

where a_n are the expansion coefficients of $f(x)$ and are given by,

$$a_n = \int w(x) f(x) F_n(x) dx. \tag{2.2.3}$$

The expansion coefficients can be evaluated numerically with the quadrature rule in Eq.(2.1.9), and

$$a_n = \sum_{j=1}^{N} w_j f(x_j) F_n(x_j). \tag{2.2.4}$$
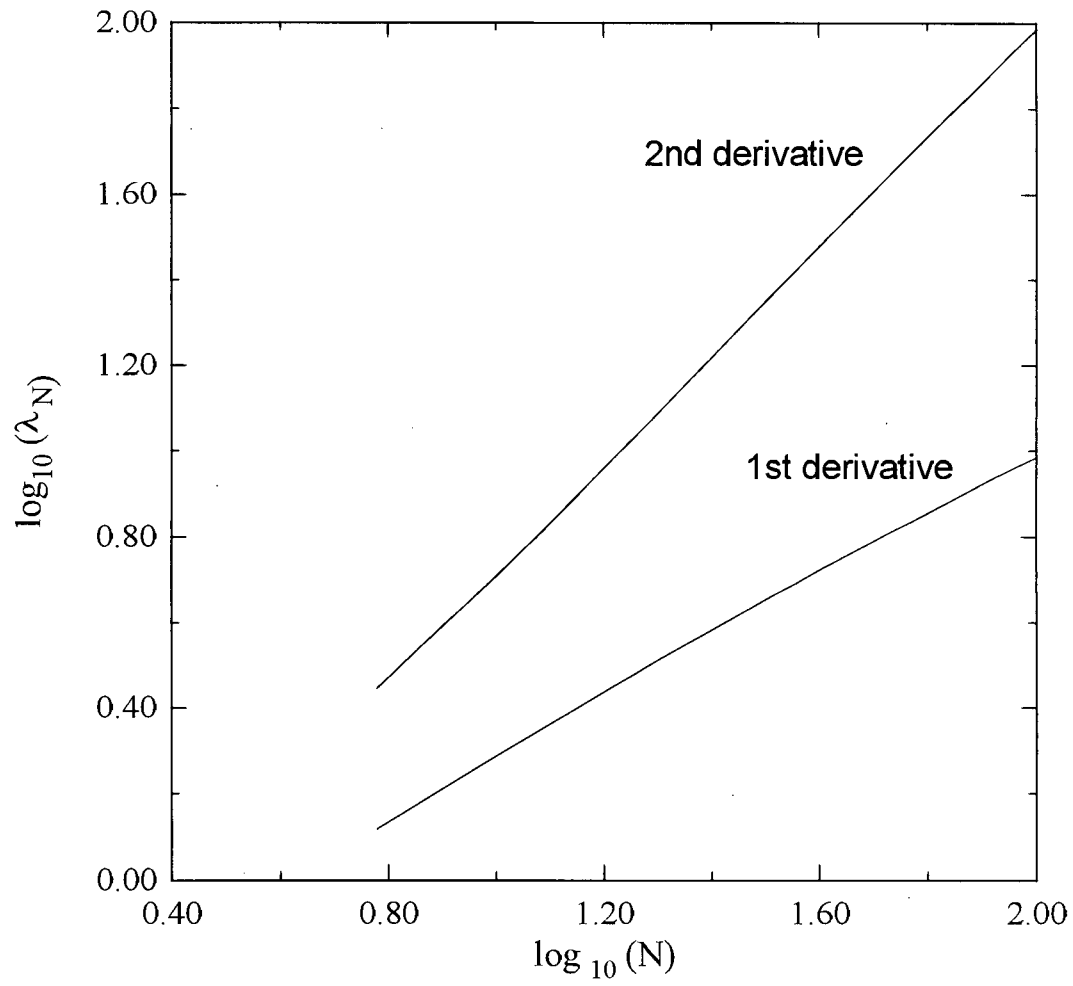
Figure 2.7: Largest eigenvalues of the 1st and 2nd derivative matrices calculated by the Hermite method.

Eq. (2.2.4) gives the transform from the physical space $\{f(x_i)\}$ to the transform space $\{a_n\}$. If we use Eq.(2.2.4) to evaluate $f(x)$ at the quadrature points x_i we have another transform that does the reverse transformation which is from the transform space $\{a_n\}$ to the physical space $\{f(x_i)\}$,

$$f(x_i) = \sum_{n=1}^{N} a_n F_n(x_i). \tag{2.2.5}$$

Substituting Eq. (2.2.4) into Eq. (2.2.2), we obtain

$$f(x) = \sum_{n=1}^{N} \sum_{j=1}^{N} w_j f(x_j) F_n(x_j) F_n(x). \tag{2.2.6}$$

The above equation indicates that $f(x)$ can be calculated at any point from its values $f(x_j)$, that is,

$$f(x) = \sum_{j=1}^{N} l_j(x) f(x_j), \tag{2.2.7}$$

where the interpolation polynomial $l_j(x)$ is given by

$$l_j(x) = w_j \sum_{n=1}^{N} F_n(x_j) F_n(x), \tag{2.2.8}$$

and satisfies

$$l_j(x_i) = \begin{cases} 0, & \text{if } i \neq j \\ 1, & \text{if } i = j \end{cases} \tag{2.2.9}$$

If Eq. (2.2.7) is differentiated, one obtains

$$\frac{df(x_i)}{dx} = \sum_{j=1}^{N} \Delta_{ij} f(x_j), \tag{2.2.10}$$

where Δ_{ij} are the entries of the derivative matrix $\boldsymbol{\Delta}$ and are defined by

$$\Delta_{ij} = l_j'(x_i) = \sum_{n=1}^{N} w_j F_n(x_j) F_n'(x_i). \tag{2.2.11}$$

It is easy to notice that the transformations between the physical space and transform space shown in Eq. (2.2.4) and Eq. (2.2.5) are not symmetric. To symmetrize the transformations, we consider an alternative function $\tilde{f}$ defined by

$$\tilde{f}(x) = \sqrt{w_i} f(x). \tag{2.2.12}$$

If the expansion coefficients of $f(x)$ in the basis set $F_n(x)$ are a_n, then there is a unitary (or orthogonal) transformation between the physical and transform spaces, that is,

$$\tilde{f}(x_i) = \sum_{n=1}^{N} \sqrt{w_i} F_n(x_i) a_n, \tag{2.2.13}$$

$$a_n = \sum_{j=1}^{N} \sqrt{w_j} F_n(x_j) \tilde{f}(x_j), \tag{2.2.14}$$

where the matrix elements of the symmetric transformation $\mathbf{T}$ are $T_{in} = \sqrt{w_i} F_n(x_i)$.

If in Eq. (2.2.13), x_i is replaced with x, and Eq. (2.2.14) is used for a_n, one obtains a Nth-order interpolation, given by

$$\tilde{f}(x) = \sum_{j=1}^{N} I_j(x) \tilde{f}(x_j), \tag{2.2.15}$$

where the interpolation polynomial $I_j(x)$ is given by

$$I_j(x) = \sqrt{w_i w_j} \sum_{n=1}^{N} F_n(x_j) F_n(x). \tag{2.2.16}$$

The algorithm for differentiation in the discrete basis is given by differentiating Eq. (2.2.15) and using Eq. (2.2.16) one has that

$$\frac{d\tilde{f}(x_i)}{dx} = \sum_{j=1}^{N} D_{ij} \tilde{f}(x_j), \tag{2.2.17}$$

where the derivative operator, $D_{ij} = \sqrt{w_i w_j} I_j'(x_i)$ is given by

$$D_{ij} = \sqrt{w_i w_j} \sum_{n=1}^{N} F_n(x_j) F_n'(x_i). \tag{2.2.18}$$

We refer to the derivative matrix $\mathbf{D}$ with the elements D_{ij} as the QDM modified derivative matrix. We have the following relation between the derivative matrices Δ_{ij} and D_{ij}

$$\Delta_{ij} = \sqrt{w_j/w_i} D_{ij}. \tag{2.2.19}$$

The matrix element of the derivative operator d/dx in the transform space (also called Galerkin 's matrix) is

$$d_{nm} = \int w(x) F_n(x) F_m'(x) dx. \tag{2.2.20}$$

If we evaluate it with the quadrature rule in Eq.(2.1.9), we have that,

$$d_{nm} = \sum_{j=1}^{N} w_k F_n(x_k) F'_n(x_k). \qquad (2.2.21)$$

For some specific physical models, using the transform matrix have an attractive advantage that the resulting differential matrix in the transform space may be banded [29,142].

If we transform the derivative matrix $\mathbf{d}$ back to the physical space with transform matrix $\mathbf{T}$, we obtain the QDM derivative matrix $\mathbf{D} = \mathbf{T}\mathbf{d}\mathbf{T}^T$, that is.

$$D_{ij} = \sum_{n=1}^{N} \sum_{m=1}^{N} B_n(x_i)\sqrt{w_i}[\sum_{k=1}^{N} w_k F_n(x_k) F'_m(x_k)] F_m(x_j)\sqrt{w_j}. \qquad (2.2.22)$$

The sum over n yields δ_{ik} and the sum over k can subsequently be performed and one obtains D_{ij} given by Eq. (2.2.18)

The second derivative matrix $\mathbf{\Delta}^{(2)}$ or $\mathbf{D}^{(2)}$ can be obtained simply by multiplying it by itself. It is easy to show that the matrix elements for $\mathbf{\Delta}^{(2)}$ and $\mathbf{D}^{(2)}$ satisfies

$$\Delta_{ij}^{(2)} = \sqrt{w_j/w_i} D_{ij}^{(2)}. \qquad (2.2.23)$$

The application to differential equations is based on the algorithm for numerical differentiation, defined by,

$$[\frac{df}{dx}]_{x=x_i} = \sum_{j=1}^{N} \Delta_{ij} f(x_j), \qquad (2.2.24)$$

or

$$\sqrt{w_i}[\frac{df}{dx}]_{x=x_i} = \sum_{j} D_{ij} f(x_j)\sqrt{w_j}, \qquad (2.2.25)$$

where the matrix Δ_{ij} and D_{ij} are defined in equations (2.2.11) and (2.2.18) respectively.

Generally speaking, the matrix representation of a differential equation can be written in a simple way by replacing derivatives with Δ_{ij} or D_{ij} and function with their values at set of points x_i. The advantage of introducing the new derivative matrix $\mathbf{D}$ will be demonstrated later in this chapter and in the applications as shown in chapter 3 and chapter 4.

The QDM method is analogous to the collocation method by using the classical sets of polynomials (e.g. Jacobi polynomial, Hermite polynomial, etc.) and their corresponding weight functions to generate weights and points to construct the differential matrix. The advantage of the QDM over the traditional pseudospectral method is that it allows the use of arbitrary orthogonal polynomial basis sets or equivalently arbitrary weight functions. This give us a much wider choice of the collocation points and weights to apply to a specific problem. The main idea is to choose a weight function related to the physical nature of the problem to be solved such that the solution converges rapidly.

2.2.2   Generation of orthogonal polynomials, quadrature weights and points

There have been several discussions on the generation of a set of polynomials orthogonal to each other with respect to some weight function $w(x)$. This is a numerically unstable problem [143,75] and a practical approach, referred to as the discretized Stieltjes's procedure, has been provided recently by Gautschi [134].

Basis set generation; The Stieltjes's procedure:

The generation of a set of polynomials orthogonal with respect to some weight function $w(x)$ has been discussed in several texts [135] and papers [71,72,75]. For a nonclassical weight function, the usual Schmidt procedure [144] which involves orthogonalization of a given member of the set to all the functions of lower order and then normalized, is highly unstable due to roundoff errors and is not practical. The Schmidt procedure is analogous to methods based on the moments of the weight function. The best approach is one based on the three term recurrence relation of the polynomials $\{Q_n(x)\}$ with $Q_0 = 1$, given by

$$Q_{n+1}(x) = (x - \alpha_n)Q_n(x) - \beta_n Q_{n-1}(x). \tag{2.2.26}$$

It can be shown that the two recurrence relations Eq.(2.1.5) and Eq.(2.2.26) are equivalent and satisfy

$$\alpha_n = -\frac{\sigma_n}{\rho_n}, \tag{2.2.27}$$

$$\beta_n = -\frac{\tau_n}{\rho_n \rho_{n-1}}, \tag{2.2.28}$$

and

$$Q_n = \frac{u_n}{\rho_{n-1}\rho_{n-2}\cdots\rho_1}. \tag{2.2.29}$$

For the classical polynomials, the coefficients α_n and β_n are known and exact. For example, $\alpha_n = 0$, $\beta_1 = 1/3$ and $\beta_n = n^2/(4n^2 - 1)$ $(n > 1)$ for the Legendre case; $\alpha_n = 0$, $\beta_1 = 1/2$ and $\beta_n = 1/4$ $(n > 1)$ for the Chebyshev case; and $\alpha_n = 0$, $\beta_1 = 1/2$ and $\beta_n = n/2$ $(n > 1)$ for the Hermite case. The polynomials generated by Eq. (2.2.26) are not normalized. The corresponding normalized polynomials $P_n(x) = Q_n(x)/\sqrt{\gamma_n}$ satisfy the recurrence relation

$$xP_n(x) = \sqrt{\beta_{n+1}}P_{n+1}(x) + \alpha_n P_n(x) + \sqrt{\beta_n}P_{n-1}(x), \tag{2.2.30}$$

where the normalization factors are given by

$$\gamma_n = \int w(x)Q_n^2(x)dx. \tag{2.2.31}$$

For the QDM, we are interested in the non-classical sets of orthogonal polynomials and α_n, β_n are usually unknown and calculated numerically. The recurrence coefficients in Eq. (2.2.26) are given by

$$\alpha_n = \frac{\int w(x)xQ_n(x)dx}{\int w(x)Q_n^2(x)dx}, \tag{2.2.32}$$

and

$$\beta_n = \frac{\int w(x)Q_n^2(x)dx}{\int w(x)Q_{n-1}^2(x)dy}. \tag{2.2.33}$$

One of the practical approaches of numerical computation of α_n and β_n in Eqs. (2.2.32) and (2.2.33) is the Stieltjes's procedure introduced by Gautschi [134]. The method involves the accurate calculation of the integrals in Eqs. (2.2.32) and (2.2.33) by subdividing the domain of interest into many subdomains and evaluating the contribution from each subdomain with a high order quadrature. Gautschi discusses the use of Gauss-Legendre and Feijer quadrature rules. The calculation begins with $Q_{-1} = 0$, $Q_0 = 1$ and $\alpha_0 = \beta_0 = 0$. Equation (2.2.26) can then be used to generate Q_1 and then α_1 and β_1 with Eqs. (2.2.32) and (2.2.33). In this way all the recurrence coefficients are calculated. The quadrature weights and points are calculated as discussed elsewhere [135,75]. The discretized Stieltjes's procedure was used to calculate the recurrence coefficients for several nonclassical weight functions reported in previous papers. It is found to work remarkably well as long as care is taken to ensure the accuracy of the integrals by a judicious choice for the number of subdivisions and the order of the quadrature in each interval.

Since there is no analytic solution of α_n and β_n for most non-classical recurrence relations, the accuracy of the numerical calculation of α_n and β_n will be essential to the later calculation of quadrature points and weights as well as the derivative matrices. To investigate the accuracy of the Stieltjes's procedure we calculate the α_n and β_n for up to 100 quadrature points for the classical polynomials with the Stieltjes's procedure and compare the results with the known analytic solution.

The maximum errors E^∞ in α_n and β_n computed by Stieltjes's procedure for several classical polynomials with N quadrature points are shown in Table 2.2. The error curves for the α_n and β_n with $N = 50$ is given in Fig. 2.8. As shown in the table, the maximum errors in β_n for both Legendre and Hermite polynomials and in α_n for all the polynomials are very small and at most $O(10^{-13})$. The maximum error in β_n for the Chebyshev polynomials are 7.76×10^{-5}. It is unchanged with changing N because the maximum error eventually occurs at the first coefficient β_1. The reduced accuracy of

N	$E^\infty_{\alpha_n}$	$E^\infty_{\beta_n}$
	Chebyshev	
5	9.528058591081317e-17	7.763988590681060e-05
10	5.386806816078257e-16	7.763988590681060e-05
20	9.710341644410283e-16	7.763988590681060e-05
50	1.805638645361598e-15	7.763988590681060e-05
100	2.490836730411662e-15	7.763988590681060e-05
	Legendre	
5	7.070397677170780e-16	3.053113317719181e-15
10	7.070397677170780e-16	3.053113317719181e-15
50	4.679789671731484e-15	3.053113317719181e-15
100	6.021950962055382e-15	3.164135620181696e-15
	Hermite	
5	4.996208974320000e-15	9.103828801930001e-15
10	4.996208974320000e-15	4.840572387370000e-14
50	2.609915956900000e-14	3.375077994860000e-13
70	5.530643324450000e-14	4.760636329590000e-13
100	5.530643324450000e-14	7.034373084020000e-13

Table 2.2: Maximum error in α_n and β_n calculated by the Stieltjes's procedure.

the recurrence coefficients β_n's for the Chebyshev polynomial is due to the less accurate intergrations. Recall the weight function for Chebyshev polynomial is $w(x) = \frac{1}{\sqrt{1-x^2}}$ in interval [-1,1] and it is divergent as x tends to the end points. When one integrates a polynomial with respect to this weight function numerically, a large round-off error is involved and results in poor accuracy of the integration. For all the computations, the maximum errors are insensitive to the changes in N.

Theoretically, for polynomials defined in an infinite domain, the integrals for α's and β's are evaluated in the entire domain. When numerical integration is applied, one has to truncate the domain into a finite one. If the truncated domain for the integration is
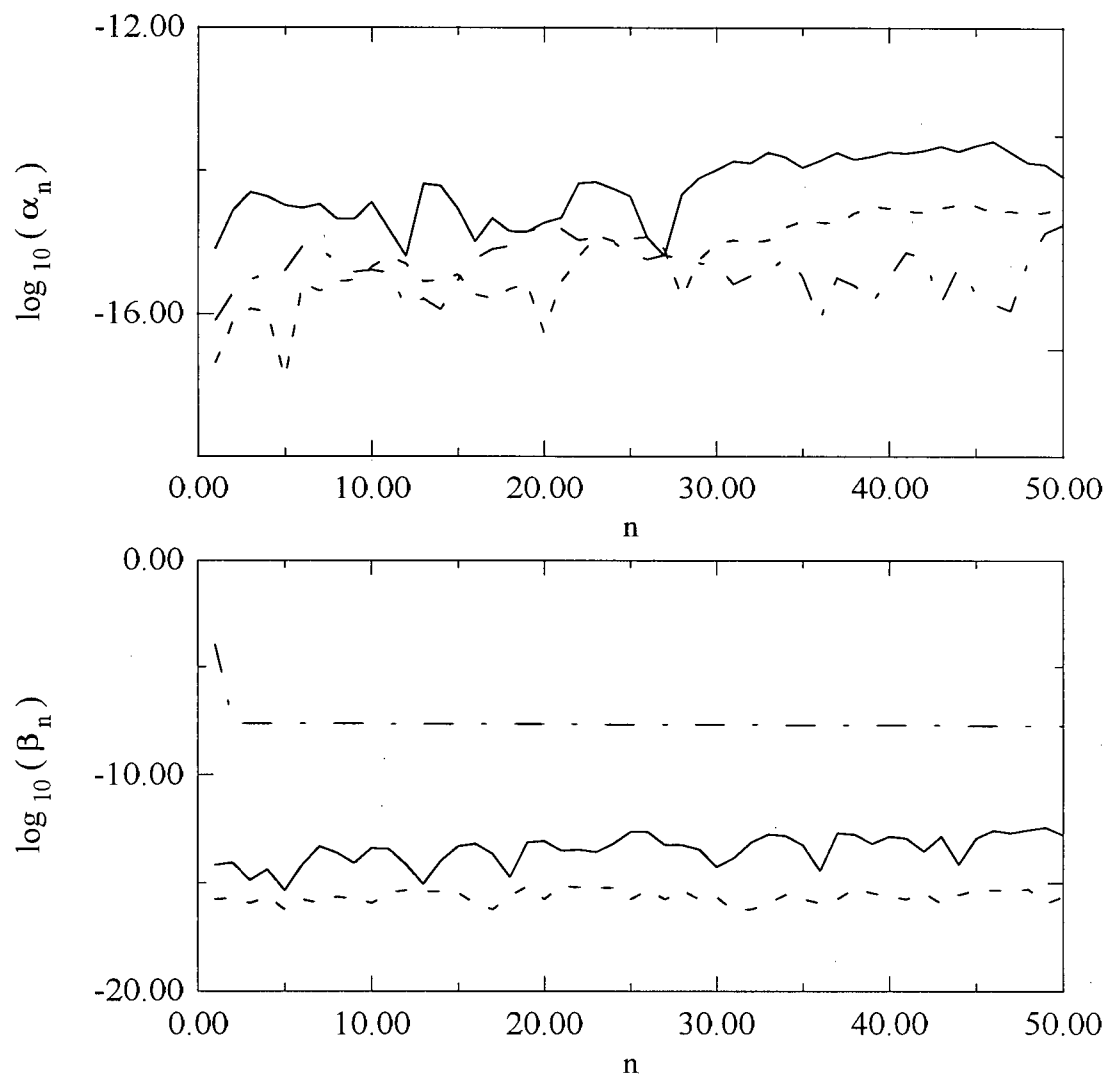
Figure 2.8: Errors in α_n and β_n calculated by the Stieltjes's procedure with N=50. The dash dotted curve is for Chebyshev polynomials, the dashed curve is for the Legendre polynomials and the solid curve is for the Hermite polynomials.

N	$E_{\alpha_n}^{\infty}$	$E_{\beta_n}^{\infty}$
	[-20, 20]	
5	4.996208974320000e-15	9.103828801930001e-15
10	4.996208974320000e-15	4.840572387370000e-14
50	2.609915956900000e-14	3.375077994860000e-13
70	5.530643324450000e-14	4.760636329590000e-13
90	5.530643324450000e-14	7.034373084020000e-13
100	5.530643324450000e-14	7.034373084020000e-13
	[-5, 5]	
5	2.346651055977530e-15	7.246219748680005e-06
10	1.263572315381132e-14	2.919377614958041e-02
50	3.598600987376839e-14	1.874888749856461e+01
100	8.320267776295266e-14	4.374979589455547e+01
	[-50, 50]	
5	6.658312592764631e-16	1.154631945610163e-14
10	1.382306109940420e-15	3.907985046680551e-14
50	1.895834758617558e-14	1.492139745096210e-13
70	3.565939958333915e-14	2.060573933704291e-13
>91	overflow	

Table 2.3: Maximum error in the numerical solution of α_n and β_n for the Hermite polynomials on three intervals [-20,20], [-5, 5] and [-50, 50].

too small, the truncation error for the integration is large and results in low accuracy for the calculation of α_n and β_n. If the domain is too large, the integrals can be very large and cause number overflow for the computer. Careful choice of domain cutoff for the numerical integration is therefore needed for the accuracy and stability of the results for the numerical calculation of α_n and β_n. The computer overflow in the integration of low degree polynomials is rare so that it is not necessary a worry if number of quadrature points required is not large. The error estimation of α_n and β_n for the Hermite polynomials calculated by Stieltjes's procedure with several choices of integration intervals are given in Table 2.3.

Calculation of quadrature points and weights

If the α_n and β_n for the recurrence relation are known, the quadrature points which are the roots of the Nth polynomial constructed from the recurrence can be calculated by diagonalizing the tri-diagonal matrix [136]

$$J = \begin{pmatrix} \alpha_0 & \sqrt{\beta_1} & 0 & \ldots & 0 & 0 \\ \sqrt{\beta_1} & \alpha_1 & \sqrt{\beta_2} & \ldots & 0 & 0 \\ 0 & \sqrt{\beta_2} & \alpha_2 & \ldots & 0 & 0 \\ \vdots & \vdots & \vdots & & & \\ 0 & 0 & 0 & \ldots & \alpha_{N-1} & \beta_{N-1} \\ 0 & 0 & 0 & \ldots & \beta_{N-1} & \alpha_N \end{pmatrix}. \tag{2.2.34}$$

The points are the eigenvalues of the matrix of J. The corresponding weights are given in the terms of the first component of the ith normalized eigenvector of the matrix J [136,134].

In Table 2.4 we give the points and weights of several previous cases studied in the above section. In order to study the effect of the error of the calculated α_n and β_n, we

N	E_{pt}^{∞}	E_{wt}^{∞}
	Chebyshev	
5	2.954894016793386e-05	7.806354429684692e-05
20	7.757441346845083e-06	2.321553559997414e-05
50	3.121430352637233e-06	9.635848417718917e-06
100	1.569879214957659e-06	4.898200317991069e-06
	Legendre	
5	2.220446049250313e-15	3.774758283725532e-15
50	1.415534356397075e-15	5.384581669432010e-15
100	3.885780586188049e-15	7.507883204027621e-15
	Hermite	
	[-20, 20]	
5	4.440892098500626e-15	1.032507412901395e-14
50	5.773159728050815e-14	1.271205363195804e-14
70	7.460698725481052e-14	1.068589661201713e-14
100	9.592326932761353e-14	1.276756478318930e-14
	[-5, 5]	
5	1.495381356519943e-07	5.903613908841976e-08
50	4.192398352706889e+00	5.962550119618734e-02
100	8.408353932924946e+00	8.056316459982088e-02
	[-50, 50]	
5	2.664535259100376e-15	2.109423746787797e-15
50	5.417888360170763e-14	5.828670879282073e-15
70	4.618527782440652e-14	5.190292640122607e-15

Table 2.4: Maximum error for the numerical approximation of points and weights.
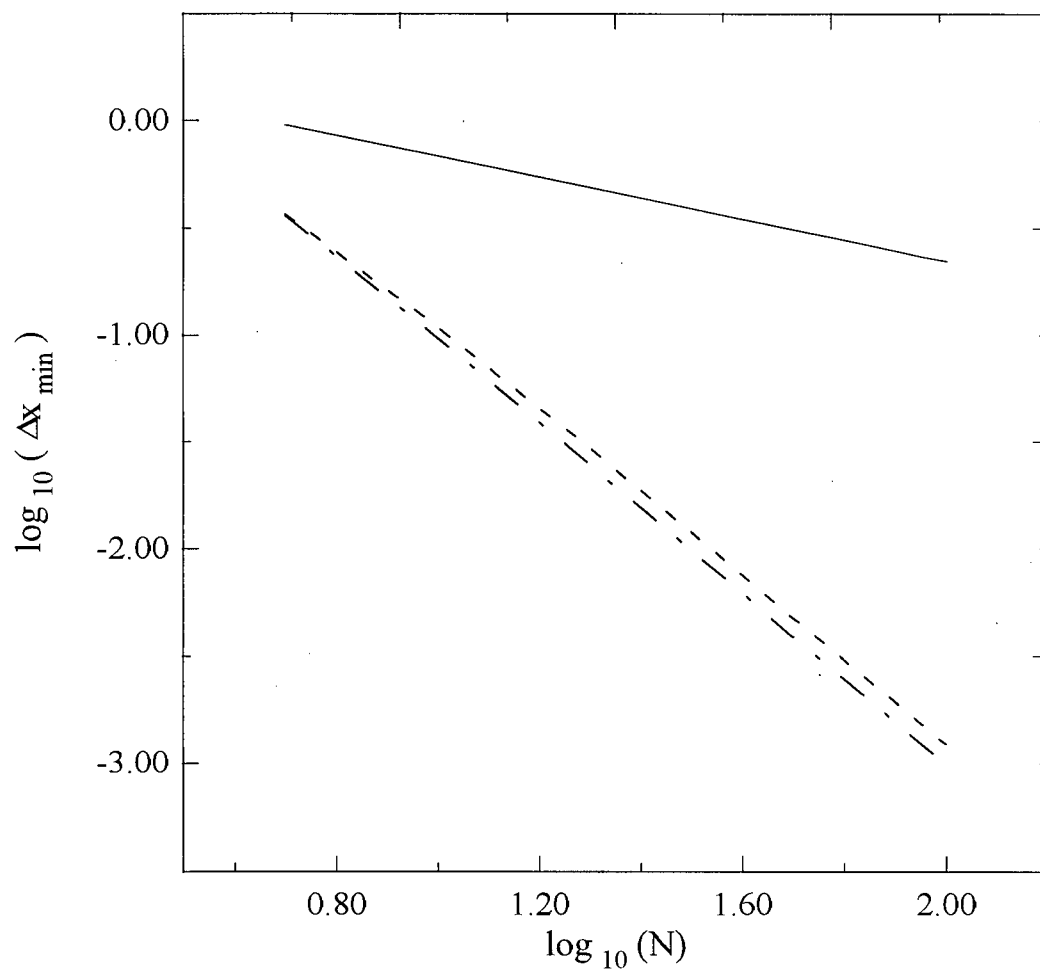
Figure 2.9: Minimum spacing of points versus number of quadrature points N. The dash dotted curve is for Chebyshev points; the dashed curve is for Legendre points and the solid curve is for Hermite points.

compare the results calculated directly from the exact α_n and β_n, as well as the exact points and weights where it is applicable.

The results from Table 2.4 show no sign of the extra error involved for the calculated points and weights except the error from the errors of α_n and β. If we can produce the recurrence coefficient accurately enough, the accuracy of the points and weights will not be affected.

The minimum spacing between adjacent quadrature points is plotted in Figure 2.9, The minimum spacing satisfies $\Delta_{min}x \approx 9.87/N^2$, $\Delta_{min}x \approx 12.2/N^2$, and $\Delta_{min}x \approx 2.22/\sqrt{N}$ for the Chebyshev, Legendre, and Hermite points, respectively. Again, the results show that the minimum spacing is decreased at rate of $O(1/N^2)$ for the Chebyshev and Legendre points and $O(1/\sqrt{N})$ for the Hermite points as number of quadrature points N increases.

2.3 Time integration

In most applications to the PDE, the spatial discretization uses the QDM but the temporal discretization uses conventional finite difference.

Consider a time dependent PDE

$$\frac{\partial u}{\partial t} = f(u, t) \quad t > 0, \tag{2.3.1}$$

where the general (linear or nonlinear) operator f contains the spatial part of the PDE. After discretizing the spatial operator by the QDM, the semi-discretized version of Eq. (2.3.1) becomes

$$\frac{dU}{dt} = F(U), \tag{2.3.2}$$

where $U(t)$ is the set of grid values of $u(x, t)$, F is the discretization representation of the operator f. In this section, we confine our discuss to the linearized version of (2.3.2),

i.e., we consider

$$\frac{dU}{dt} = LU, \tag{2.3.3}$$

where L is the matrix resulting from the linearization of (2.3.2).

If $F(U)$ is linear, i.e., $L = F$, and L is a diagonalizable matrix, we can solve Eq. (2.3.3) by eigenfunction expansion.

Eigenfunction expansion

The eigenvalue problem of Eq. (2.3.3) is defined by

$$L\phi_n(x) = -\epsilon_n\phi_n(x), \tag{2.3.4}$$

where ϵ_n are the eigenvalues and $\phi_n(x)$ are the eigenfunctions. The linear time-dependent equation, admits a solution of the form

$$u(x,t) = \sum_{n=0}^{\infty} c_n e^{-\epsilon_n t}\phi_n(x), \tag{2.3.5}$$

where the coefficients c_n are determined from the initial condition, $u(x,0)$, and are given by

$$c_n = \int u(x,0)\phi_n(x)dx. \tag{2.3.6}$$

In actual calculations, the solution $u(x,t)$ given by Eq. (2.3.5) must be truncated at $n = N$, and evaluated at quadrature points. It is essential that the lower eigenvalues and eigenfunctions converge accurately and rapidly in order to achieve a fast accurate approximation of the solution.

Since no numerical approximation involved in temporal variable t, the accuracy of the solution of Eq. (2.3.3) is of the same order as the numerical method applied to approximate the differential operator L. In the case that the eigenvalues are easy to calculate accurately and converge very fast, the eigenfunction expansion technique is a super choice

for the solution of the time dependent problem. The convergence could be difficult at small times depending on the choice of the initial condition. For most applications to solve time dependent problem, temporal discretization is a more popular approach.

Temporal discretization

Most temporal discretization uses a finite difference method. The eigenvalue spectrum of the discretization matrix in space determines the stability of the time-discretization. The region of the absolute stability of a numerical method is defined for the problem

$$\frac{dU}{dt} = \lambda U \qquad (2.3.7)$$

to be the set of all $\lambda \Delta t$ such that $\|U\|$ is bounded as $t \to \infty$. A method is called A-stable if the region of the absolute stability includes the region $Re\{\lambda \Delta t\} \leq 0$.

The most simple and popular schemes widely used in the applications are the first order forward Euler (FE) and backward Euler (BE) method, as well as the second order Crank-Nicolson (CN) method. The discretization formula for Eq. (2.3.3) of these methods are as following: for the forward Euler method,

$$U^{n+1} = U^n + \Delta t L^n. \qquad (2.3.8)$$

For the backward Euler method,

$$U^{n+1} = U^n + \Delta t L^{n+1}, \qquad (2.3.9)$$

and for the Crank-Nicolson method,

$$U^{n+1} = U^n + \frac{1}{2}\Delta t[L^{n+1} + L^n]. \qquad (2.3.10)$$

The FE method is an explicit method and the absolute stability region is $|1 + \lambda \Delta t| < 1$. If the eigenvalue λ is real, then $-2 < \lambda \Delta t < 0$. Both FE and CN are implicit methods and are A-stable, i.e. they are absolutely stable in the entire left-half plane.

N	QDM1	QDM2	QDM3	QDM4
4	7.08(-03)	3.11(-03)	9.26(-02)	9.62(-02)
6	1.59(-02)	4.47(-03)	9.26(-03)	1.18(-02)
8	5.25(-04)	1.99(-04)	4.01(-04)	6.10(-04)
10	2.66(-05)	5.43(-06)	1.04(-05)	1.85(-05)
12	4.43(-07)	9.86(-08)	1.84(-07)	3.75(-07)
14	8.77(-09)	1.29(-09)	2.36(-09)	5.43(-09)
16	8.59(-11)	1.28(-11)	2.31(-11)	5.90(-11)
20	1.20(-14)	4.44(-15)	3.48(-15)	6.78(-15)
25	4.95(-14)	7.35(-15)	1.05(-14)	1.23(-14)

Table 2.5: Standard error for the numerical approximation of $u'' = \sin(\pi x)$ for the four QDM methods.

The detailed discussion of these methods and other high order and more complicated numerical schemes are out of the scope of this thesis and can be found in standard references [1–6].

2.4 Numerical tests and results

In this section, we give three analytic examples to study the properties of the QDM.

2.4.1 One-dimensional Poisson equation

The first example we discuss is the one-dimensional Poisson problem in section 2.1 defined by Eq. (2.1.12). We compared the convergence of the solution of the Poisson problem between the classical Legendre method and a second order FD method. Since the intention of the QDM is to use nonclassical base functions, in this section we applied four nonclassical polynomial sets based on four weight functions. They are $w_1(x) = \sin^2(\pi x)$, $w_2(x) = e^{x^2}$, $w_3(x) = e^{-x^2}$, and $w_4(x) = 1 - x^2$. We refer to the QDM based on these weight functions as QDM1, QDM2, QDM3 and QDM4, respectively.

The standard errors of the numerical solution for the four methods are given in Table

2.5. All the methods work remarkly well and the rate of convergence is exponential. With 20 quadrature points, the numerical approximations of the solution is at least 14 digits accurate. The rate of convergence for the QDM competes well with that for the classical Legendre method and the method is much faster than the FD method (see Table 2.1). We also study the largest eigenvalue of the derivative operators based on the nonclassical QDM, the result is similar to the classical methods, that is, the largest eigenvalue of the first derivative matrix grows like $O(N^2)$ and of the second derivative matrix grows like $O(N^4)$.

2.4.2 An analytic example

In order to demonstrate the applicability of the QDM and some of its properties, we consider a time-dependent Fokker-Planck equation defined by

$$\frac{\partial}{\partial t} P(x,t) = \frac{\partial}{\partial x} [A(x)P(x,t)] + \frac{\partial^2}{\partial x^2} [B(x)P(x,t)], \tag{2.4.1}$$

where,

$$A(x) = \tanh(x)[1 + 2\text{sech}^2(x)]/4, \quad B(x) = \text{sech}^2(x)/2. \tag{2.4.2}$$

The physical interpretation of $P(x,t)$ is the probability density function. It is defined in $x \in (-\infty, \infty)$, and satisfies $P(\pm\infty, t){=}0$. With a δ-function initial condition at x_0, Eq. (2.4.1) has an analytic solution

$$P(x,t) = \frac{\cosh(x)}{\sqrt{4\pi(1-z^2)}} e^{-\frac{[\sinh(x)-\sinh(x_0)z]^2}{4(1-z^2)}}, \tag{2.4.3}$$

where $z = e^{-1/4}$. The equilibrium solution as $t \to \infty$ is given by

$$P_0(x) = \frac{cosh(x)}{\sqrt{4\pi}} e^{-\sinh(x)^2/4}. \tag{2.4.4}$$

If we set $P(x,t) = P_0(x)g(x,t)$, then the equation for $g(x,t)$ is given by,

$$\begin{aligned} \frac{\partial g(x,t)}{\partial t} &= -A(x)\frac{\partial g(x,t)}{\partial x} + B(x)\frac{\partial^2 g(x,t)}{\partial x^2} \\ &= -\mathbf{L}g(x,t), \end{aligned} \tag{2.4.5}$$

It is easily shown that the operator $\mathbf{L}$ is self-adjoint with respect to the equilibrium solution $P_0(x)$.

1. *Eigenvalue problem.*

First, we consider the eigenvalue problem of Eq. (2.4.5):

$$-\mathbf{L}\phi_n(x) = [-A(x)\frac{\partial}{\partial dx}) + B(x)\frac{\partial^2}{\partial x^2}]\phi_n(x) = -\lambda_n\phi_n(x), \qquad (2.4.6)$$

where λ_n and ϕ_n are the eigenvalues and eigenfunctions, respectively. The exact eigenvalues of Eq. (2.4.6) are

$$\lambda_n = n/4, \quad n = 0, 1, 2, ... \qquad (2.4.7)$$

Three set of polynomials are applied in the QDM to solve the eigenvalue problem Eq. (2.4.6). They are scaled Legendre polynomials with weight function $w_1(x) = 1$ in a finite interval, scaled Hermite polynomials with weight function $w(x) = e^{-4x^2}$, and nonclassical polynomials with weight function $w(x) = P_0(x)$. We refer to the methods based on these polynomials as Legendre, Hermite, and QDM, respectively.

The discretization matrix $\mathbf{L_N}$ of the differential operator in Eq. (2.4.4) is in the form

$$-\mathbf{L_N} = -\mathbf{A}\boldsymbol{\Delta} + \mathbf{B}\boldsymbol{\Delta}^2 \qquad (2.4.8)$$

where, $\mathbf{A}$ and $\mathbf{B}$ are the diagonal coefficient matrices of $A(x)$ and $B(x)$, $\boldsymbol{\Delta}$ is the derivative matrix with its entries defined in Eq. (2.2.11).

If we use the equilibrium solution $P_0(x)$ as weight function, the Galerkin matrix $\tilde{\mathbf{L}}_{\mathbf{N}}$ of the operator $\mathbf{L}$ can be obtained in a simple form

$$\tilde{\mathbf{L}}_{\mathbf{N}} = \mathbf{B}\mathbf{D}\mathbf{D}^{\mathbf{T}}, \qquad (2.4.9)$$

where $\mathbf{D}$ is the modified QDM derivative matrix with its elements defined in Eq. (2.2.18). The detailed derivation of the matrix is given in Chapter 3. We refer this approach of

N	λ_1	λ_5	λ_{10}	λ_{15}	λ_{20}
Exact	0.25	1.25	2.5	3.75	5.0
Error					
			Hermite		
4	.218(-01)				
6	.123(-02)	.465(+01)			
10	.592(-06)	.524(+00)	.186(+02)		
15	.205(-12)	.682(-02)	.278(+01)	.319(+02)	
20	.104(-13)	.889(-04)	.126(+00)	.616E+01	.458(+02)
25	.905(-14)	.146(-07)	.504(-01)	.654(+00)	.103(+02)
30	.133(-13)	.184(-08)	.192(-01)	.919(+00)	.171(+01)
40	.508(-13)	.389(-12)	.681(-04)	.574(+00)	.168(+01)
50	.143(-13)	.913(-13)	.777(-07)	.285(+00)	.141(+01)
			QDM		
4	.205(-02)				
6	.467(-04)	.204(+00)			
10	.530(-08)	.242(-02)	.576(+01)		
15	.722(-15)	.308(-05)	.282(+00)	.124(+02)	
20	.999(-15)	.212(-07)	.104(-01)	.140(+01)	.213(+02)
25	.000(+00)	.206(-11)	.506(-04)	.230(+00)	.358(+02)
30	.666(-15)	.422(-14)	.453(-07)	.152(-01)	.100(+01)
40	.555(-15)	.666(-14)	.151(-13)	.767(-06)	.227(-01)
50	.355(-14)	.000(+00)	.444(-14)	.439(-12)	.577(-05)
			MQDM		
4	.154(-03)				
6	.257(-05)	.388(+00)			
10	.347(-07)	.216(-01)	.306(+01)		
15	.158E-08)	.180(-06)	.408(+00)	.808(+01)	
20	.140(-11)	.999(-09)	.447(-02)	.151(+01)	.153(+02)
25	.934(-13)	.107(-11)	.193(-03)	.402(-02)	.369(+01)
30	.433(-14)	.102(-13)	.163(-07)	.315(-01)	.559(+00)
40	.278(-15)	.666(-15)	.431(-13)	.312(-05)	.759(-02)
50	.472(-14)	.688(-14)	.160(-13)	.276(-11)	.240(-05)

Table 2.6: Numerical error in the eigenvalues of the analytic example for the Hermite and QDM methods.

N	λ_1	λ_5	λ_{10}	λ_{15}	λ_{20}
Exact	0.25	1.25	2.5	3.75	5.0
Error					
			Legendre[a]		
4	.295(-02)				
6	.102(-03)	.500(+00)			
10	.143(-06)	.230(+00)	.845(+01)		
15	.105(-11)	.192(-01)	.259(+01)	.207(+02)	
20	.156(-13)	.140(-02)	.978(+00)	.823(+01)	.386(+02)
25	.354(-10)	.125(-04)	.395(+00)	.453(+01)	.174(+02)
30	.491(-08)	.242(-06)	.854(-01)	.268(+01)	.113(+02)
40	.462(-04)	.691(-03)	.128(-02)	.672(+00)	.466(+02)
50	.414(+00)	.341(+00)	.583(+00)	.523(+00)	.137(+01)
			Legendre[b]		
4	.250(-01)				
6	.262(-02)	.761(+00)			
10	.468(-06)	.292(+00)	.186(+01)		
15	.200(-12)	.568(-01)	.928(+00)	.606(+01)	
20	.247(-14)	.566(-05)	.424(+00)	.128(+01)	.127(+02)
25	.164(-14)	.143(-07)	.656(-01)	.796(+00)	.118(+02)
30	.239(-14)	.770(-11)	.199(-03)	.845(-02)	.511(+01)
40	.711(-14)	.134(-12)	.128(-09)	.109(-03)	.440(-00)
50	.799(-14)	.222(-12)	.695(-12)	.102(-05)	.728(-00)
			Legendre[c]		
4	.105(+00)				
6	.313(-01)	.901(+00)			
10	.297(-04)	.739(+00)	.255(+00)		
15	.137(-09)	.494(+00)	.168(+01)	.133(+01)	
20	.927(-14)	.314(+00)	.139(+01)	.257(+01)	.424(+01)
25	.255(-14)	.465(-01)	.109(+01)	.229(+01)	.343(+01)
30	.555(-14)	.942(-05)	.916(+00)	.194(+01)	.317(+01)
40	.389(-15)	.443(-11)	.388(+00)	.135(+01)	.250(+01)
50	.178(-14)	.254(-10)	.216(-05)	.841(+00)	.183(+01)

Legendre points in [a] (-2,2); [b] (-3,3); [c] (-4,4).

Table 2.7: Numerical error in the eigenvalues of the analytic example for the Legendre method.

discretization as modified QDM (MQDM). The main advantage of using the MQDM representation is that the differential matrix is simple to construct. The matrix representative is symmetric and the eigenvalues are all real.

The matrix representations in Eq. (2.4.8) and Eq. (2.4.9) are diagonalized to give the approximate eigenvalues and eigenfunctions. The convergence of the eigenvalue λ_1, λ_5, λ_{10}, λ_{15}, and λ_{20} is shown in Table 2.6 and 2.7 for each method. The exact eigenvalues are given in the top of the tables. Table 2.6 compares the errors of these eigenvalues calculated by the Hermite, QDM and MQDM. As we can see from the table, QDM and MQDM give relatively the same rate of convergence for most eigenvalues, and the error of eigenvalues decays very fast. As N increases, the convergence of the first eigenvalue λ_1 for the MQDM is slightly slower than that for the QDM. To obtain 14 decimal places accuracy of λ_1 it requires $N = 30$ points for the MQDM in comparison with $N = 15$ points for the QDM. The Hermite method calculates small eigenvalues (e.g. λ_1, λ_5) very well but the results for the larger eigenvalues (e.g. λ_{15}, λ_{20}) are not as good. The eigenvalue λ_{20} is only accurate to $O(1)$ for the Hermite method with $N = 50$ in comparison with $O(10^{-5})$ for the QDM and MQDM.

For the QDM, the points spread over the interval $(-\infty, \infty)$. As N increases, the domain is getting larger. Since we use the equilibrium function $P_0(x)$ as the weight function, the resulting domain reflects the natural property of the solution. At the boundary points, the rate of decay of the the solution is the same as the exact solution. We may refer to this domain as natural domain of the problem. With the same number of quadrature points on a larger domain, some points are beyond the natural domain and can not contribute to improve the accuracy. Therefore the rate of convergence is expected to be slower. If the domain is much smaller than the natural domain, the boundary condition may not be accurately applied, which results in low accuracy in the solution. Therefore, choosing the weight function is very crucial for the convergence of
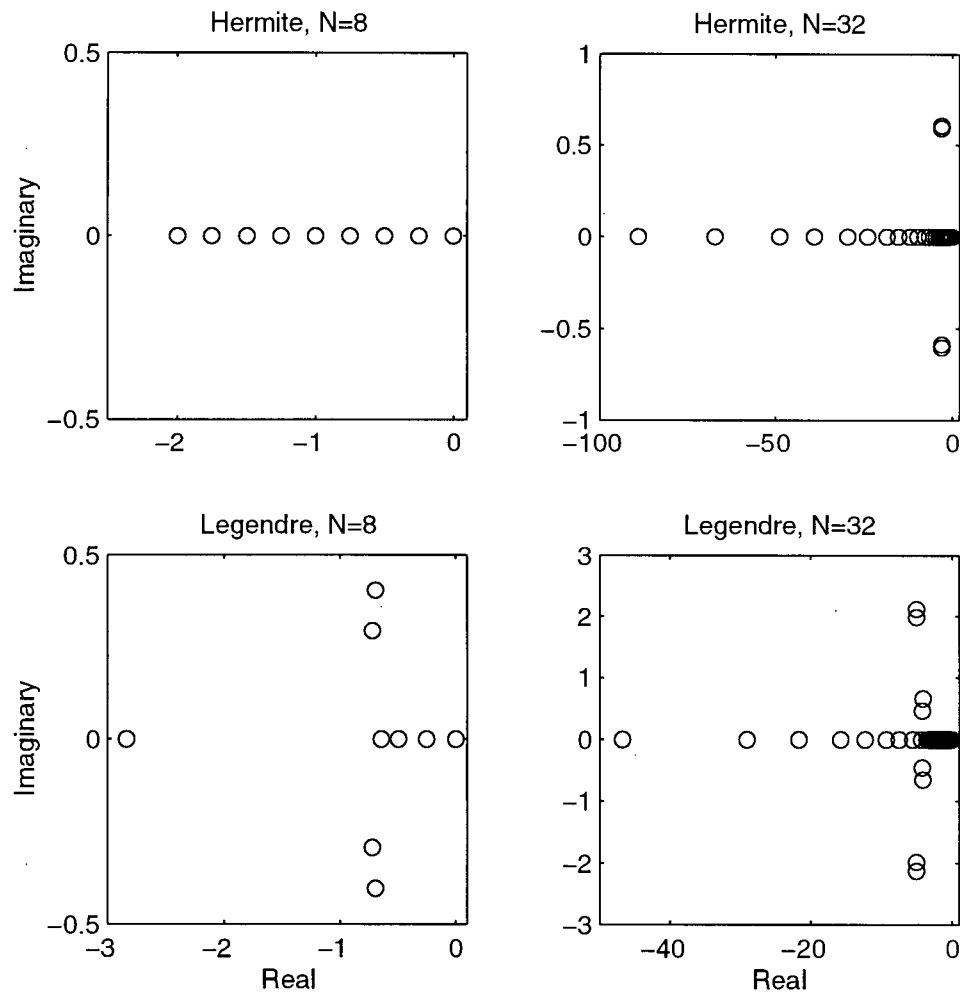
Figure 2.10: Numerical approximation of the eigenvalues for the analytic FPE problem.

N	QDM	Hemite
4	(-1.834, 1.834)	(-1.010, 1.010)
6	(-2.077, 2.077)	(-1.326, 1.326)
10	(-2.375, 2.375)	(-1.834, 1.834)
15	(-2.605, 2.605)	(-2.344, 2.344)
20	(-2.764, 2.764)	(-2.775, 2.775)
25	(-2.885, 2.885)	(-3.155, 3.155)
30	(-2.983, 2.983)	(-3.498, 3.498)
40	(-3.136, 3.136)	(-4.106, 4.106)
50	(-3.252, 3.252)	(-4.632, 4.632)

Table 2.8: Domain generated from the QDM and Hermite weight function for the analytic FPE example.

the solution. We will discuss more about the choice of the weight function in Chapter 3 and Chapter 4. Table 2.8 gives the domains for the QDM and Hermite method versus number of grid.

To apply the Legendre points, one has to truncate the infinite domain $(-\infty, \infty)$ into a finite domain $(-c, c)$. Table 2.7 gives the numerical error of these eigenvalues calculated by Legendre method in the intervals a: (-2,2), b: (-3,3), and c: (-4,4), respectively. We refer to the above three Legendre methods as Legendre^a, Legendre^b and Legendre^c method, respectively. As we can see from the table, the Legendre^b method on interval (-3,3) is the best among the three Legendre methods. As N increase, the error of the eigenvalues calculated by the Legendre^a method decays initially, and then increase. This is because the truncated domain is too small, and with N increasing, the truncation error caused by the boundary cut off accumulates and is getting larger and larger. The Legendre^c method is in general slower than Legendre^b method, since the domain (-4,4) is wider than it requires and some points near the boundary are not contributing. In comparison with the QDM and MQDM, the convergence of the Legendre^b method is

slower, especially for the large eigenvalues, but it is better than the Hermite method.

For the Hermite and Legendre methods, some of the eigenvalues of the differential matrices are imaginary as shown in Fig. 2.10 with $N = 8$ and $N = 32$. For the QDM and MQDM, all the eigenvalues are real. This property is obviously important with regard to CPU time and memory, especially for higher dimensional problems.

Fig. 2.11 compares the largest eigenvalues of the differential matrix versus number of quadrature points for each method. The largest eigenvalue grows like $O(N^{1.76})$ for the QDM, $O(N^{1.85})$ for the MQDM, $O(N^{1.2})$ for the Hermite, and $O(N^2)$ for the Legendre method as N increases ($N < 100$). It worth to point out that, although the largest eigenvalue of the second derivative matrix for the Legendre method grows at much faster pace ($O(N^4)$), this property is not shown in this application.

2. *Time dependent solution*

We intend to solve the Eq. (2.4.1) with a δ-function at x_0 as initial condition. The application of the eigenvalue expansion stated in section 2.3 in the solution the the time-dependent problem with x_0 chosen as one of the quadrature points is straight forward. In this section our interest is to apply the temporal propagation techniques such as forward Euler or/and backward Euler method to solve the time-dependent the FPE problem. We set $x_0 = 1$. Since it is very hard to discretize the δ-function numerically based on the quadrature points, in order to compare the numerical result with the exact solution, we use the exact solution at time t=1 as the initial distribution. Both forward and backward Euler are used to solve the problem. Since the real part of the eigenvalues are all negative for the QDM, Hermite and Legendre differential matrices, backward Euler method is always stable, the choice of the time step is depended on the accuracy requirement of the solution. For the forward Euler method, the time step Δt has to satisfy the condition $\Delta t < 2/\lambda_{max}$, where λ_{max} is the largest eigenvalue of the differential
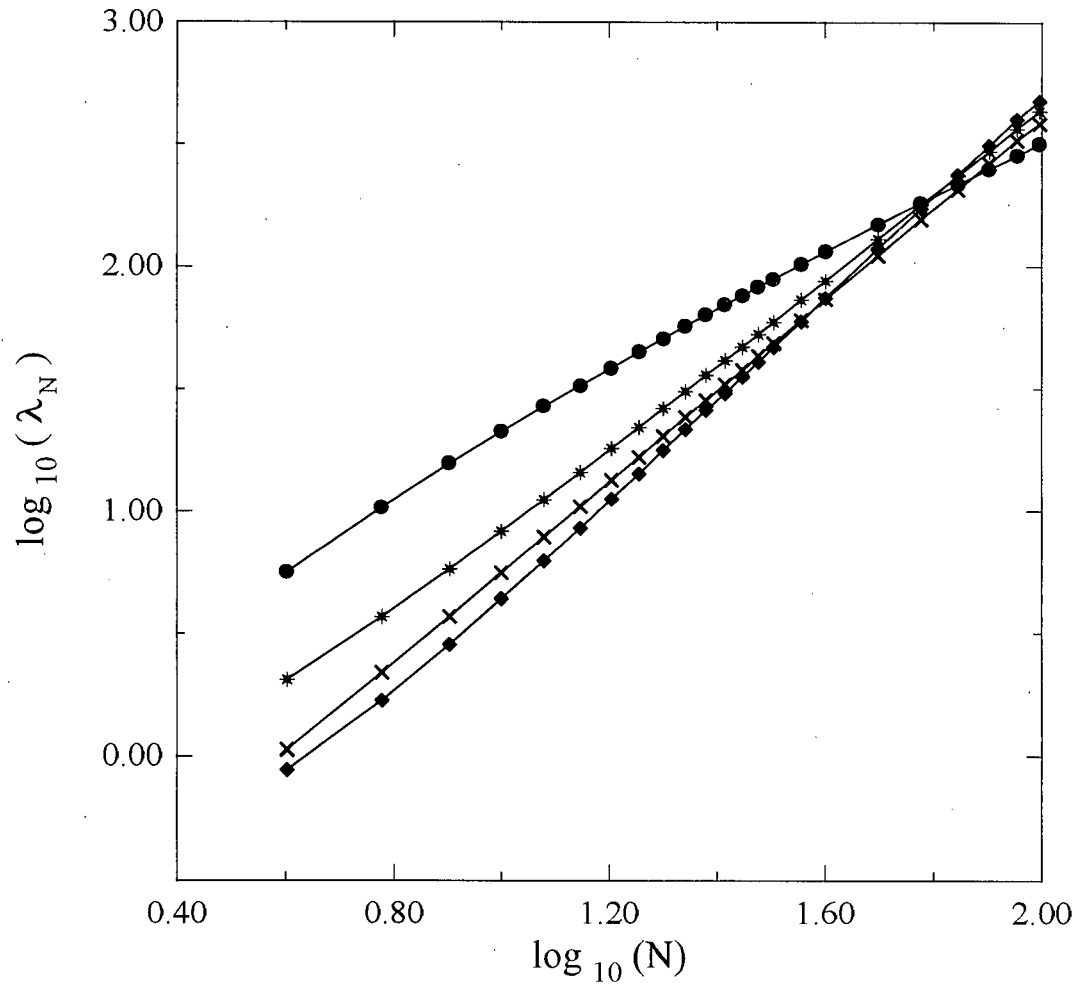
Figure 2.11: Largest numerical eigenvalues for the analytic FPE example. The results with the QDM, MQDM, Hermite and Legendre are denoted by solid lined with asterisks, crosses, solid circles and diamonds, respectively.

N	QDM	Hermite	Legendre
10	0.24	0.094	0.45
15	0.12	0.056	0.20
20	0.075	0.039	0.11
25	0.051	0.030	0.071
30	0.037	0.024	0.048
35	0.028	0.020	0.035
40	0.022	0.017	0.026
50	0.015	0.013	0.016
60	0.011	0.010	0.011
70	0.0085	0.0093	0.0084
80	0.0067	0.0079	0.0063
90	0.0054	0.0070	0.0050

Table 2.9: Maximum time step in the FE time integration.

matrix. Table 2.9 gives the maximum time step for the forward Euler method for the QDM, Hermite and Legendre differential matrix.

The numerical solution of Eq. (2.4.1) solved by the forward Euler method with $\Delta t = 0.01$ is given in Fig. 2.12 and Fig. 2.13 with $N = 6$ and $N = 15$ quadrature points respectively. In the figures, the solid line is the exact solution. As we can see from Fig. 2.12, with only six quadrature points, the QDM approximates the exact solution very well. Among the three discretization methods in spatial dimension, the QDM approximation is the best. The Legendre method is better than the Hermite method, but still a little bit off the exact solution. Hermite method approximate poorly to the exact solution for large times. With increasing number of quadrature points to $N = 15$ (Fig. 13), all the numerical approximations can not distinguish from the exact solution in the figure.

3. An equivalent problem

If we make a simple change of variable $y = \frac{1}{2}\sinh x$ and let $\tilde{P}(y,t) = \frac{1}{2}\cosh x P(x,t)$
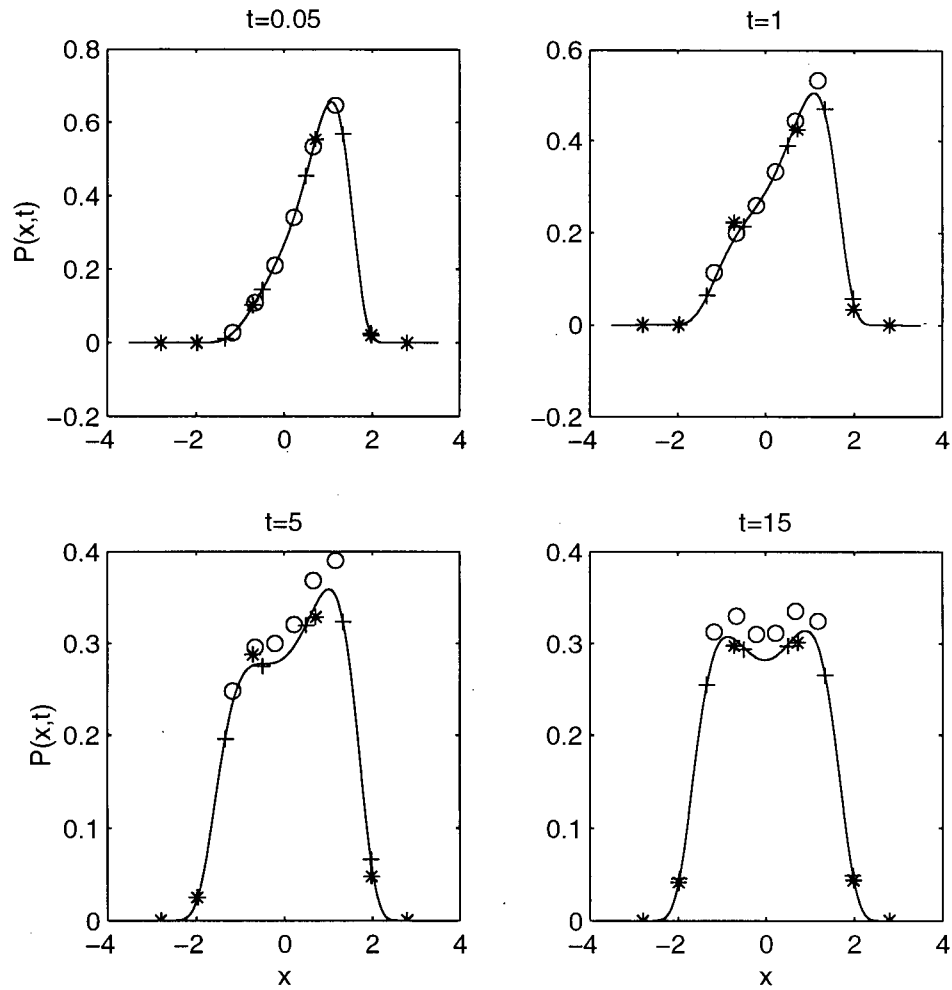
Figure 2.12: Numerical solution of the time dependent FPE with $N = 6$. The solid lines are the exact solution. The plus signs are the results with the QDM, the asterisks are the result for the Legendre method and the circles are the results with the Hermite method.
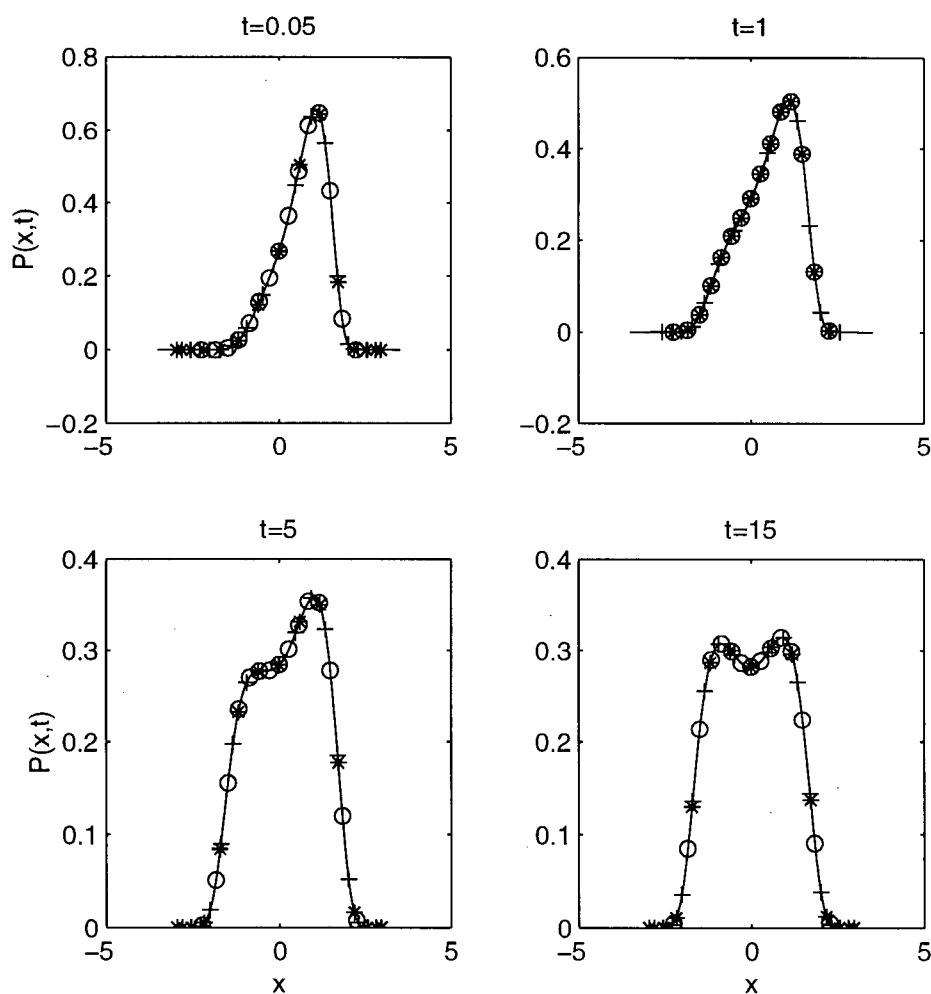
Figure 2.13: Numerical solution of the time dependent FPE with $N = 15$. The solid lines are the exact solution. The plus signs are the results with the QDM, the asterisks are the result for the Legendre method and the circles are the results with the Hermite method.

in Eq. (2.4.1) and (2.4.2), one finds the equation,

$$\frac{\partial \tilde{P}(y,t)}{\partial t} = \frac{1}{4} \Big[\frac{\partial \tilde{P}(y,t)}{\partial y} + \frac{1}{2} \frac{\partial \tilde{P}^2(y,t)}{\partial y^2} \Big]. \tag{2.4.10}$$

The equilibrium solution of this equation is

$$\tilde{P}_0(y) = \frac{1}{\sqrt{\pi}} e^{-y^2}, \tag{2.4.11}$$

which is the weight function for Hermite polynomials. If we set $\tilde{P}(y,t) = \tilde{P}_0(y)\tilde{g}(y,t)$, we obtain the self-joint equation of $\tilde{g}(y,t)$

$$\frac{\partial \tilde{P}(y,t)}{\partial t} = -\frac{1}{4} \frac{\partial \tilde{P}(y,t)}{\partial y} + \frac{1}{8} \frac{\partial \tilde{P}^2(y,t)}{\partial y^2}. \tag{2.4.12}$$

The eigenvalues of its eigen-problem are $n/4, (n = 0, 1, ..., N)$ and the eigenfunctions are the normalized Hermite polynomials $H_n(y)$. We solve the eigen-problem numerically by the QDM and MQDM with $w(y) = \tilde{P}_0(y)$ and Legendre methods in the interval (-6,6). Since the eigenfunctions are polynomials, we expect accurate results in numerical approximations. Table 2.10 gives the convergence of the eigenvalues for the three methods. For the QDM and MQDM, the solutions are exact. While for the Legendre method, the eigenvalues are exact for small N and the error is getting larger with increasing N after a certain level of N. The poor approximations are a result of the domain cutoff for the Legendre method. Furthermore we should point out that, the Galerkin matrix in transform space (see Eq. (3.2.12), Chapter 3 for detail) is diagonal with the Hermite polynomials as basis set. The diagonal elements are the eigenvalues of the eigen-problem of Eq. (2.4.12). The eigenfunction matrix is the transform matrix defined in Eq. (2.2.15).

In comparison with the current eigen-problem, the convergence of the eigenvalues of the eigen-problem Eq. (2.4.6) is much slower because the eigenfunctions of the problem are not polynomials.

Since the QDM and MQDM are exact for the problem, it is easy to know that the largest eigenvalue is $O(N)$. For the Legendre method we applied, the largest eigenvalue

N	domain	λ_1	λ_5	λ_{10}	λ_{15}	λ_{20}
		Exact				
		0.25	1.25	2.5	3.75	5.0
		Error				
		Hermite				
4	(-2.020, 2.020)	.555(-16)				
10	(-3.668, 3.668)	.222(-15)	.222(-15)	.111(-13)		
20	(-5.550, 5.550)	.111(-14)	.266(-14)	.311(-14)	.755(-14)	.109(-12)
30	(-6.996, 6.996)	.178(-14)	.155(-14)	.666(-14)	.933(-14)	.400(-13)
40	(-8.213, 8.213)	.888(-15)	.799(-14)	.933(-14)	.933(-14)	.320(-13)
50	(-9.284, 9.284)	.355(-14)	.666(-15)	.266(-14)	.355(-14)	.258(-13)
70	(-11.14, 11.14)	.160(-13)	.622(-14)	.311(-14)	.444(-14)	.977(-14)
90	(-12.74, 12.74)	.738(-14)	.533(-14)	.191(-13)	.933(-14)	.888(-15)
		Legendre				
4	(-6, 6)	.111(-15)				
10		.222(-15)	.205(-12)	.129(-11)		
20		.833(-15)	.566(-12)	.183(-09)	.141(-09)	.768(-10)
30		.350(-14)	.169(-12)	.133(-09)	.317(-08)	.549(-07)
40		.173(-13)	.187(-12)	.223(-09)	.647(-08)	.342(-06)
50		.533(-14)	.571(-13)	.127(-10)	.331(-07)	.128(-05)
70		.279(-13)	.400(-09)	.250(+00)	.496(+00)	.994(+00)
90		.192(-13)	.240(+01)	.449(+01)	.100(+01)	.979(+00)

Table 2.10: Comparison of the numerical error of the eigenvalues of Eq. (2.4.12) for the Hermite and the Legendre methods.

is marginally $O(N)$. One should notice that the largest eigenvalue approximated by the Legendre method for this problem is much smaller than the largest eigenvalue of the second derivatives (which is $O(N^4)$). It occurs to us that the condition of a differential matrix is related to both differential operator and boundary conditions. It doesn't have to be of the same order as of the highest derivative in the differential operator.

For the time integration by the explicit forward Euler method, the time step restriction should be $O(N^{-1})$.

As we recall the maximum time step is around $O(N^2)$ for the time integration for the solution of Eq. (4.2.1) and (4.2.2).

For the above examples, it is interesting to point out that although the condition number (or the largest eigenvalue) of the first and second derivative matrices depends on the minimum spacing of the grid as we discussed previously, it doesn't seem true for the differential operator. For the Legendre points, the minimum spacing is $O(N^2)$, and the condition number of the second derivative matrix is $O(N^4)$. However, the condition numbers of the differential matrix representatives for the above examples are $O(N^2)$ and $O(N)$, respectively.

2.4.3 Three-dimensional Poisson problems

In one dimensional examples, we already show that the QDM provides very high accuracy and fast convergence in the solution of differential equations. In comparison with the FD method, the QDM usually requires much coarser grid of points for the solution to converge to the same accuracy. This indicates a great advantage of the QDM in solving high dimensional problems. Our interest in this section is to solve the three dimensional Poisson equation of the form,

$$\frac{\partial^2 u}{\partial x^2} + \frac{\partial^2 u}{\partial x^2} + \frac{\partial^2 u}{\partial x^2} = f(x, y, z), \qquad (2.4.13)$$

	$f(x, y, z)$	Boundary Condition	$u(x, y, z)$
A	$3e^{(x+y+z)}$	exact solution	$e^{(x+y+z)}$
B	$-20\pi^2\phi(x,y,z)^* + \sin(4\pi x)\sin(2\pi y)a(z)^*$	$u\|_{BC} = 0$	$\phi(x,y,z)^*$

* $\phi(x,y,z) = \sin(4\pi x)\sin(2\pi y)[1 - e^{-5(z^2-1)}]$, $a(z) = 10(1 - 10z^2)e^{-5(z^2-1)}$.

Table 2.11: Examples of Poisson problems

subject to Dirichlet boundary conditions. The specific examples in Table 2.11 are considered.

Numerical solution of example A is calculated by a second order central differencing FD method and the QDM on a IBM RS6000 computer. Two set of polynomials are applied in the QDM. One is the classical Chebyshev polynomials. Since the main intention of the QDM is to use nonclassical polynomial basis set, we also applied a set of nonclassical polynomials associated with an arbitrary weight function $w(x) = e^{6x^2}$. For convenience, we use the same set of polynomials and the same number of grid points in each dimension. As we will see later in Chapter 4, sometimes it is necessary to use different grids in different dimension in order to obtain superior convergence of the solution.

The standard errors (E_2) of the solution and the CPU time of the calculation for each numerical method are given in Table 2.12. In the table, N is the number of grid points. For the QDM with nonclassical polynomials, the first CPU time is for the calculation of the points and the QDM derivative matrix associated with the weight function $w(x) = e^{6x^2}$. The second CPU time is for solving the discretized algebraic equation. As seen from the table, the error of the solution calculated with the FD method decays at the rate

FD			Chebyshev			QDM			
N	E_2	CPU	N	E_2	CPU	N	E_2	CPU1	CPU2
4	.754(-2)	0.01s	4	.486(-3)	0.01s	4	.113(-2)	1.72s	0.00s
10	.143(-2)	0.03s	6	.263(-5)	0.03s	6	.882(-5)	1.76s	0.00s
20	.366(-3)	0.39s	8	.731(-8)	0.05s	8	.254(-7)	1.77s	0.01s
30	.163(-3)	1.99s	10	.136(-10)	0.10s	10	.478(-10)	1.81s	0.03s
40	.920(-4)	6.75s	12	.122(-12)	0.21s	12	.145(-12)	1.83s	0.08s
50	.589(-4)	16.5s	16	.522(-13)	0.50s	16	.631(-13)	1.86s	0.15s
70	.300(-4)	61.1s							
90	.182(-4)	182.s							

Table 2.12: Standard Error and CPU time for the numerical approximations of example A of the Poisson problems.

of $O(1/N^2)$ as N increases, whereas the error of the solution calculated with the QDM decays at a much faster rate. With $N = 10$, or $10 \times 10 \times 10$ grid, $E2 = 0.136 \times 10^{-10}$ for the Chebyshev approximation, and $E_2 = 0.478 \times 10^{-10}$ for the QDM. For the FD method, $E_2 = 0.589 \times 10^{-4}$ with $N = 50$, or $50 \times 50 \times 50$ grid. To achieve accuracy of $O(10^{-12})$, only a $12 \times 12 \times 12$ grid is needed, and it costs less than a second for both QDM and Chebyshev method. However, for the FD method, with $90 \times 90 \times 90$ grid, it takes about 3 minutes and one can only obtain accuracy of $O(10^{-4})$. Comparing the CPU time, the QDM is much faster than the FD method if the same accuracy of the solution is required.

Although the FD method performs relatively poorly in the calculation of Example A in comparison with the QDM, the result calculated by it is still acceptable. In some cases, the FD method may fail while the QDM can do very well. To show this point, we studied example B of the Poisson problems described in Table 2.11. Fig. 2.14 plots the exact solution of this problem at $z = 0$, i.e., $u(x, y, 0) = (1 - e^5) \sin(4\pi x) \sin(2\pi y)$. As seen in the figure, the solution of the problem is highly oscillated in x and y dimensions. The Poisson problem is solved by the three methods used in Example A. Fig. 2.15 shows the

N	FD		Chebyshev		QDM	
	E_2	CPU	E_2	CPU	E_2	CPU
10	.218(02)	0.04s	.154(02)	0.06s	.272(02)	1.77s
16	.732(01)	0.19s	.121(00)	0.18s	.375(00)	1.89s
20	.452(01)	0.44s	.144(-02)	0.44s	.492(-02)	2.33s
26	.261(01)	1.19s	.449(-06)	1.18s	.186(-05)	3.22s
30	.194(01)	2.20s	.947(-09)	2.07s	.460(-08)	4.19s
34	.150(01)	3.67s	.137(-11)	3.49s	.719(-11)	5.59s
40	.108(01)	7.15s	.267(-12)	6.73s	.849(-12)	8.94s
50	.688(00)	17.4s				
70	.349(00)	36.5s				
90	.211(00)	118.s				

Table 2.13: Comparison of the standard Error E_2 and CPU times for the three numerical approximations of example B of the Poisson problems.

standard error of the numerical solution versus $log_{10}N$ for the three numerical methods. The comparison of errors is given in Table 2.13.

The results indicate that the numerical solution calculated by the FD method converges very slowly. Even with a $90 \times 90 \times 90$ grid, the FD solution barely reaches 1 decimal place accuracy. While for the Chebyshev method and the QDM, the numerical solution can achieve 11 decimal place accuracy with $40 \times 40 \times 40$ grid.

For both examples, it is evident that the QDM based on nonclassical polynomials competes well with the traditional Chebyshev method in the accuracy and convergence of the solution of PDEs.
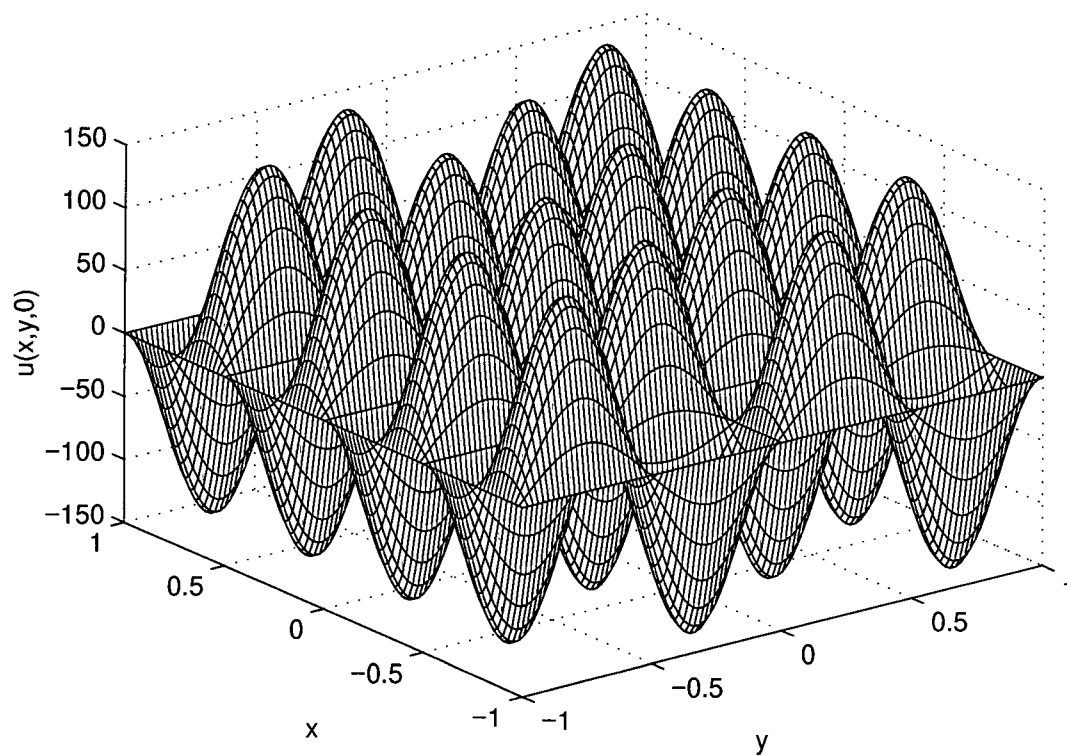
Figure 2.14: Exact solution for example B at $z = 0$.
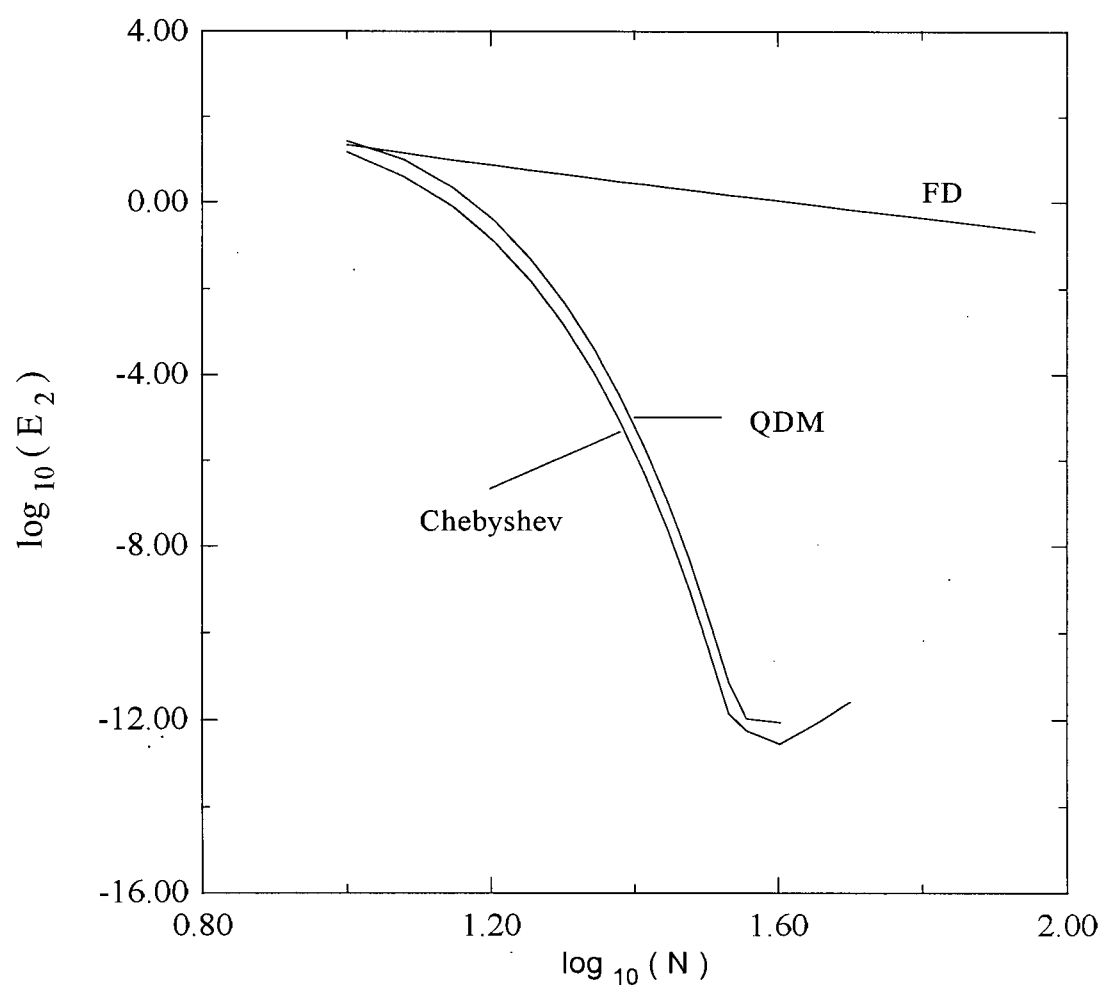
Figure 2.15: Standard error of the solution for example B.

Chapter 3

Applications of the QDM to the Solution of Fokker-Planck Equation

3.1 Introduction

The Fokker-Planck equation was introduced by *Fokker* and *Planck* to describe the Brownian motion of particles [76,77]. For the past several decades, there has been an ongoing interest by numerous researchers in the description of nonequilibrium phenomena modeled with a Fokker-Planck equation (FPE). This interest continues unabated to the present date [78] - [91]. The basis for many of these models is the Brownian diffusion in a potential characterized by Gaussian white noise. This leads to a time dependent linear FPE with drift and diffusion coefficients which can be nonlinear functions of the independent variable of interest. The theoretical basis for this approach has been provided in several standard references [92] - [94]. A general Fokker-Planck equation in one dimension is of the form

$$\frac{\partial P(x,t)}{\partial t} = \frac{\partial A(x)P(x,t)}{\partial x} + \frac{\partial^2 B(x)P(x,t)}{\partial^2 x}. \tag{3.1.1}$$

where $P(x,t)$ is related to probability density function of x and $A(x)$ and $B(x) > 0$ are referred to as the drift and diffusion coefficients, and depend on the particular application considered. The detail of the derivation of the Fokker-Planck equation can be found in the book by Risken [93].

The main objective in many of studies in Fokker Planck equation is the approach of some initial probability density function (PDF) to equilibrium, which in some applications may be characterized by two or more stable states. Examples of systems

studied with a FPE include, model systems [78]- [80], [145]- [146], electron relaxation in gases [147], reactive systems [83,148,149], polymer dynamics [84], optical bistability [70,150,151], nucleation [152], dielectric relaxation [153], climate models [154], biological applications [155], astrophysical problems [86,100,156], economics [89], ionospheric applications [87,91], plasma physics [88], nuclear dynamics [90], and numerous other applications. These Fokker-Planck equations are strictly linear although the coefficients may be nonlinear functions of the independent variable. The main objective of the present chapter is to provide an efficient and rapid numerical method of solution of this large class of Fokker-Planck equations.

The traditional method for the solution of the FPE usually involves the expansion of the probability density function in a suitable basis set, and the reduction of the differential equation to a set of algebraic equations for the expansion coefficients. This is referred to as spectral method of solution as discussed at length by Funaro [39] and Canuto et al [18,36]. An alternate approach involves the discretization of the PDF on a grid of points. This discrete approach in the solution of differential and/or integral equations has been used by researchers in other fields, notably neutron transport [95], radiative transfer [96], and computational fluid dynamics [18,36]. If the grid corresponds to the roots of the Nth order polynomial of some basis set, the solution procedure is referred to as a pseudospectral approach as described by Fornberg [19]. Fourier series or Chebyshev polynomials are almost exclusively chosen as basis functions in the application of the pseudospectral approach. Other popular discretization schemes are based on the finite-difference technique such as those proposed by Chang and Cooper [97], Larsen et al [98] and Epperlein [99] primarily for the solution of a nonlinear FPE that arises in plasma physics. Park and Petrosian [100] have recently provided a detailed comparison of several different methods of solution of Fokker-Planck equations applied to astrophysical problems.

The purpose of the present work is to apply the QDM to the solution of several

Fokker-Planck equations. The FPE describes the relaxation of some non-equilibrium distribution, $P(x, t)$, to a "steady distribution", $P_0(x)$, at infinite time which can be written in the form,

$$P_0(x) = e^{-U(x)}, \tag{3.1.2}$$

with

$$U(x) = \int_0^x \frac{A(x')}{B(x')} dx' + \ln B(x). \tag{3.1.3}$$

This steady distribution, characterized by the "potential" U(x), is the eigenfunction of the Fokker-Planck operator with zero eigenvalue, that is the "ground" state. In the QDM, the steady distribution given by Eq. (3.1.2) is employed as the weight function for the polynomials used to generate the quadrature grid. In the present work, we consider these weight functions together with alternate choices in order to maximize the rate of convergence of the solutions. We use Gautsch's Stielties procedure [134] to generate the polynomial sets orthogonal with arbitrary weight function. This permits the construction of polynomial basis sets and the corresponding quadrature grids for any appropriate weight function that accelerates the convergence of the solutions.

Although the present work is restricted to Markovian processes and a linear FPE, it is anticipated that the present methodology will be easily adapted to nonlinear and multidimensional problems. The distinction between the FPE considered here with drift and diffusion coefficients which are nonlinear functions of the independent variable x and "truly" nonlinear equations was made clearer by Drozdov and Morillo [157]. For the non-Markovian situations, several workers have derived approximate FPEs in one and two dimensions [158]. We anticipate that the QDM will provide an accurate and efficient approach to these problems.

3.2 The QDM matrix representation of the Fokker-Planck operator

Equation (3.1.1) can be rewritten as

$$\frac{\partial P(x,t)}{\partial t} = \frac{\partial}{\partial x}\left[A(x)P(x,t) + \frac{\partial B(x)P(x,t)}{\partial x}\right] \tag{3.2.1}$$

and has a stationary solution at infinite time given by Eq. (3.1.2). If we set $P(x,t) = P_0(x)g(x,t)$, then the equation for $g(x,t)$ is given by,

$$\begin{aligned}\frac{\partial g(x,t)}{\partial t} &= -A(x)\frac{\partial g(x,t)}{\partial x} + B(x)\frac{\partial^2 g(x,t)}{\partial x^2} \\ &= -\mathbf{L}g(x,t),\end{aligned} \tag{3.2.2}$$

It is easily shown that the operator L is self-adjoint with respect to the equilibrium solution $P_0(x)$. Direct application of the QDM derivative matrix to the "spatial" operator L gives the matrix "representative"

$$\mathbf{L}g_i = -A(x_i)\sum_{j=1}^{N}\Delta_{ij}g_j + B(x_i)\sum_{j=1}^{N}\Delta_{ij}\sum_{k=1}^{N}\Delta_{jk}g(x_k). \tag{3.2.3}$$

which is not symmetric and its eigenvalues may be imaginary. It is therefore important to construct a symmetric representative of the operator L.

Let's consider the matrix representative of operator L in the transform space,

$$L_{nm} = \int w(x)F_n(x)LF_m(x)dx, \tag{3.2.4}$$

where $F_n(x)$ is the set of polynomials orthonormal with respect to the weight function $w(x)$, that is

$$\int w(x)F_n(x)F_m(x)dx = \delta_{nm}. \tag{3.2.5}$$

For convenience, it will be useful to introduce a second set of orthogonal functions, defined by

$$Q_n = \sqrt{\frac{w(x)}{P_0(x)}}F_n(x), \tag{3.2.6}$$

which are orthogonal with respect to equilibrium solution $P_0(x)$, that is,

$$\int P_0(x)Q_n(x)Q_m(x)dx = \delta_{nm}. \tag{3.2.7}$$

The matrix elements of the operator L in the basis set $\{Q_n(x)\}$ are given by

$$\begin{aligned} L_{nm} &= \int P_0(x)Q_n(x)LQ_m(x)dx, \tag{3.2.8} \\ &= \int P_0(x)Q_n(x)(A(x)Q_m'(x) - B(x)Q_m''(x))dx. \end{aligned}$$

Integrating by parts on Eq. (3.2.8),

$$\begin{aligned} L_{nm} &= -B(x)P_0(x)Q_n(x)Q_m'(x) \tag{3.2.9} \\ &\quad + \int A(x)P_0(x)Q_n(x)Q_m'(x) + (B(x)P_0(x)Q_n'(x)Q_m''(x)dx, \\ &= -B(x)P_0(x)Q_n(x)Q_m' \\ &\quad + \int (A(x)P_0(x) + (B(x)P_0(x))')Q_n(x)Q_m'(x) + B(x)P_0(x)Q_n(x)'Q_m'(x)dx, \end{aligned}$$

and using the facts that $P_0(x) = 0$ at the boundaries and $A(x)P_0(x) + \frac{dB(x)P_0(x)}{dx} = 0$ for all x on the defined interval, we obtain that

$$L_{nm} = \int P_0(x)B(x)Q_n'(x)Q_m'(x)dx. \tag{3.2.10}$$

In terms of the polynomial basis $\{F_n(x)\}$ and weight function $w(x)$, upon which the quadrature rule is based, we have, substituting Eq. (3.2.6) into Eq. (3.2.10), that

$$L_{nm} = \int B(x)w(x)[\frac{d}{dx} + q(x)]F_n(x)[\frac{d}{dx} + q(x)]F_m(x)dx, \tag{3.2.11}$$

where

$$q(x) = \frac{w'(x)}{2w(x)} - \frac{P_0'(x)}{2P_0(x)}. \tag{3.2.12}$$

If the weight function $w(x)$ could be chosen equal to $P_0(x)$ then $q(x) = 0$. Applying the quadrature rule Eq. (2.1.9), we have that

$$L_{nm} \approx \sum_{k=1}^{N} B(x_k)w_k[F_n'(x_k) + q(x_k)F_n(x_k)][F_m'(x_k) + q(x_k)F_m(x_k)], \tag{3.2.13}$$

where x_k, $k = 1, 2, ..., N$ are the quadrature points which are the zeros of $F_N(x)$. The matrix representative L_{nm} is transformed back to the physical space with transformation matrix $\mathbf{T}$ defined in Chapter 2, that is, $T_{in} = \sqrt{w_i} F_n(x_i)$ and we obtain

$$L_{ij} = \sum_{n=1}^{N} \sum_{m=1}^{N} T_{in} L_{nm} T_{mj}, \tag{3.2.14}$$

Substituting Eq (3.2.13) and transformation matrix $\mathbf{T}$ into Eq.(3.2.14), that is,

$$L_{ij} = \sum_{n=1}^{N} \sum_{m=1}^{N} \sqrt{w_i} F_n(x_i) \sum_{k=1}^{N} B(x_k) w_k [F_n'(x_k) + q(x_k) F_n(x_k)][F_m'(x_k) + q(x_k) F_m(x_k)] \sqrt{w_i} F_m(x_j), \tag{3.2.15}$$

and using the fact that

$$\sum_{n=1}^{N} w_k F_n(x_k) F_n(x_i) = \delta_{ik} \tag{3.2.16}$$

and

$$\sum_{k=1}^{N} w_k F_n(x_k) F_m(x_k) = \delta_{nm}, \tag{3.2.17}$$

one finds that

$$L_{ij} = \sum_{k=1}^{N} B(x_k)[D_{ki} + q(x_k)\delta_{ki}][D_{kj} + q(x_k)\delta_{kj}], \tag{3.2.18}$$

where D_{ij} are the elements of derivative matrix defined in Eq. (2.2.18). It is obvious that this matrix representation is symmetric. For the case when the weight function $w(x) = P_0(x)$, or $q(x) = 0$, the matrix elements of operator $\mathbf{L}$, L_{ij}, is simplified as

$$L_{ij} = \sum_{k=1}^{N} B(x_k) D_{ki} D_{kj} \tag{3.2.19}$$

The great advantage of the QDM is that the matrix representation of the Fokker-Planck operator is easily constructed and evaluated for arbitrary coefficients $A(x)$ and $B(x)$. Since any set of orthogonal polynomials could be employed, it provides more opportunity to choose the weight function or basis set to optimize the matrix for rapid convergence and high accuracy of the solutions. It is expected that the convergence would be rapid for $w(x) = P_0(x)$ although this is not always the case. The use of the modified

derivative operator D_{ij} rather than derivative operator Δ_{ij} provides a symmetric matrix representation of FP operator. It is essential for the stability in the time integration of the ODE system

$$\frac{\partial g(x_i, t)}{\partial t} = -\sum_{j=1}^{N} L_{ij} g(x_j, t). \tag{3.2.20}$$

3.3 Eigenfunction expansion

The formal solution of the Fokker-Planck equation, Eq. (3.2.1), may be evaluated by eigenfunction expansion. If $\phi_n(x)$ are the eigenfunctions of operator $\mathbf{L}$ in Eq. (3.2.3), the eigenvalue problem of the FP equation is defined by

$$L\phi_n(x) = -\epsilon_n \phi_n(x), \tag{3.3.1}$$

where ϵ_n are the eigenvalues and $\phi_n(x)$ are the eigenfunctions. The linear time-dependent equation, Eq. (3.2.1), admits a solution of the form

$$P(x, t) = P_0(x) \sum_{n=0}^{\infty} c_n e^{-\epsilon_n t} \phi_n(x), \tag{3.3.2}$$

where the coefficients c_n are determined from the initial condition, $P(x, 0)$, and are given by

$$c_n = \int P(x, 0) \phi_n(x) dx. \tag{3.3.3}$$

The eigenvalues in Eq. (3.3.1) and Eq. (3.3.2) are in units of reciprocal time. The ground state eigenfunction is the equilibrium distribution $P_0(x)$ with zero eigenvalue. The eigenvalues ϵ_n are real and satisfy $\epsilon_n > 0$, for $n > 0$.

In actual calculations, the solution $P(x, t)$ given by Eq. (3.3.2) must be truncated at $n = N$. It is essential that the lower eigenvalues and eigenfunctions converge accurately and rapidly in order to achieve a fast accurate approximation of the solution. To obtain rapid convergence of the eigenvalues and eigenfunctions of the FP operator, the choice of the weight function or the basis functions plays an important role.

Since no numerical approximation involved in temporal variable t, the accuracy of the solution (3.3.2) is as the same order as the numerical method applied to approximate the differential operator L.

3.4   Temporal discretization

Numerical schemes for temporal discretization of the Fokker-Planck equations have been studied by several researchers [97–100]. Most of the methods used are finite difference methods. Chang and Cooper [97] used centered differences on the diffusion term and weighted differences on the drift term of the FP equation. Their method corresponds to a standard finite difference scheme for solving time-dependent FP equations and was used in many applications [154]. Larsen *et al* [98] then generalized the Chang-Cooper method to allow for more efficient solution of the nonlinear FP equation using larger time steps. More recently, Epperlein [99] developed a scheme which extended the standard Chang-Cooper scheme by providing not only number density conservation but also energy conservation and allowed much larger time steps for stable and accurate solutions. The schemes are implicit in the temporal discretization. In a review of numerical methods for solving FP equations of stochastic acceleration, Park *et al* [100] compared several finite difference schemes, including the Chang-Cooper method, the method by Larsen *et al*, and some semi-implicit schemes based on the above two schemes. They pointed out that the fully implicit Chang-Cooper method is the most robust finite difference method. Other methods suffer from instability and accuracy problems when dealing with some FP equations. Although there is some success of these methods, the finite difference methods generally encounter some difficulties that would be easy to solve or avoid in the QDM. First, the FP equation is defined over a infinite interval. To avoid this problem for the finite difference methods, one has to evaluate the equation over a finite interval

and impose boundary conditions on the newly defined boundaries. This implementation usually would cause some boundary effects in the numerical calculation. Second, the current finite difference methods available are at most 2nd order accurate in the spatial dimension, while the QDM is spectral accurate. Furthermore, since the differential matrix constructed in the finite difference schemes is usually not positive definite, an implicit or semi-implicit time discretization has to be performed to obtain a stable solution. With the QDM, the differential matrix of the FP operator is symmetric and the eigenvalues of the matrix are positive. This indicates that one can even use explicit time discretization to obtain a stable solution of the problem if the condition number of the matrix is not very large. For a implicit method, there is no restriction to the choice of time steps for a stable solution. Finally, the QDM differential matrix is very easy to construct and the method is very easy to implement. The finite difference schemes seem more complex to implement. At present, for simplicity, we only use the first order implicit and explicit Euler discretization in the time intergration.

3.5   Applications and results

In this section, we apply the methodology of the previous sections to several different systems described with a FPE with bistable states. Our main objective is to determine the optimum basis sets with the QDM formalism for the evaluation of the eigenvalues and eigenfunctions of the Fokker-Planck operator. The time dependent solutions are then expressed in terms of an eigenfunction expansion.

(1) The Quartic Potential:

A very popular model system is the quartic potential,

$$U(x) = \frac{x^4}{4} - \frac{x^2}{2} \qquad\qquad (3.5.1)$$

defined by choosing, $A(x) = x^3 - x$ and $B(x) = \epsilon$ with $x \in [-\infty, \infty]$. The equilibrium PDF, $P_0(x)$, exhibits a bimodal form indicative of two stable states that occur for $x = \pm 1$. This system has been considered by many authors in a study of the role of fluctuations in systems far from equilibrium and the subsequent evolution of such systems. Several workers have sought numerical and semianalytical solutions to this system. Eigenvalues for this system were reported by Dekker and van Kampen [146] with a finite difference approximation, by Risken [93] with a matrix continued fraction technique and Indira et al [145] with a finite difference scheme to solve the time dependent FPE. Blackmore and Shizgal [71] employed the QDM, with a quadrature based on the steady equilibrium PDF as the weight function.

Since the equivalent Schrödinger equation (see section 4.2 for detail) has three wells at $x = 0$ as well as at $x = \pm 1$ (see Fig. 2 of reference [71]), in this work we use three different weight functions and compare the results for each. We choose (a) the equilibrium PDF $w_a(x) = P_0(x) = \exp[-(x^4/4 - x^2/2)/\epsilon]$, (b) a Gaussian weight function centered at the origin, $w_b(x) = \exp(-x^2/2\epsilon)$, (c) a second narrower Gaussian weight function centered at the origin, $w_c(x) = \exp(-4x^2/\epsilon)$, and (d) the sum of the equilibrium PDF and a Gaussian weight function peaked at the origin, $w_d(x) = P_0(x) + \exp(-x^2/2.37\epsilon)$. The motivation for these different choices becomes clear when the variation of the eigenfunctions are seen. The widths of the Gaussian functions were chosen by trial and error to optimize the rate of convergence.

The eigenfunctions for $\epsilon = 0.01$ and $\epsilon = 0.001$ are plotted in Fig. 3.1. The dotted curves are for $\epsilon = 0.01$ and the solid curves are for $\epsilon = 0.001$. It is clear that the eigenfunctions are symmetric for n even and antisymmetric for n odd. For $\epsilon = 0.01$, some of the eigenfunctions are localized either near the origin and/or near ± 1, whereas others are spread over the domain. For $\epsilon = 0.001$, the eigenfunctions are generally concentrated either near $x = \pm 1$ and/or near $x = 0$. The eigenfunctions are concentrated in the
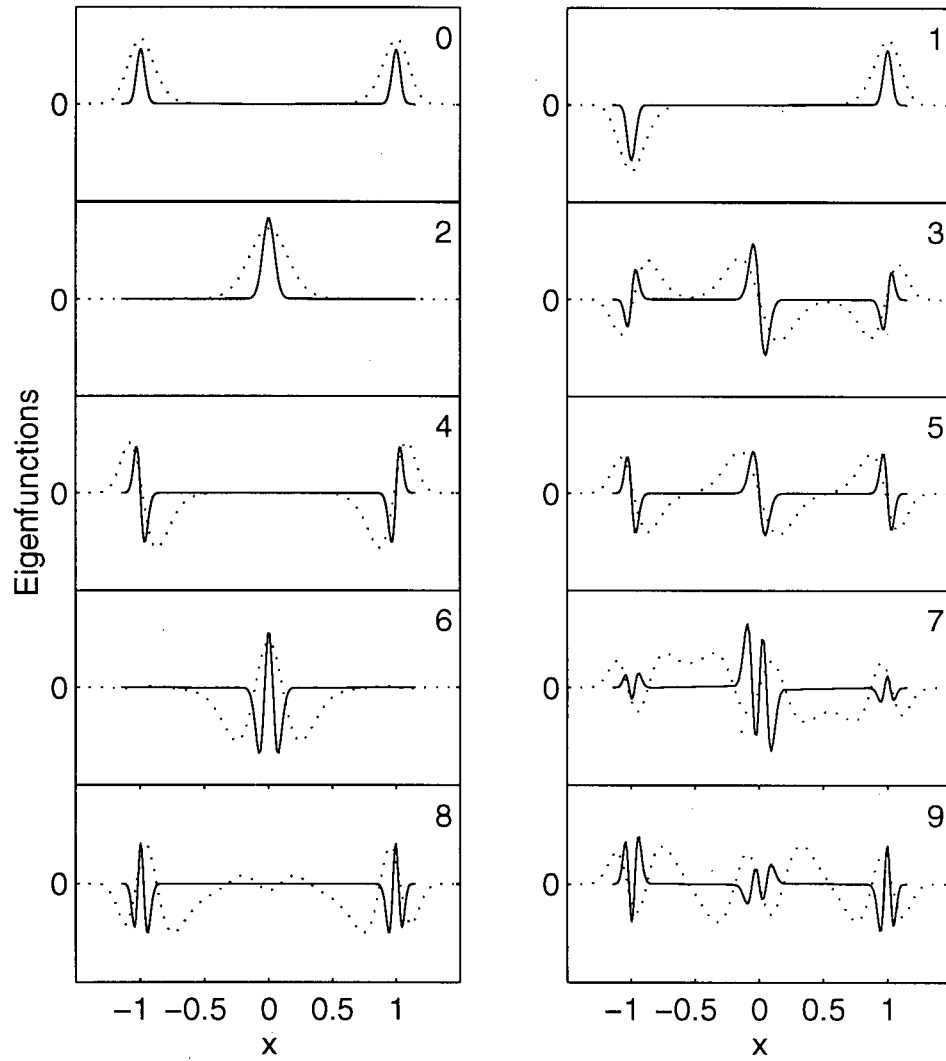
Figure 3.1: First ten eigenfunctions for the quartic potential model. The dotted curves are for $\epsilon = 0.01$ and the solid curves are for $\epsilon = 0.001$.

regions of the minima in the potential of the Schrödinger equation [71]. For $\epsilon = 0.01$, the eigenfunctions are not as localized as for $\epsilon = 0.001$. The eigenfunctions are concentrated in the three regions corresponding to the extrema of the quartic potential, i.e., $x = 0$ and $x = \pm 1$, respectively. Therefore, for small ϵ this suggests choosing a weight function $w_d(x)$ with peaks at three extrema of the potential. This results in a set of quadrature points concentrated in these three regions where the eigenfunctions are localized. It is anticipated that this choice will provide a rapid convergence of the eigenvalues and eigenfunctions. In the previous work by Blackmore and Shizgal [71], only the weight function $w_a(x)$ was used.

The convergence of the lower order eigenvalues with several different weight functions for $\epsilon = 1.0$, 0.01 and 0.001 is shown in Table 3.1. The last entry in each column is the eigenvalue converged to the figures shown. For $\epsilon = 1.0$, the eigenfunctions are not very localized and with the equilibrium PDF, $w_a(x)$, as weight function the rate of convergence of the eigenvalues is quite rapid . For the next set of results with $\epsilon = 0.01$, a Gaussian weight function centered at the origin is used and the convergence of the eigenvalues is slower than for $\epsilon = 1.0$. The convergence to 5 significant figures is achieved with 60 quadrature points. The first eigenvalue becomes extremely small with decreasing ϵ and the convergence is very slow and this behavior is discussed further with regard to the other applications. As $\epsilon \to 0$, the eigenvalues λ_3, λ_4 and λ_5 are triply degenerate [71] and tend towards 2. Similarly, the eigenvalues λ_7, λ_8 and λ_9 tend towards 4. Hence, with decreasing ϵ the calculation of the splitting of these nearly degenerate eigenvalues becomes more difficult, as seen for $\lambda_3 \to \lambda_5$. Results for $\epsilon = 0.01$ with the equilibrium distribution as weight function give the same final converged values for the eigenvalues but the rate of convergence is different. The difference in the results for these weight functions is demonstrated further for $\epsilon = 0.001$.

The results for $\epsilon = 0.001$ in Table 3.1 are reported for three different weight functions,

N	λ_1	λ_2	λ_3	λ_4	λ_5	λ_6	λ_7	λ_8	λ_9
				$\epsilon = 1.0^a$					
10	0.79216	3.5537	6.8623	11.065	15.910	23.238	30.185	46.074	
15	0.79209	3.5489	6.8441	10.829	15.445	20.607	26.644	33.051	42.023
20	0.79209	3.5489	6.8436	10.827	15.415	20.543	26.161	32.291	38.846
30			6.8435		15.415	20.540	26.153	32.219	38.709
40							26.153	32.219	38.709
				$\epsilon = 0.01^b$					
10		0.96787		1.8659		2.6791		3.4024	4.0276
15		0.96786		1.8658		2.6776		3.3652	3.8922
20						2.6768	3.3328	3.3441	3.7107
30					1.7728	2.6765	2.9702	3.3321	3.5456
40	1.7206(-3)		1.8642		1.8708	2.6772	3.3050	3.3689	3.4526
50	6.9871(-6)		1.8645		1.8670	2.6772	3.3045	3.3655	3.4515
60	6.0771(-8)*				1.8670		3.3044	3.3655	3.4515
				$\epsilon = 0.001^a$					
4				1.9960	2.0060				
6				1.9880	1.9882			3.9999	4.0268
8				1.9879	1.9879			3.9529	3.9547
10					1.9879			3.9512	3.9513
15								3.9512	3.9512
				$\epsilon = 0.001^b$					
4		0.99698	1.9880						
6			1.9879			2.9727	3.9524		
8						2.9726	3.9513		
10							3.9512		
				$\epsilon = 0.001^d$					
6		1.0096	2.0220	2.0383					
8		0.82578	1.9897	2.0024	3.6293	4.0967			
10		1.0016	1.9912	1.9933	4.1423	4.1748	17.0192	18.3206	
15		0.99953	1.9879	1.9879	1.9900	3.1069	3.9524	3.9546	4.3375
20		0.99698			1.9885	2.9723	3.9511	3.9512	4.0025
30					1.9879	2.9727	3.9512		3.9541
40						2.9726			3.9512

Table 3.1: Convergence of the eigenvalues for the quartic potential. $^a w(x) = P_0(x)$; $^b w(x) = e^{-x^2/(2\epsilon)}$; $^d w(x) = P_0(x) + e^{-x^2/(2.37\epsilon)}$. $P_0(x) = e^{-(\frac{x^4}{4} - \frac{x^2}{2})/\epsilon}$ is the equilibrium solution of the Fokker-Planck equation.

the equilibrium distribution (w_a), a Gaussian centered on the origin (w_b), and the sum of the equilibrium and a Gaussian at the origin (w_c). With the equilibrium distribution, only the eigenvalues λ_4, λ_5, λ_8 and λ_9, are calculated (see Fig. 3.1: solid curves), whereas for the Gaussian weight function centered at the origin, only the eigenvalues λ_2, λ_3, λ_6, λ_7 and λ_{10}, are calculated. In both cases, the convergence is very rapid. This demonstrates that the choice of weight function which determines the distribution of grid points is extremely important. The eigenfunctions ϕ_4, ϕ_5, ϕ_8 and ϕ_9 in Fig. 3.1 have their greatest variation near $x = \pm 1$ and the equilibrium distribution provides the required distribution of grid points for the rapid convergence obtained. By contrast, the eigenfunctions ϕ_2, ϕ_3, ϕ_6 and ϕ_7 have their greatest variation near $x = 0$ and the Gaussian distribution centered at the origin provides the required distribution of grid points for the rapid convergence of these eigenfunctions. The eigenfunction pairs ϕ_3 and ϕ_5, and ϕ_7 and ϕ_9, are antisymmetric (see Fig. 3.1) and the corresponding eigenvalues are (nearly) degenerate (see Table 3.1).

The final entry in Table 3.1 is for $\epsilon = 0.001$ and a weight function which is the sum of the equilibrium distribution and a Gaussian weight function centered at the origin. In this case, all the eigenvalues are calculated and the convergence is moderately rapid, more so than with only the equilibrium distribution as weight function.

A summary of the rate of convergence of the eigenvalues is presented in Table 3.2. Here, N_a, N_b, N_c and N_d are the number of quadrature points associated with the four weight functions shown at the bottom of the table. The entries in the table are the approximate numbers of points required to calculate the eigenvalues shown to 5 significant figures. As can be seen in the results, the rate of convergence of the eigenvalues is extremely rapid for $\epsilon = 1.0$ with both weight function $w_a(x)$ and $w_c(x)$, for $\epsilon = 0.01$ with weight function $w_b(x)$, and for $\epsilon = 0.001$ with weight function $w_d(x)$. For $\epsilon = 1.0$, the convergence is twice as slow with the weight function $w_b(x)$ because the Gaussian function employed is too narrow and there is an insufficient number of points in the

	λ_1	λ_2	λ_3	λ_4	λ_5	λ_{10}	λ_{15}	λ_{20}	λ_{25}
$\epsilon = 1.0$									
λ	0.79209	3.5489	6.8435	10.827	15.415	45.599	85.415	133.03	187.38
N_a	15	15	30	20	20	40	40	50	60
N_b	50	70	50	70	70	90	110	140	160
N_c	20	20	20	15	20	30	50	40	50
$\epsilon = 0.01$									
λ	6.16(-12)	0.96786	1.8645	1.8658	1.8670	3.9435	5.9608	8.7931	12.269
N_a	50	80	80	40	70	90	100	110	100
N_b	80	15	50	20	50	60	60	70	60
$\epsilon = 0.001$									
λ	1.2016(-109)[a]	0.99698	1.9879	1.9879	1.9879	4.9234	7.8013	9.6867	11.545
N_a		**	**	8	8	**	20	**	30
N_b		4	6	**	**	10	**	20	**
N_d		20	15	15	30	40	40	50	60

[a]The value is estimated by Kramers' approximation.
**More than 200 quadrature points are required for convergence.

Table 3.2: Comparison of the rate of convergence of the eigenvalues for the quartic potential. N_a, N_b, N_c, and N_d are the number of quadrature points for weight function $w_a(x) = P_0(x)$, $w_b(x) = e^{-x^2/(2\epsilon)}$, $w_c(x) = e^{-x^2/(0.25\epsilon)}$ and $w_d(x) = P_0(x) + e^{-x^2/(2.37\epsilon)}$, respectively.

interval where the eigenfunctions are large. The first eigenvalue decreases extremely rapidly with decreasing ϵ and the value for $\epsilon = 0.001$ in Table 3.2 is determined with the Kramers' approximation; see Eqs. (3.5.2) and (3.5.3).

Generally speaking, for large ϵ, the eigenvalues and eigenfunctions can converge very fast with a weight function equal to either the equilibrium distribution or a Gaussian centered near the origin (as long as a proper width is selected). For $\epsilon = 0.01$, the eigenvalues converge faster with the equilibrium function $P_0(x)$, i.e. $w_a(x)$, as weight function than with a Gaussian weight function $w_b(x)$ shown in the Table 3.2. For $\epsilon = 0.001$, the rate of convergence improves dramatically for certain eigenvalues with $w_a(x)$ and for others with $w_b(x)$. But both weight functions fail to provide accurate results for other eigenvalues.

ϵ	λ_1	λ_2	λ_3
		QDM	
50	9.041867	30.45742	56.83964
100	13.04778	43.49627	81.02501
200	18.71484	61.94008	115.2331
300	23.06393	76.09384	141.4834
400	26.73058	88.02646	163.6139
		Wu and Kapral	
50	9.04	30.5	56.8
200	13.1	43.5	81.0
200	18.7	61.9	115
300	23.1	76.1	142
400	26.7	88.0	164

Table 3.3:   Comparison of the eigenvalues for large ϵ for the quartic potential. $w(x) = P_0(x) = \exp[-(\frac{x^4}{4} - \frac{x^2}{2})/\epsilon]$, $N = 20$.

By adding these two weight functions together all the eigenvalues can be calculated with a moderately rapid convergence. The first 25 eigenvalues can be calculated in this way to 5 significant figures with 60 points. For large ϵ, the eigenvalues and eigenfunctions can converge very fast with either the equilibrium solution or a Gaussian centered in the middle (as long as a proper width is selected) as weight function.

Wu and Kapral [149] employed this Fokker-Planck equation to study the barrier crossing dynamics in terms of the spectral properties of the Fokker-Planck operator. They studied the chemical rate problem in terms of the eigenvalue spectrum of the Fokker-Planck operator and a second projected operator defined in their paper. They were primarily interested in the very low barrier limit, that is for $\epsilon \gg 1$. They expanded the eigenfunctions in a set of scaled Hermite polynomials and diagonalized the matrix representative of the Fokker-Planck operator in this basis set. They mention that the choice of scaling parameter is particularly important. Wu and Kapral reported the first

ϵ	λ_1^{QDM}	$\lambda_1^{Kramers}$	$(\lambda_1^{Kramers} - \lambda_1^{QDM})/\lambda_1^{QDM}$
0.01	6.1596(-12)	6.2518(-12)	0.0150
0.02	1.6232(-6)	1.6776(-6)	0.0335
0.04	8.0874(-4)	8.6901(-4)	0.0752
0.05	2.7761(-3)	3.0331(-3)	0.0926
0.06	6.3146(-3)	6.9792(-3)	0.1052
0.08	1.7774(-2)	1.9779(-2)	0.1128
0.1	3.3545(-2)	3.6951(-2)	0.1015
0.15	8.2136(-2)	8.5024(-2)	0.0352
0.2	1.3478(-1)	1.2897(-1)	-0.0431
0.25	1.8717(-1)	1.6560(-1)	-0.1152
0.3	2.3802(-1)	1.9564(-1)	-0.1781
0.4	3.3407(-1)	2.4095(-1)	-0.2787
0.45	3.7934(-1)	2.5828(-1)	-0.3191
0.5	4.2294(-1)	2.7303(-1)	-0.3544

Table 3.4: Variation of λ_1 versus ϵ for the quartic potential: Comparison with the Kramers' estimate.

three eigenvalues for several large values of ϵ. These are shown in Table 3.3 in comparison with the QDM results with the equilibrium distribution as weight function and N = 20. For these large values of ϵ, the QDM is extremely efficient and the results in Table 3.3 are converged to the number of significant figures shown. The more difficult numerical problem is for smaller values of ϵ.

The Wu and Kapral paper is but one of many models of chemical reactions viewed as the rate of passage of reactants in one well over the barrier to the second well which represents the product states. Usually, the initial distribution is taken to be the equilibrium distribution restricted to one well that is in the region $-\infty < x < 0$. The solution of the Fokker-Planck equation is then given by Eq. (3.3.2) and the rate of change of the density of reactants as the integral of the PDF over half the domain. The rate becomes
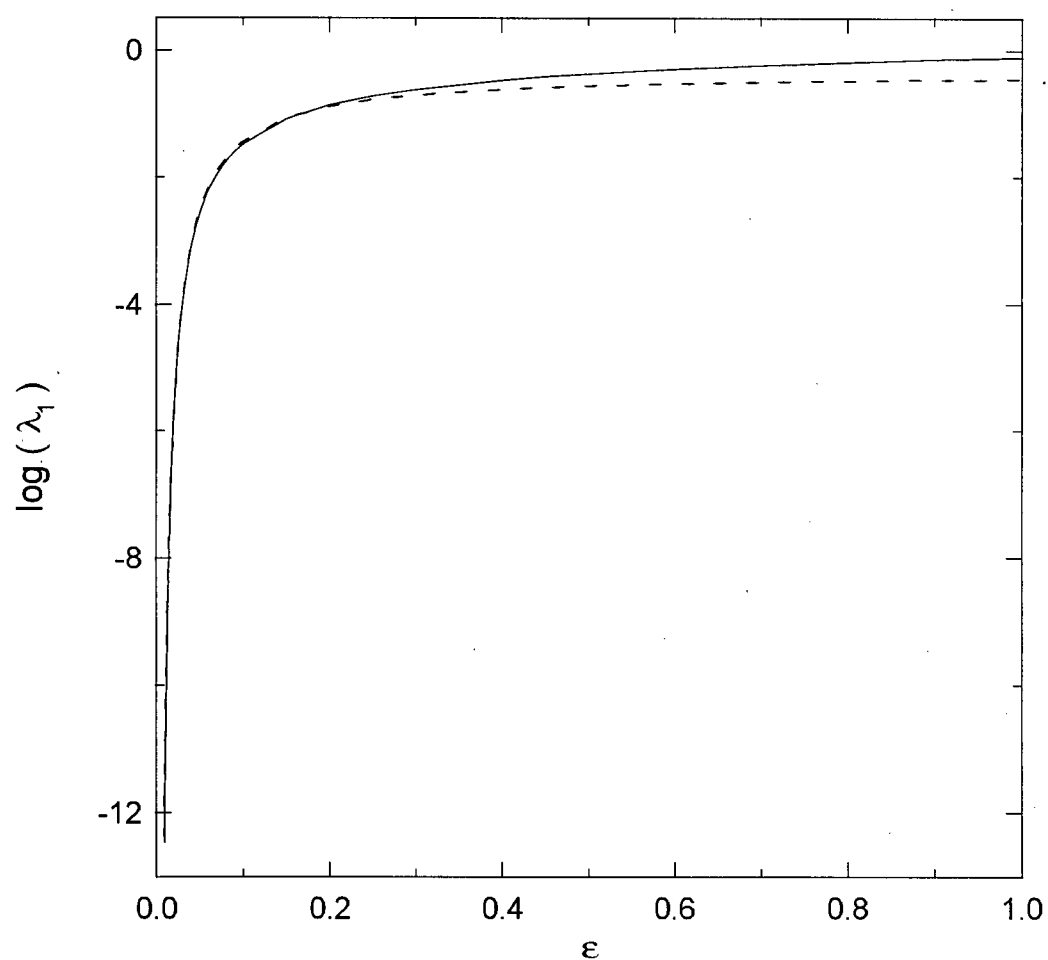
Figure 3.2: The variation of the lowest nonzero eigenvalue, λ_1 versus ϵ for the quartic potential. The solid line is the converged result with the QDM. The dashed line is the Kramers' approximation, Eqs. (3.5.2) and (3.5.3).

purely exponential after an initial transient if the smallest non-zero eigenvalue is well separated from the higher eigenvalues, i.e. $\lambda_1 \ll \lambda_2 < \lambda_3 \ldots\ldots$ The rate coefficient is then approximated by $1/\lambda_1$. A well known approximation for the reaction dynamics in a bistable potential, that is, for λ_1 is the result obtained by Kramers over fifty years ago [159]. This asymptotic result derived elsewhere [93,159] is given by,

$$\lambda_1 \approx \frac{1}{2\pi}\sqrt{U''(0)|U''(1)|}\,e^{-(U(0)-U(1))/\epsilon}. \tag{3.5.2}$$

With the explicit expression for $U(x)$ for the quartic potential, we get that,

$$\lambda_1 \approx \frac{1}{\pi}e^{-1/4\epsilon}. \tag{3.5.3}$$

A comparison of the converged QDM results for λ_1 with the approximate result, Eq. (3.5.3), is shown in Table 3.4 and Figure 3.2. The graph demonstrates the very rapid decrease in λ_1 with decreasing ϵ consistent with the form given by Eq. (3.5.3). Departures from Kramers' result can be either positive or negative and become significant for $\epsilon > 0.2$.

(2) Optical Bistability.

Optical bistability refers to the phenomenon which can arise when light is transmitted in an optical cavity containing a medium. For particular conditions, the transmitted light intensity, I_t, is a nonlinear function of the incident light intensity, I_i. The relationship between the incident and transmitted light intensities depends critically on the parameter $C = \alpha L/2T$ where α is the linear absorption coefficient, L is the length of the cavity and T is the mirror transmissivity coefficient. When C exceeds a critical value, the I_t versus I_i is then discontinuous and this system is characterized by two stable states. Further detailed discussions of this phenomenon can be found elsewhere [150,151].

The behavior of this physical system can, within certain constraints, be modeled with

a one-dimensional FPE with coefficients,

$$A(x) = y - x - \frac{2C}{1 + x^2},$$ (3.5.4)

and

$$B(x) = \frac{2qx^2}{(1 + x^2)^2}.$$ (3.5.5)

The dimensionless input and output amplitudes are denoted by y and $x \in [0, \infty]$, respectively. The parameter $q = C/2N_s$ where N_s is the saturation photon number. The stationary distribution $P_0(x)$ can be bimodal for particular values of the parameters, in particular q and y. The variation of the potential in the equilibrium distribution, Eq. (3.1.2), is shown in Fig. 3.3 for $q = 0.4$, and different y values for which there exists either a single state potential or a bistable potential.

Previous work by Blackmore *et al* [70] employed a weight function which approximated the bimodal $P_0(x)$ as a sum of two Gaussians. In this work, we choose $w_a(x) = P_0(x)$ and a second weight function made up of two equilibrium distributions, that is, $w_b(x) = P_0(x) + 0.33P_0(0.33x + 6.6)$. The quadrature weights and points are calculated as discussed in Sections 2.2 and 2.3.

The first ten eigenfunctions for $C = 8$, $q = 0.4$, and $y = 8$ and $y = 9$ are shown in Fig. 3.4. The dotted curves are for $y = 8.0$ and the solid curves are for $y = 9.0$. The eigenfunctions for $y = 9.0$ in Fig. 3.4 are localized in two regions; one is near $x = 0$ and the other near $x = 6.6$. On the other hand, the equilibrium distribution (the $n = 0$ eigenfunction in Fig. 3.4) has only one peak near $x = 6.6$. If the equilibrium distribution were used as the weight function, the quadrature points generated would be concentrated in this region. The eigenfunctions for $y = 9$ are more localized in the two regions than for $y = 8$.

A comparison of the numerical convergence of the eigenvalues, λ_n, with weight functions $w_a(x)$ and $w_b(x)$ is shown in Table 3.5 for $C = 8$, $q = 0.4$ and several y values.
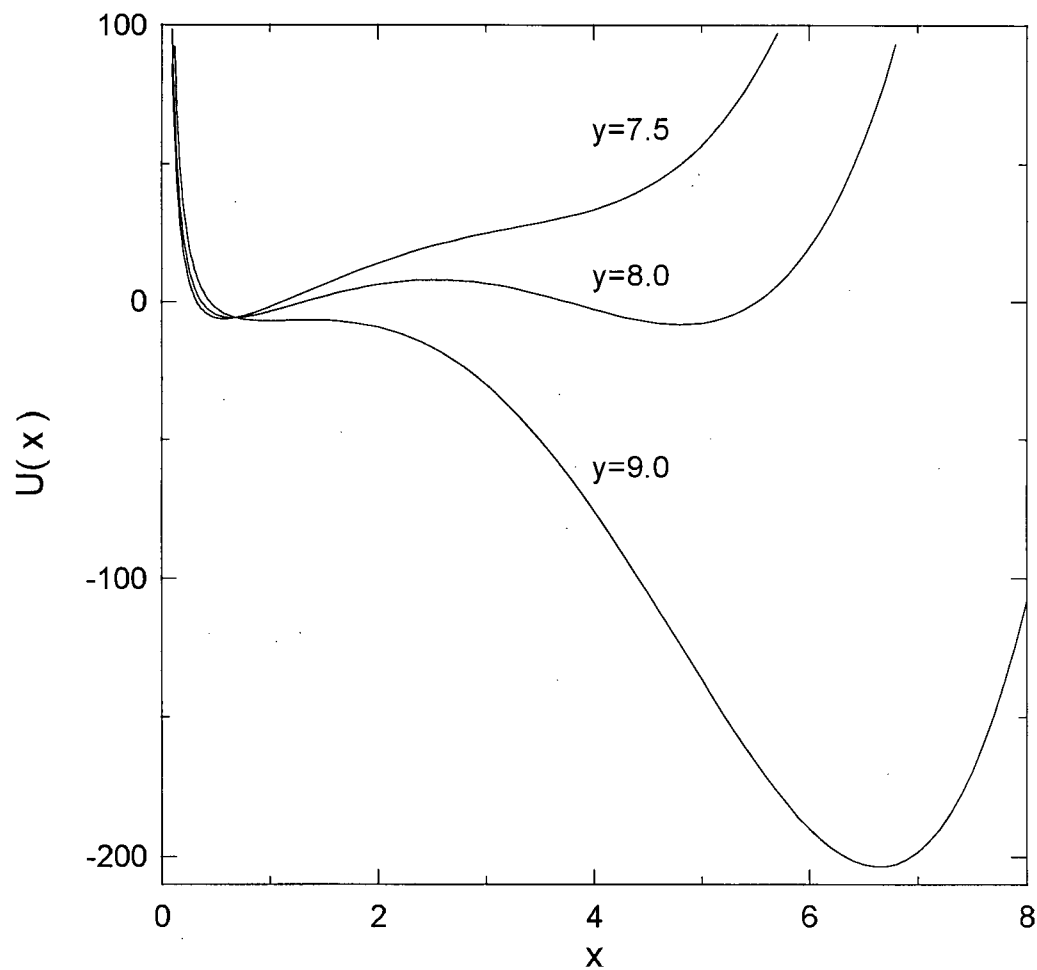
Figure 3.3: The potential $U(x)$ in the equilibrium distribution for the optical bistability problem, $C = 8$ and $q = 0.4$.
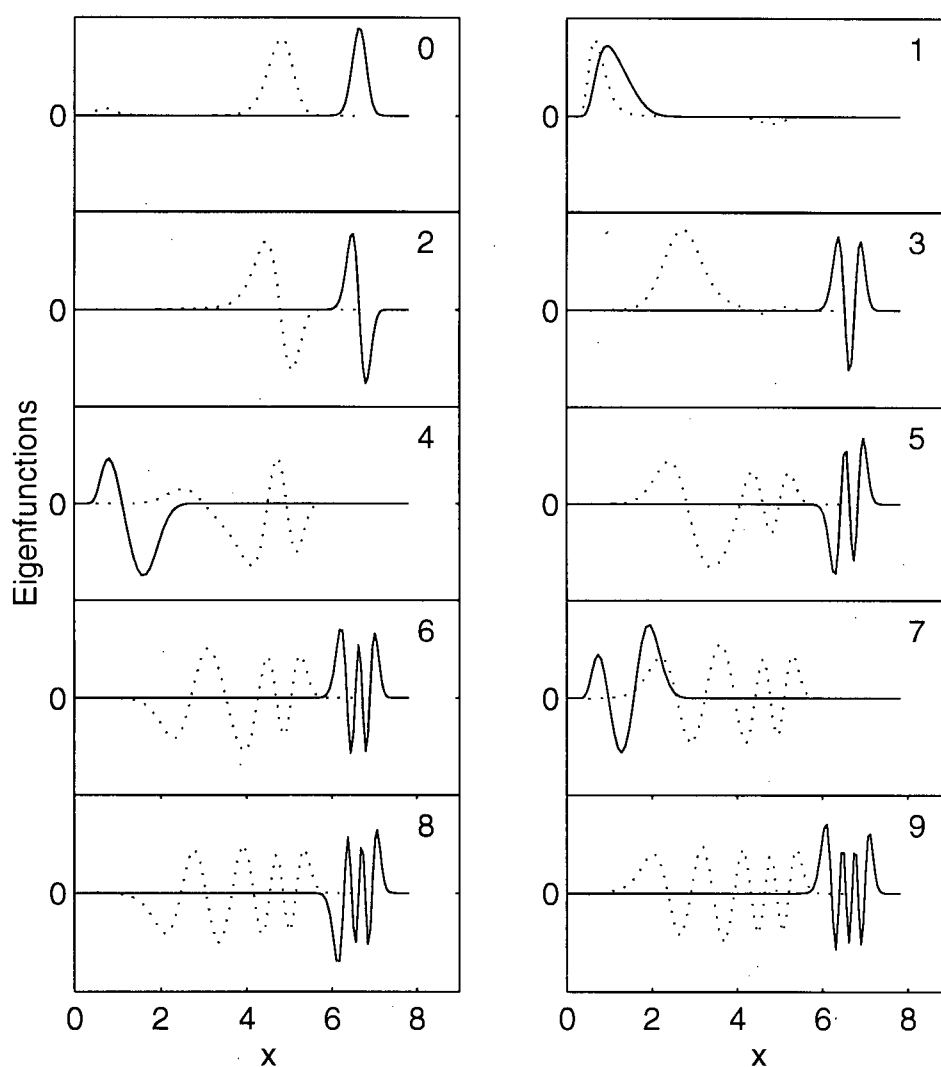
Figure 3.4: The first ten eigenfunctions of the Fokker-Planck operator for the optical bistability problem with $C = 8$, $q = 0.4$. The dotted curves are for $y = 8.0$ and the solid curves are for $y = 9.0$.

N	λ_1	λ_2	λ_3	λ_4	λ_5	λ_6	λ_7	λ_8	λ_9
				$y = 7.5^a$					
10	0.7779	3.4958	5.4983	6.7301	9.2306	13.2532	19.6935	29.7897	46.2350
20	0.5809	0.9297	1.3063	1.7289	2.1979	2.7500	3.7418	5.4299	5.7352
30		0.9291	1.3033	1.6991	2.1135	2.5445	2.9903	3.4510	3.9434
40						2.5440	2.9886	3.4455	3.9132
				$y = 8.0^a$					
10	1.609(-5)	0.3773	0.7078	1.0355	1.4857	2.1358	3.7191	7.3766	16.4200
20	5.494(-7)	0.3771	0.6692	0.7342	0.9843	1.2403	1.5440	1.9160	2.3760
30	6.653(-7)		0.5255	0.6980	0.8822	1.0626	1.3013	1.5612	1.8527
40	4.642(-7)		0.5210	0.6976	0.8729	1.0468	1.2742	1.5206	1.7880
45	4.641(-7)		0.5209	0.6976	0.8728	1.0467	1.2738	1.5195	1.7860
50							1.2738	1.5195	1.7858
				$y = 9.0^a$					
2		0.6606							
4		0.6605	1.3178		1.9735				
6					1.9718	2.6224		3.2768	
8						2.6223		3.2693	3.9130
10									3.9126
				$y = 9.0^b$					
6	0.1721	0.6613	1.3510	40.5944					
8	0.04931	0.6606	1.3219	2.0198	5.0508				
10	0.1482	0.6606	1.3172	1.3946	2.0090	3.3048	21.3499		
20	0.2064	0.6605	1.3178	1.4933	1.9718	2.6223	2.9576	3.2698	3.9180
30	0.2063		1.3178	1.4849	1.9718	2.6223	2.9039	3.2693	3.9126
35				1.4849			2.8388	3.2693	3.9126
40							2.8388		

Table 3.5: Convergence of the eigenvalues for the optical bistability model with $q = 0.4$. $^a w(x) = P_0(x)$. $^b w(x) = P_0(x) + 0.33 P_0(0.33x + 6.6)$. $P_0(x)$ is the normalized equilibrium solution of the Fokker-Planck equation.

As can be seen from the results, the rate of convergence of the eigenvalues is extremely rapid for the smaller y values with both weight functions. For $y = 9$, the convergence of some of the eigenvalues is extremely rapid with $w_a(x)$, whereas other eigenvalues are not calculated. With the weight function $w_b(x)$, we are able to calculate the first nine eigenvalues to 5 significant figures with 40 quadrature points.

A comparison of the rate of convergence of several weight functions used for constructing the QDM matrix in the present and in the previous work is shown in Table 3.6. For the weight functions we used in our present work, $w_a(x)$ and $w_b(x)$, the rate of convergence of the eigenvalues is more than twice as fast as that for weight functions $w_c(x) = x^2 \exp(-x^2)$ and $w_d(x) = x^2 \exp(-x^2) + x^2 \exp[-(x - 6.6)^2/0.1)]$ used in the previous work by Blackmore *et al* [70]. For $q = 0.4$ and $y = 7.5$ and 8, the convergence is the same with both $w_a(x)$ and $w_b(x)$. The so-called "speed" quadrature points with $w_c(x)$ gives poorer convergence. For $y = 9$, $w_a(x)$ is superior for some of the eigenvalues and worse for others. For example, for $y = 9$ and $q = 0.4$, the eigenvalues λ_1, λ_4 and λ_7 converge with 90 to 110 points, while eigenvalues λ_2, λ_3, λ_5, λ_6, λ_8 and λ_9 converge with less than 10 points. This is because that the eigenfunctions for $y = 9$ are concentrated in two regions; one is near $x = 0$, the other is near $x = 6.6$. However, the peak of the weight function $w_a(x) = P_0(x)$ at $x = 6.6$ dominates and, with small N, most of the quadrature points are distributed near this region. Since there are not enough points or none in the $x = 0$ region, the eigenvalues corresponding to the eigenfunctions in this region are not calculated. With increasing N, there are more points near $x = 0$, and the "missing" eigenvalues are recovered. With w_b as weight function, the grid points are better distributed and all the eigenvalues converge quickly. The results for $q = 1$ are also shown in Table 3.6 and the results are similar to those obtained for $q = 0.4$.

	λ_1	λ_2	λ_3	λ_4	λ_5	λ_6	λ_7	λ_8	λ_9
				$y = 7.5$	$q = 0.4$				
λ	0.5809	0.9291	1.3033	1.6991	2.1135	2.5440	2.9886	3.4455	3.9132
N_a	20	30	30	30	30	40	40	40	40
N_b	20	30	30	30	30	40	40	40	40
N_c	30	40	40	50	60	70	80	80	80
				$y = 8.0$	$q = 0.4$				
λ	4.642(-7)	0.3771	0.5209	0.6976	0.8728	1.0467	1.2738	1.5195	1.7858
N_a	40	20	50	40	50	50	50	50	50
N_b	40	20	50	40	50	50	50	50	50
N_c	60	60	40	70	70	70	80	80	90
				$y = 9.0$	$q = 0.4$				
λ	0.2063	0.6605	1.3178	1.4849	1.9718	2.6223	2.8388	3.2693	3.9126
N_a	90	4	4	100	6	6	110	8	10
N_b	30	20	20	30	20	20	40	30	30
N_c	30	100*	100	30	100*	100*	30	100*	100*
N_d	30	60	70	40	90*	90*	50	90*	90*
				$y = 7.5$	$q = 1.0$				
λ	0.3037	0.6883	1.1146	1.5723	2.0519	2.5446	3.0443	3.5542	4.0872
N_a	20	20	20	20	30	30	30	30	30
N_b	20	20	20	20	30	30	30	30	30
N_c	30	30	40	40	40	40	50	50	60
				$y = 8.0$	$q = 1.0$				
λ	1.514(-3)	0.3343	0.4922	0.7460	1.0443	1.3761	1.7367	2.1225	2.5324
N_a	20	30	30	30	30	30	30	30	30
N_b	20	30	30	30	30	30	30	30	30
N_c	40	40	40	50	50	60	60	60	70
				$y = 9.0$	$q = 1.0$				
λ	0.3166	0.6592	1.3099	1.8157	1.9516	2.5835	3.2045	3.2588	3.8136
N_a	50	4	6	60	6	8	10	70	10
N_b	40	20	20	30	30	40	50	40	50
N_c	30	80	100	30	100	100	100	100	100

*Converge to essentially 3 figures.

Table 3.6: Comparison of the rate of the convergence of the eigenvalues for the optical bistability model. $^a w_a(x) = P_0(x)$; $^b w_b(x) = P_0(x) + 0.33 P_0(0.33x + 6.6)$; $^c w_c(x) = x^2 e^{-x^2}$; $^d w_d(x) = x^2 e^{-x^2} + x^2 e^{-(x-6.6)^2/0.1}$.

(3) Climate Models.

Nicolis and Nicolis [154] presented a stochastic model for climatic transitions. The independent variable x in the Fokker-Planck equation represents the globally averaged surface temperature, T. The time dependent PDF of the temperature is then given by Eq. (3.1.5) with $B(T) = q^2/2$ and

$$A(T) = Q[1 - a(T)] - \epsilon\sigma T^4, \qquad (3.5.6)$$

with

$$
\begin{aligned}
1 - a(T) &= \gamma_1, T < T_1, & (3.5.7) \\
1 - a(T) &= \gamma_0 + \beta T, T_1 < x < T_2; \\
1 - a(T) &= \gamma_2, T > T_2.
\end{aligned}
$$

The coefficient $A(T)$ is the difference between the solar influx $Q[1-a(T)]$ (Q being related to solar constant, taken to be $340\mathrm{Wm^{-2}}$ with a the albedo) and the infrared cooling rate, $\epsilon\sigma T^4$, (ϵ being the emissivity and σ the Stefan constant). In Eq. (3.5.7), γ_0, γ_1 and γ_2 are constants and β is a temperature feedback coefficient. The values of the parameters used in this model are defined as $Q = 340$, $\epsilon = 0.61$, $\sigma = 5.67\mathrm{x}10^{-8}$, $T_2 = 297.0$, $\gamma_1 = 61.2$, $\gamma_2 = 0.75$, and for the continuity of $A(x)$, γ_0 and T_1 are defined by $\gamma_0 = \gamma_2 - \beta T_2$ and $T_1 = (\gamma_1 - \gamma_0)/\beta$, respectively.

For appropriate values of these parameters the system is bistable, and the corresponding climate potential has two minima at $T = T_\pm$ and a maximum at $T = T_0$ which lies between T_+ and T_-. It is important to mention that the defined $A(T)$ is a nonsmooth piecewise continuous function.

The equilibrium distribution can be written in the form:

$$P_0(T) = \exp\left(-\frac{2}{q^2}U(T)\right), \qquad (3.5.8)$$

	λ_1	λ_2	λ_3	λ_4	λ_5	λ_{10}	λ_{15}	λ_{20}	λ_{25}
10	1.3990(-4)	0.57262	1.0695	1.1826	1.8395				
20	3.6683(-5)	0.51358	0.65862	1.0430	1.1819	3.5430	7.6004		
30	3.3949(-5)	0.49091	0.61516	0.94902	1.1703	2.9259	5.9582	10.019	15.110
40	3.3889(-5)	0.48983	0.61350	0.94177	1.1687	2.7497	5.2499	8.6076	12.757
50	3.3888(-5)	0.48981	0.61347	0.94160	1.1687	2.7335	5.0674	8.0389	11.684
60		0.48980	0.61347	0.94160		2.7331	5.0466	7.8278	11.045
70							5.0458	7.7945	10.865
80								7.7931	10.824
90									10.822

Table 3.7: Convergence of the eigenvalues for the climate model with $\beta = 0.007123$ and $q = 7.13$.

where $U(T)$ is the climate potential defined by

$$U(T) = -\int^T A(T')dT'. \tag{3.5.9}$$

Nicolis and Nicolis were particularly interested in the long time evolution of this system, namely, the time scale determined by the lowest non-zero eigenvalue of the Fokker-Planck operator. They employed a finite difference scheme proposed by Chang and Cooper [97] and integrated the FPE numerically to determine this long time dependence. Figure 3.5 displays the graphs for steady state function, $P_0(T)$, and the potential, $U(T)$, for several values of β with $q = 7.13$ yr^{-1}K^2. With an increase in β, the steady state moves from one peak at T_+ to two peaks at T_+ and T_-, and then one peak at T_-. In this way, there is a transition of the global average temperature from a warm to a cold state. The form of the potential changes from one well near T_+ to two wells near T_+ and T_-, and then again to one well near T_-. For convenience, we first rescale Eq. (3.5.6) with a linear transformation given by, $T = 38.5x + 243.5$ to position the two minima around $x = \pm 1$ and the maximum around $x = 0$. The results are studied versus the parameters β and q which determine the nature of the potential.

The QDM is applied to this system with the equilibrium function $P_0(x)$ as weight
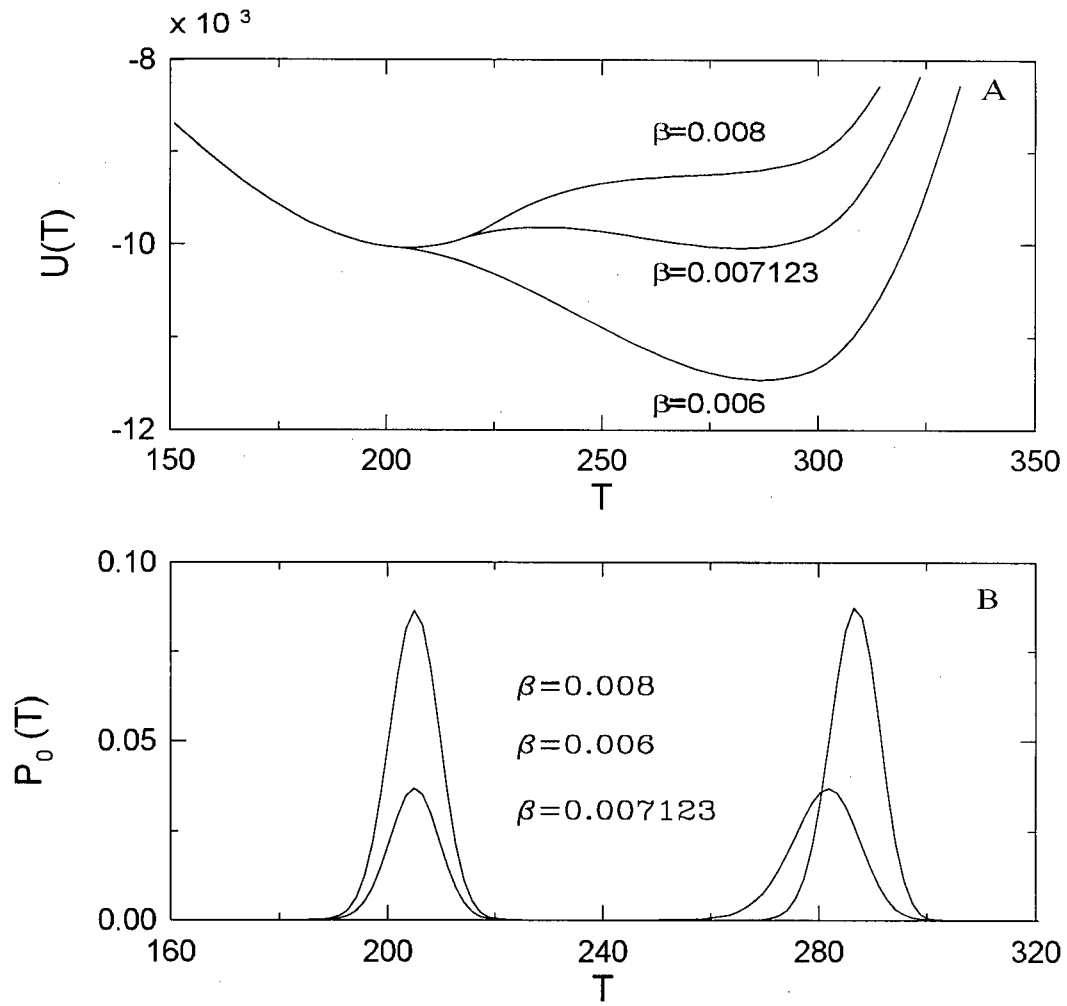
Figure 3.5: (A) The potential $U(T)$ and (B) the equilibrium distribution $P_o(T)$ for the climate model, $q = 7.13 \text{ yr}^{-1}\text{K}^2$.

function. In Fig. 3.6, we show the first ten eigenfunctions for $q = 7.13\text{yr}^{-1}$ K^2 and β = 0.007123, corresponding to the symmetric potential and symmetric stationary distribution function in Fig. 3.5. The convergence of the eigenvalues corresponding to these eigenfunctions is shown in Table 3.7, and 25 eigenvalues can be calculated to 5 significant figures with 90 quadrature points. The behavior of this system is similar to the other bistable systems. The calculations of the eigenvalues converge very quickly for small barriers, that is, for q large. The convergence is slower as q decreases as was the case for the quartic potential for small ϵ. The calculations also converge quickly for values of β which yield a potential with a single well at either cold or hot temperatures.

As with the other bistable systems, the long time behavior of the system is determined by the first eigenvalue which can be very well separated from the higher eigenvalues. The variation of $\log_{10}(\lambda_1)$ versus β for several q values is shown in Fig. 3.7. The decrease in λ_1 as β increases is because of the increasing barrier between the two states until β = 0.007123 where λ_1 reaches a minimum. It then increases for increasing β as the barrier again decreases until there is only one well at high temperatures. The behavior shown in Fig. 3.7 is referred to as "critical slowing down" and is determined in the present work in a more direct approach than by Nicolis and Nicolis. The minimum value of λ_1 in Fig. 3.7 which occurs for β = 0.007123, decreases as q decreases and as the barrier between the two wells increases. The dashed curves in Fig. 3.7 are the estimates of λ_1 determine with Kramers' approximation, Eq. (3.5.2), modified to take into account the contribution from both potential minima. The approximation is surprisingly accurate for the range of q and β in Fig. 3.7.

For all the bistable systems studied in this chapter, the time dependent probability density functions are given by Eq. (3.3.2). We show only one example in Fig. 8 of the probability density for the climate model ($q = 7.13$ and $\beta = 0.007123$) with an initial
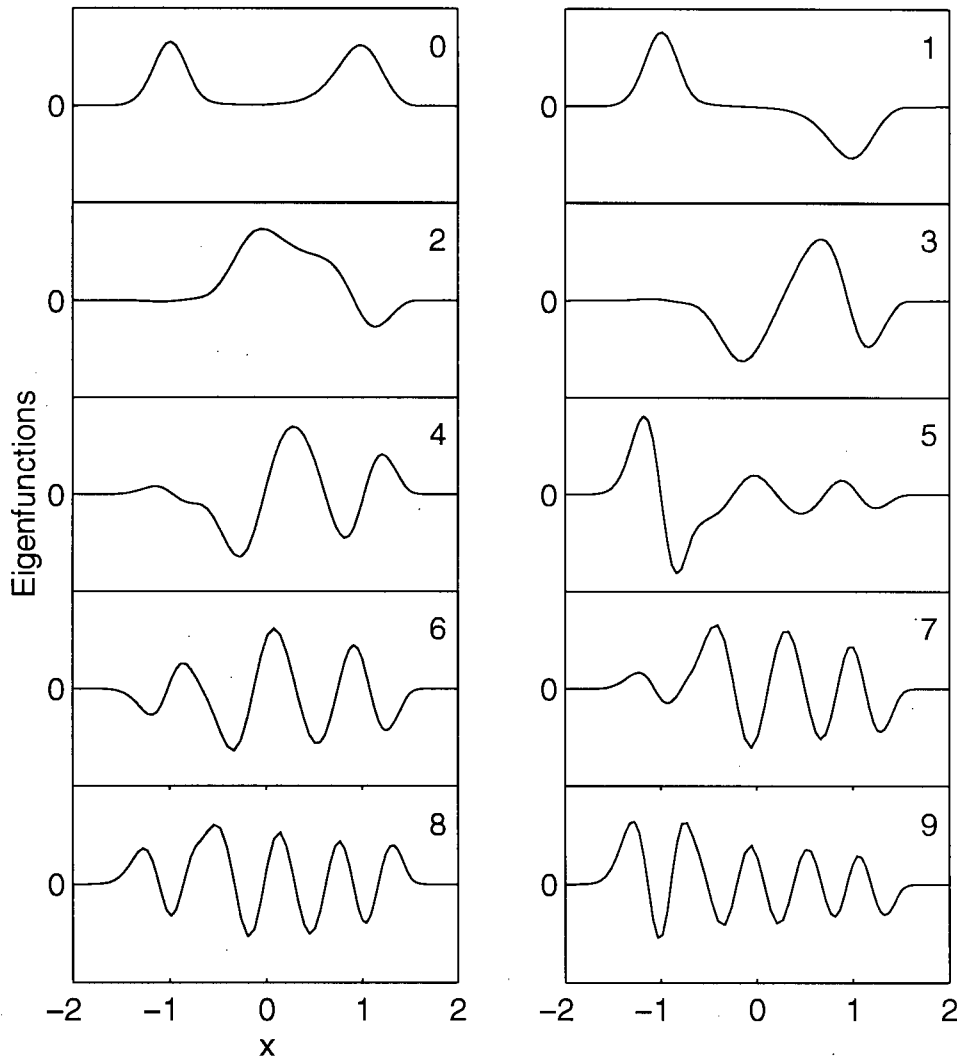
Figure 3.6: The first ten eigenfunctions of the Fokker-Planck operator for the climate model $q = 7.13$ yr^{-1}K^2, and $\beta = 0.007123$.
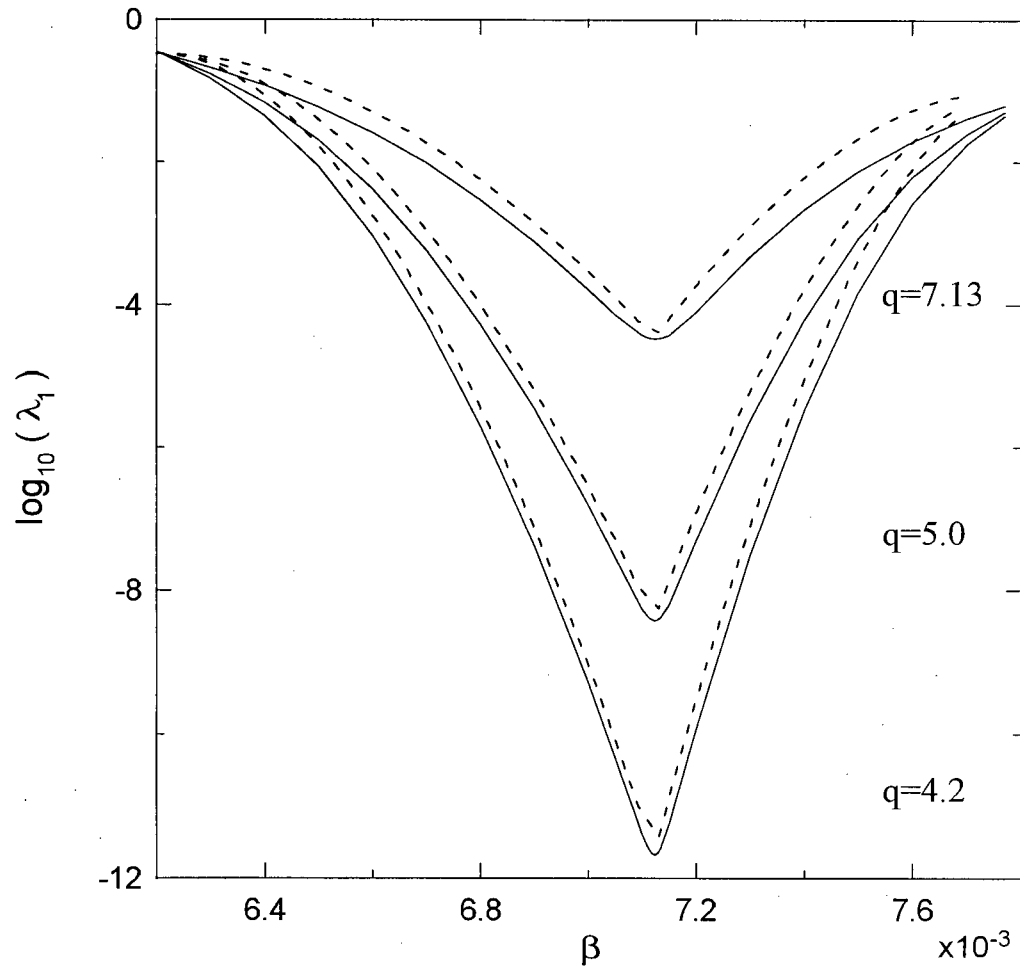
Figure 3.7: The variation of the lowest nonzero eigenvalue, λ_1 for the climate model. The solid line is the converged result with the QDM. The dashed line is the Kramers' approximation, Eq. (3.5.2).

delta-function distribution and reduced temperature $x = 1.5$ or $T(0) = 301K$. The distribution function initially broadens, with the peak moving to lower x and then there is a bifurcation with a second peak appearing at $x = \pm 1$. With increasing time there is a decrease in the peak at $x = 1$ and an increase in the peak at $x = -1$. At equilibrium, the two peaks are equal in magnitude.

The time dependent solution of the probability density function $P(x,t)$ for the climate model for $q = 7.13$ yr^{-1}K^2, and $\beta = 0.007123$ with δ function at $x = 1.5$ (at high temperature T=401K) as initial condition is shown in Fig. 8. Implicit backward Eular scheme was used to calculate the time evolution. The One peak initial distribution is quickly transform into distribution with two peaks at $x = \pm 1$ (T=250K and T=282K) and stablized gradually.

The time dependence of the global average temperature corresponding to the distribution in Fig. 3.8 is shown by the solid curve in Fig. 3.9. The time scale is determined by λ_1 listed in Table 3.7. Because of the very large separation in the value of λ_1 relative to the higher eigenvalues listed in Table 3.7, the initial transient is not discernible in Fig. 3.9. There is a very rapid, almost instantaneous decrease in the temperature to about 280K and then the gradual slow decrease. The dashed curve is the single exponential decay with decay constant equal to λ_1.

Comparison between the QDM and other numerical methods of solution of Fokker-Planck equation are available in the papers by Chen *et al* [45] and Leung *et al* [47]. Some of the results are shown in Figure 3.10 and Figure 3.11. Detailed discussion can be found in the papers.
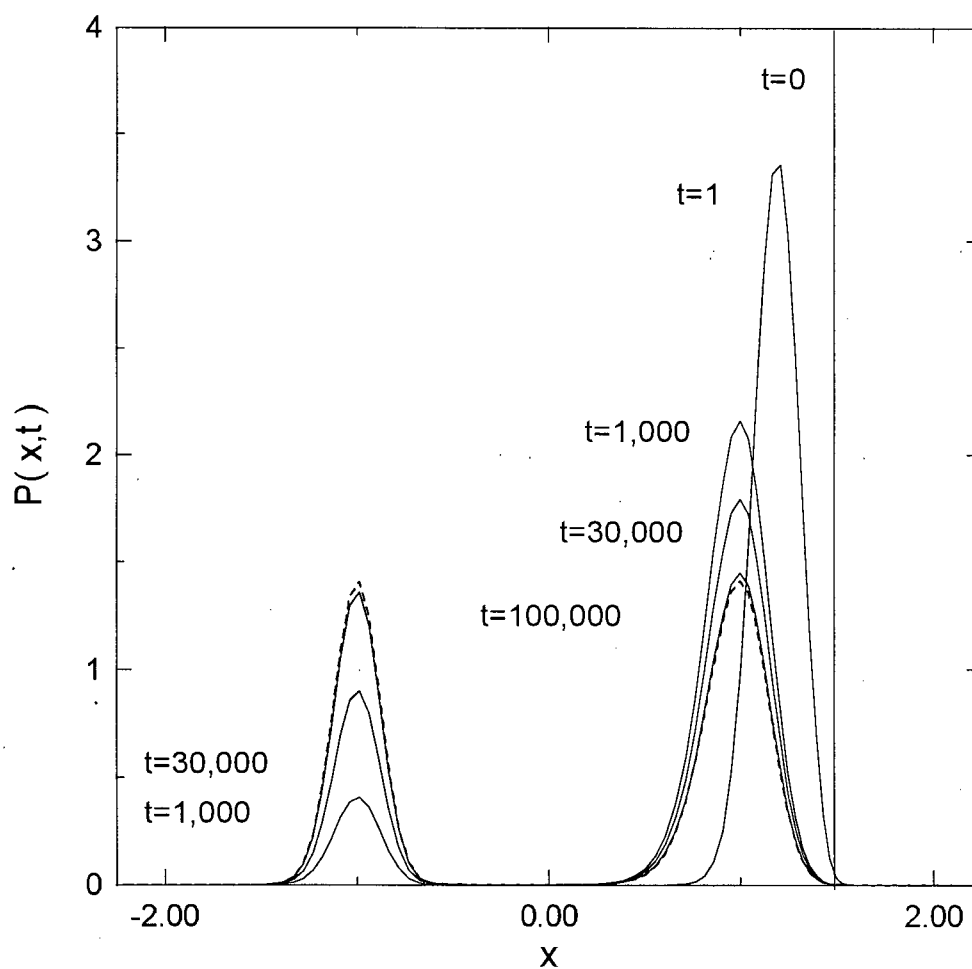
Figure 3.8: Time dependence of the probability density function for the climate model for $q = 7.13$ yr^{-1}K^2, and $\beta = 0.007123$. The initial distribution is a delta function at $T = 301K$ corresponding to $x = 1.5$.
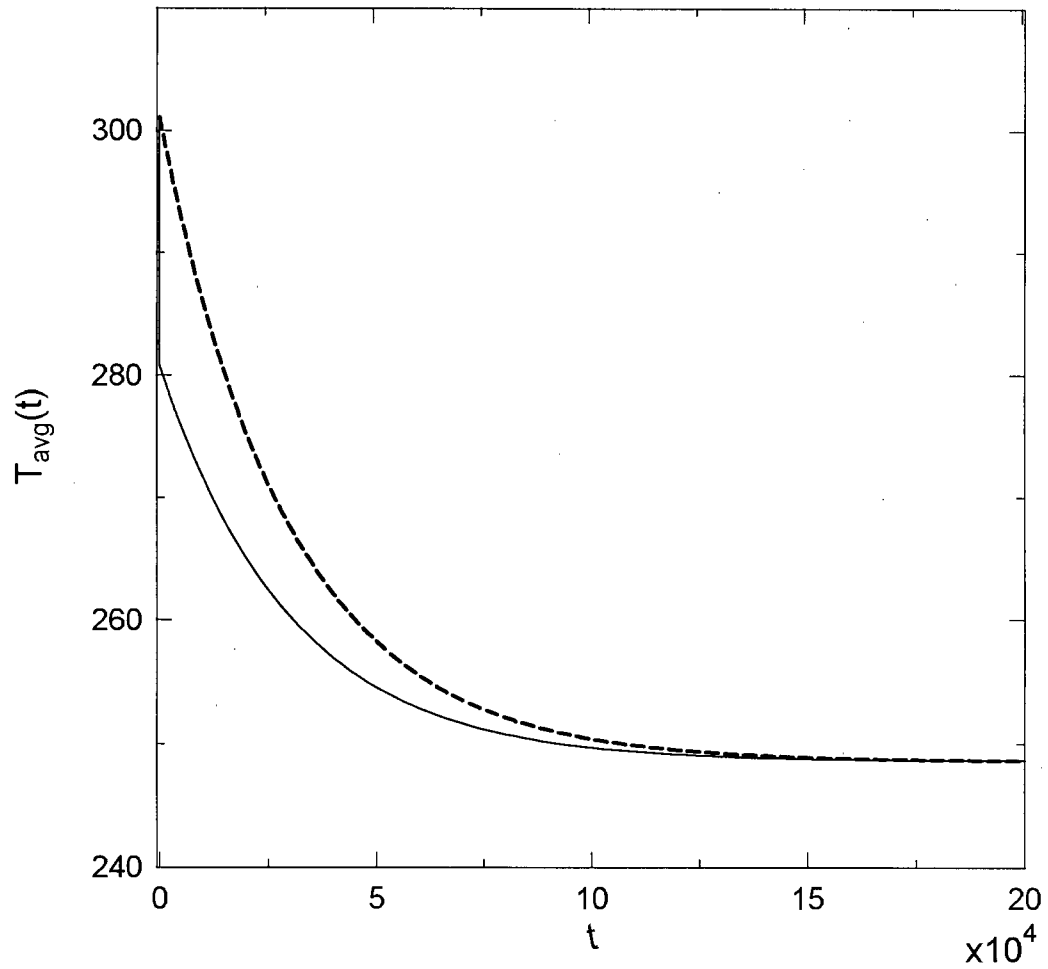
Figure 3.9: The variation of the global average temperature corresponding to the distribution in Fig. 7. The solid line is the result all terms in the eigenfunction expansion whereas the dashed line is the result with just two terms corresponding to λ_0 and λ_1.
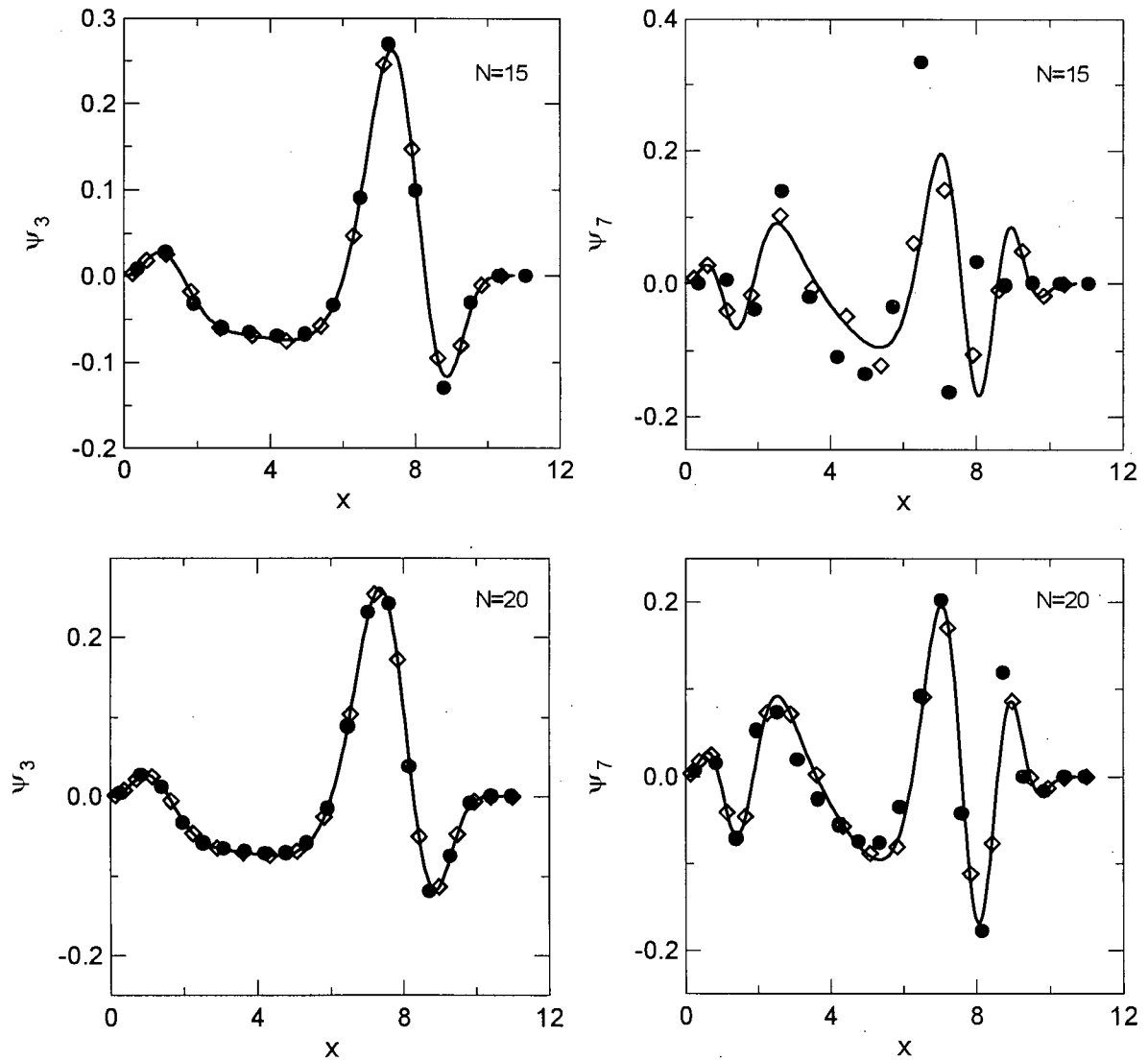
Figure 3.10: Eigenfunctions of the Fokker-Planck operator for electron relaxation in Xe, $E/n = 0.25$ Td. The solid lines represent the exact results. The circle symbols are the results with the QDM and the plus signs are the results with a finite difference method.
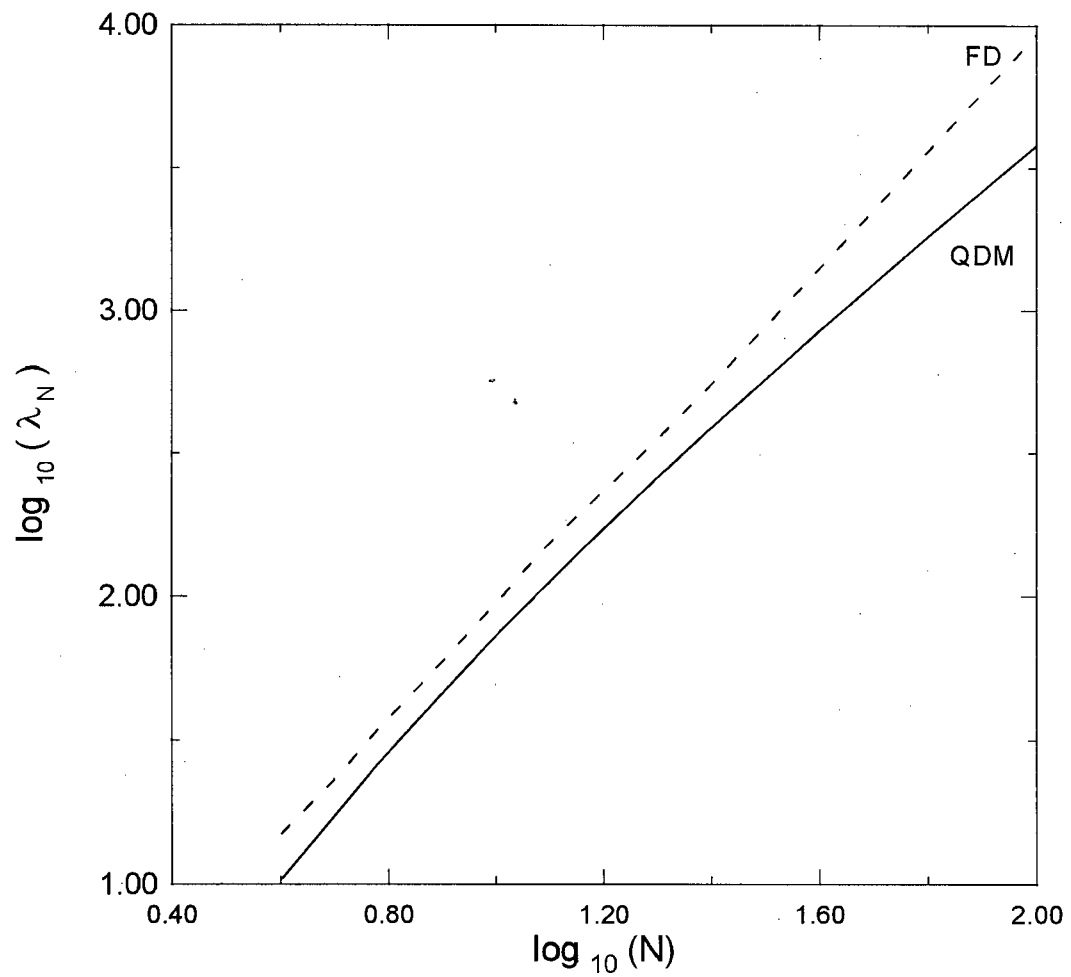
Figure 3.11: Variation of the maximum eigenvalue λ_N versus the grid size, N, for a finite difference approach and the QDM.

3.6 Summary

In the present chapter, we have demonstrated that accurate eigen-solutions of different Fokker-Planck equations can be determined with the QDM. The main theme of this work is with regard to the choice of the weight function that determines the distribution of quadrature points in the QDM. We have demonstrated that the convergence of the eigen-functions and eigenvalues of the Fokker-Planck operator is rapid with the appropriate choice of weight function. For the bistable systems studied here, which include the quartic potential, optical bistability and a climate model, the first non-zero eigenvalue can be extremely small and nearly degenerate with the zero eigenvalues that characterizes the equilibrium distribution. The small difference between these nearly identical eigenvalues can be determined with the QDM. The slow approach to equilibrium is then characterized by the smallest non-zero eigenvalue. It is anticipated that the gridding technique described in this work will find important applications to multidimensional problems as well as nonlinear problems which may include time dependent forcing terms and/or time dependent drift and diffusion coefficients in the Fokker-Planck equation.

Chapter 4

Applications of the QDM to the Solution of Schrödinger equation

4.1 Introduction

There have been increased interest in the solution of the quantum mechanical problems with a discretization of the wave function in the Schrödinger equation. The traditional methods for solving a Schrödinger equation usually involve the expansion of the wave function in a suitable basis set, and the reduction of the differential equation to a set of algebraic equations for the expansion coefficients. The discrete approach in the solution of other differential and/or integral equations has been used by researchers in other fields, notably neutron transport [95], radiative transport [96], and computational fluid dynamics [18,36]. In kinetic theory, a discretization method of solution of the linear Boltzmann equation was introduced by Shizgal [75]. For this problem, the velocity distribution function for atomic species for a model reactive system was evaluated at set of quadrature points based on a set of "speed" polynomials orthogonal with weight function $x^2 \exp(-x^2)$ on the interval $[0, \infty]$.

There have been numerous papers on the solution of the elementary one-dimensional Schrödinger equation,

$$\left[-\frac{d^2}{dy^2} + V(y) \right] \psi(y) = E\psi(y) \tag{4.1.1}$$

with different methods and several choices for the potential function V(y) [101]- [131]. The details of the potentials in these references are discussed later with a rational given for those choices for benchmarking the QDM against other numerical methods. Some of

the potentials studied include the nonpolynomial oscillator (NPO)potential of the form,

$$V(y) = y^2 + \frac{\lambda y^2}{1 + g y^2}.$$ (4.1.2)

This potential is chacterized by the parameters λ and g. It is close to a harmonic oscillator except a deep and narrow anharmonic well near the origin for large λ and g. In this case numerical calculation of the solution is extremely difficult. Mitra [101] employed Hermite polynomials as basis functions and reduced the Schrödinger equation to matrix form. Mitra obtained the eigenvalues and eigenfunctions by numerical diagonalization and reported numerical results for the first three eigenvalues. Kaushal [112] described a perturbative approach and compared with the previous numerical results. Bessis and Bessis [104] demonstrated that the matrix elements of the potential with Hermite basis functions can be done analytically and the numerical integrations by Mitra are unnecessary. Flessas [126] showed that for particular relationships between λ and g there are some exact results for the eigenvalues of this potential. For example, if $\lambda = -4g - 2g^2$, then $E_1 = 1 - 2g$ and for $\lambda = -7g^2 - 6g \pm g\sqrt{25g^2 - 12g + 4}$, then $E_2 = (9g + \lambda)/g$. These results are useful for benchmarking different numerical methods. Hautot [105] reconsidered the calculation of the matrix elements of the Hamiltonian for this potential in the Hermite basis set. Lai and Lin [118] reported additional exact solutions not discovered by Flessas, and also introduced a Pade approximant analysis. Fack and Vanden Berghe [124] employed several different finite difference schemes to solve for the eigenvalues and eigenfunctions for this problem. They employed a fine grid of points and diagonalized matrices of dimensions 200×200. They compared their results with available numerical results of previous workers, as well as for models with known exact results. Varshni [128] and Witwit [121,110] extended the earlier work to a three-dimensional version of this potential. Scherrer et al [129] employed the continued fraction approach by Risken employed in the solution of the Fokker-Planck equation.

We have also considered the potential given by,

$$V(y) = y^6 - 3y^2 \qquad (4.1.3)$$

considered by Sinha et al [131]. This potential belongs to the class of potentials that arise in supersymmetric quantum mechanics [114,115], and are the same class that results in the transformation of the Fokker-Planck equation to the Schrödinger equation [51,160]. These authors consider a comparison of the SWKB results [114,115] and an exact calculation of the eigenvalues from a direct integration of the Schrödinger equation. In this application, the ground state is known and can be used as the weight function in the QDM.

Kaluza [130] considered the anharmonic sextic oscillator defined by the potential,

$$V(y) = \frac{1}{2}y^2 + 2y^4 + \frac{1}{2}y^6 \qquad (4.1.4)$$

Kaluza employed an analytical Lanczos procedure to generate the tridiagonal matrix representative of the Hamiltonian for this potential. Since the algorithm is analogous to a Schmidt orthogonalization procedure, it suffers from considerable roundoff error. This problem was alleviated by using multiple precision arithmetic. Braun *et al* [125] employed a spectral method based on Chebyshev polynomials to study the same potential and was able to reproduce the numerical results of Kaluza and extend the precision of many of the higher eigenvalues up to 18 significant figures with 512 grid points.

A fourth potential that we consider in this study is of the form,

$$V(y) = y^2 + \epsilon y^4 \qquad (4.1.5)$$

which has been studied by several workers. Banerjee et al [102] and Banerjee [103] employed a non-perturbative method with the product of scaled Gaussian and a polynomial as weight function to calculate the eigenvalues for this potential for various values of

ϵ. Fernandez et al [106] and Arteca et al [108] applied a variational method to obtain the eigenvalues and compared with Banerjee's results. Fernandez and Castro [120] obtained the eigenvalues of this potential by solving the corresponding Riccati equation with Pade approximants. Recently, Fernandez and Tipping [122] improved the solution of the Riccati equation for this potential with a separation of the eigenfunctions into odd and even parity. Fack and Vanden Berghe employed a finite difference method to solve this problem. Witwit [111,117] extended the work to two and three dimensional problems.

We also include an application of the QDM to a two-dimensional Schrödinger equation with the Henon-Heiles potential that has been used by several researchers as a benchmark of different methods [161–168]. This model has also been used to study the chaotic behaviour [169–173]. In this first instance, we choose to apply the QDM with Hermite points and weights. We also employ a grid determined by other nonclassical weight function. The result are in very good agreement with those of other researchers.

4.2 The equivalence of the Fokker-Planck eigenvalue problem and the Schrödinger equation

The eigenvalue problems of Fokker-Planck equation are equivalent to Schrödinger equations. Recall the eigenvalue problem of FPE presented in Eq. (3.3.1). If the independent variable, x, is transformed to a new variable, y,

$$y = \int^x \frac{1}{\sqrt{B(x')}} dx', \tag{4.2.1}$$

and we define $\psi_n(y)$ by

$$\psi_n(y) = \sqrt{\tilde{P}_0(x(y))} \phi_n(x(y)), \tag{4.2.2}$$

with $\tilde{P}_0(y) = \sqrt{B(x(y))}P_0(x(y))$, then the Fokker-Planck eigenvalue equation, Eq. (3.3.1), is transformed into a Schrödinger equation

$$-\frac{d^2\psi_n(y)}{dy^2} + V(y)\psi_n(y) = \epsilon_n\psi_n(y), \qquad (4.2.3)$$

$$H\psi_n(y) = \epsilon_n\psi_n(y).$$

The potential function in the Schrödinger equation is derived from the drift and diffusion coefficients in the Fokker-Planck equation, that is

$$V(y) = \frac{1}{4}W^2(y) - \frac{1}{2}\frac{dW(y)}{dy}, \qquad (4.2.4)$$

where

$$W(y) = \frac{A}{\sqrt{B}} + \frac{B'}{2\sqrt{B}}. \qquad (4.2.5)$$

The potential functions obtained in this way belong to the class of potentials that occur in supersymmetric quantum mechanics [114,115].

If $\sqrt{\tilde{P}_0}$ is differentiated twice, it is clear that it is the eigenfunction with a zero eigenvalue of the Schrödinger equation Eq. (4.2.3). The Schrödinger equation, Eq. (4.2.3), can in turn be transformed into a different Fokker-Planck equation. The equivalence of the Fokker-Planck equation with the Schrödinger equation has been discussed by several authors [160]. It can be shown that the time-dependent Fokker-Planck equation equivalent to this stationary Schrödinger equation is given by

$$\frac{\partial\tilde{P}(y,t)}{\partial t} = \frac{\partial}{\partial y}\left[W'(y)\tilde{P}(y,t) + \frac{\partial\tilde{P}(y,t)}{\partial y}\right], \qquad (4.2.6)$$

with stationary solution given by

$$\tilde{P}_0(y) = \exp\left(-\int W(y)dy\right). \qquad (4.2.7)$$

The Fokker-Planck eigenvalue problem is given by

$$W(y)\frac{d\phi_n}{dy} - \frac{d^2\phi_n}{dy^2} = \epsilon_n\phi_n \qquad (4.2.8)$$

$$\hat{L}\phi_n = \epsilon_n\phi_n,$$

where the drift coefficient, $A(y) = W(y)$, and the diffusion coefficient, $B(y) = 1$. The Fokker-Planck operator, $\hat{L}$, is self-adjoint with the equilibrium function $\tilde{P}_0(y)$.

4.3   The QDM matrix representation of the Schrödinger equations

The matrix representation of the Schrödinger equation, Eq. (4.2.3), has similar form to that of the Fokker-Planck equation. Consider the matrix elements of the Hamiltonian for a basis set $\{S_n(y)\}$ orthogonal with unit weight function, that is,

$$H_{nm} = -\int S_n(y) S_m''(y) dy + \int S_n(y) V(y) S_m(y) dy. \qquad (4.3.1)$$

With an integration by parts in the first integral, we have that

$$H_{nm} = \int S_n'(y) S_m'(y) dy + V_{nm}, \qquad (4.3.2)$$

where $V_{nm} = \int S_n(y) V(y) S_m(y) dy$. We now introduce a second polynomial set $\{F_n\}$ orthogonal with weight function $w(y)$, that is,

$$S_n(y) = \sqrt{w(y)} F_n(y), \qquad (4.3.3)$$

where $w(y) = \exp(-\int W(y') dy')$. Eq. (4.3.2) can be rewritten as

$$H_{nm} = \int w(y) [F_m' + \frac{w'}{2w} F_m][F_n' + \frac{w'}{2w} F_n] dy + V_{nm}. \qquad (4.3.4)$$

If one of the cross terms in the integrand above is integrated by parts one gets that

$$H_{nm} = \int w F_n' F_m' dy + [V_{nm} - \tilde{V}_{nm}], \qquad (4.3.5)$$

where

$$\tilde{V}(y) = \frac{1}{4} W^2(y) - \frac{1}{2} W'(y). \qquad (4.3.6)$$

If the matrix representative H_{nm} is transformed back to the discrete representation in physical space with the transformation $\mathbf{T}$, that is,

$$H_{ij} = \sum_{n=0}^{N} \sum_{m=0}^{N} T_{in} H_{nm} T_{mj}, \qquad (4.3.7)$$

one finds that

$$H_{ij} = \sum_{k=0}^{N} D_{ki}D_{kj} + [V(y_i) - \tilde{V}(y_i)]\delta_{ij}. \tag{4.3.8}$$

If the potential of interest can be factorized in accordance with Eq. (4.2.4) then a possible choice of weight function would be given by the equilibrium distribution function or the square of the ground state wave function, Eq. (4.2.7). For this choice the term $[V(y_i) - \tilde{V}(y_i)]\delta_{ij}$ is zero since $\tilde{V}(y) = V(y)$.

The method can be applied to higher dimensional problems with product space of one-dimensional bases. For a two-dimensional Schrödinger equation,

$$\left[-\frac{\partial^2}{\partial^2 x} - \frac{\partial^2}{\partial^2 y} + V(x,y) \right] \psi_{nm}(x,y) = \lambda_{nm}\psi_{nm}(x,y) \tag{4.3.9}$$

the eigenfunctions are represented by a two-dimensional grid constructed from the product space of orthogonal polynomials in x and y. The matrix representative of the two-dimensional Hamiltonian for bases set $\{X_n(x), Y_m(y)\}$ orthogonal with unit weight function is given by

$$H_{n'm',nm} = -\iint X_{n'}(x)Y_{m'}(y)\left(\frac{\partial^2}{\partial^2 x} + \frac{\partial^2}{\partial^2 y}\right)X_n(x)Y_m(y)dxdy$$
$$+ \iint X_{n'}(x)Y_{m'}(y)V(x,y)X_n(x)Y_m(y)dxdy \tag{4.3.10}$$

With an integration by parts, we obtain that

$$H_{n'm',nm} = \delta_{m'm}\int X'_{n'}(x)X'_n(x)dx + \delta_{n'n}\int Y'_{m'}(y)Y'_m(y)dy + V_{n'm',nm}, \tag{4.3.11}$$

where $V_{n'm',nm} = \iint X_{n'}(x)Y_{m'}(y)V(x,y)X_n(x)Y_m(y)dxdy$.

As for the one-dimensional case, consider polynomial sets $\{G_n(x)\}, \{E_m(y)\}$ orthogonal with weight function $u(x), v(y)$ respectively, that is,

$$X_n(x) = \sqrt{u(x)}G_n(x) \tag{4.3.12}$$

$$Y_m(y) = \sqrt{v(y)}E_m(y) \tag{4.3.13}$$

Eq. (4.3.11) can be rewritten as

$$H_{n'm',nm} = \delta_{m'm} \int u(x) G'_{n'}(x) G'_n(x) dx + \delta_{n'n} \int v(x) E'_{m'}(y) E'_m(y) dy$$
$$+ [V_{n'm',nm} - \tilde{V}_{n'm',nm}], \qquad (4.3.14)$$

where

$$\tilde{V}_{n'm',nm} = \delta_{m'm} \int (\frac{1}{4} U^2(x) - \frac{1}{2} U'(x)) u(x) G'_{n'}(x) G'_n(x) dx$$
$$+ \delta_{n'n} \int (\frac{1}{4} V^2(y) - \frac{1}{2} V'(y)) v(y) E'_{m'}(y) E'_m(y) dy, \qquad (4.3.15)$$

and $U(x), V(y)$ satisfy

$$U'(x) = -\ln u(x), \qquad (4.3.16)$$

$$V'(y) = -\ln v(y). \qquad (4.3.17)$$

We obtain the QDM representation of the Hamiltonian by transforming matrix $H_{n'n,m'm}$ to the discrete representation $H_{ij,kl}$, that is,

$$H_{ij,kl} = \delta_{kl} \sum_{k'=1}^{N_x} D_{k'i} D_{k'j} + \delta_{ij} \sum_{k'=1}^{N_y} D_{k'k} D_{k'l} + [V(x_i, y_k) - \tilde{V}(x_i, y_k)] \delta_{ij} \delta_{kl}, \qquad (4.3.18)$$

where

$$\tilde{V}(x,y) = \frac{1}{4} U^2(x) - \frac{1}{2} U'(x) + \frac{1}{4} V^2(y) - \frac{1}{2} V'(y). \qquad (4.3.19)$$

and N_x, and N_y are the numbers of quadrature points chosen in actual applications.

4.4 Applications and results

The QDM has been applied to several one-dimensional Schrödinger equations by Shizgal and Chen [51]. In this work, the QDM was applied to several one-dimensional and a two dimensional Schrödinger equations. The eigenvalues and eigenfunctions were calculated

with different choice of weight functions and were compared with the results by other authors.

The main purpose of this study is to consider the solution of the Schrödinger equation with the QDM, and to study the rate of the convergence of the eigenvalues versus the number of grid points (equivalently basis functions) for different weight functions. The basis functions, $F_n(x)$, are orthonormal with respect to the weight function, $w(x)$. Our interest is to try to suggest the weight function that provides optimal convergence of the eigenvalues. We consider four different one-dimensional potentials in the Schrödinger equation that have received considerable attention in the literature over the past decade. If the convergence for one-dimensional problems can be optimized, there would be a considerable savings in computer time when applied to two and three dimensional problems. This has been demonstrated by Shizgal and Chen [51] in the application of the QDM to the two-dimensional Henon-Heles potential.

The first potential that we have chosen and which has been studied extensively [101]-[129] is the NPO model, Eq. (4.1.2), shown in Fig. 4.1 as the solid curves. The dashed curves are the harmonic potentials, $V(y) = y^2 + \lambda/g$, for $\lambda = g = 100$ and $\lambda = g = 10$ (upper curve) and for $\lambda = 10$ and $g = 100$ (lower curve); the potential departs from harmonic in the vicinity of the origin. The deep narrow anharmonic well near the origin gets deeper and narrower with increasing λ and g. Many of the previous calculations have emphasized the calculation of the ground state eigenvalue for large g. For situations where the potential is close to harmonic, it would appear useful to use the scaled Hermite polynomials as basis functions based on the weight function, $w_1(y) = \exp(-\alpha y^2)$, where α is a scaling parameter.

For this NPO potential, we have carried out an extensive analysis of the behavior versus the two parameters g and λ and for different weight functions. The results are summarized in Tables 4.1-4.10. In Tables 4.1-4.3 with $g = 1$, 10 and 100, we use the
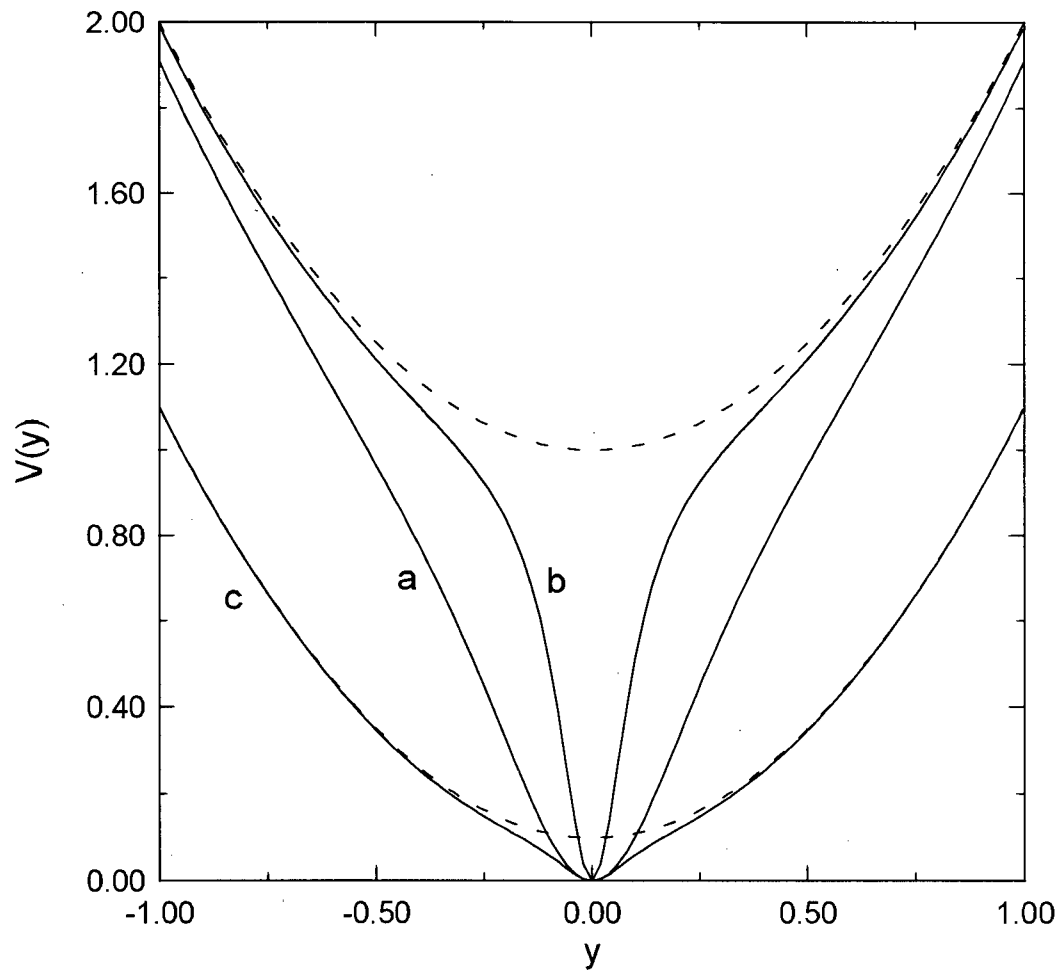
Figure 4.1: The nonpolynomial oscillator (NPO) potential, $V(y) = y^2 + \frac{\lambda y^2}{1+gy^2}$. λ and g equal to (a) 10, 10 (b) 100, 100 and (c) 10, 100. The dash lines are the corresponding harmonic potential $V(y) = y^2 + \lambda/g$.

weight function for scaled Hermite polynomials and vary the scaling parameter α for each of the first 5 eigenvalues so as to get the value of α that yields the most rapid convergence. The QDM is implemented as discussed in the previous papers [51] by constructing the orthogonal polynomials for the chosen weight function with the algorithm described by Gautschi [134]. The quadrature points are then determined [135] and the eigenvalues calculated from the numerical diagonalization of the QDM representative of the Hamiltonian, Eq. (4.3.8). The results are shown for $\lambda = 1$, 10 and 100 in each table. In Table 4.1, we reproduce exactly (to 9 significant figures) the harmonic oscillator eigenvalues for $\lambda = 0$. With increasing g, it is seen that the eigenvalues are getting increasingly equally spaced consistent with an harmonic potential. The underlined portion of each eigenvalue indicates the convergence to that number of significant figures. For $g = 1$, 10 and 100 in Tables 4.1-4.3, we get convergence of the eigenvalues with 25-45, 60-120, 170-180 quadrature points, respectively. The convergence is clearly much slower for the large values of g. The results in Table 4.3 for the largest eigenvalues are converged to no less that 3 significant figures. The slow convergence for large g is due to the narrow anharmonic form of the potential near the origin; see Fig. 4.1.

For the results in Table 4.1, the values of α were chosen arbitrarily. The interest in this study is to develop techniques to optimize the convergence by selecting a weight function related in some way to the potential. Mitra [101] chose $\alpha = \sqrt{1 + \lambda}$ and Bessis and Bessis [104] suggested $\alpha = \sqrt{1 + \lambda/(1 + 0.5g)}$. In Tables 4.4-4.6, we show the results analogous to those in Tables 4.1-4.3 using the value of α suggested by Bessis and Bessis. It is clear that the convergence in Tables 4.1-4.3 is faster than the convergence in Tables 4.4-4.6.

We have extended the previous efforts by employing a weight function chosen empirically but taking into account the form of the potential. Our previous experience [51]

N	λ_1	λ_2	λ_3	λ_4	λ_5
		$\lambda = 0$	$g = 0$		
5	1.00000000	3.00000000	5.00000000	7.00000000	9.00000000
		$\lambda = 1$	$g = 1$		
10	1.23249101	3.51099389	5.62484751	7.83801690	10.32756366
20	1.23235080	3.50738872	5.58979112	7.64836479	9.68550819
25	1.23235072	3.50738837	5.58977905	7.64820406	9.68407574
30	1.23235072	3.50738835	5.58977894	7.64820127	9.68404264
35		3.50738835	5.58977893	7.64820124	9.68404202
40			5.58977893	7.64820124	9.68404202
		$\lambda = 10$	$g = 1$		
10	2.78256744	7.41859167	10.73364911	13.61840145	16.71237123
20	2.78233128	7.41750446	10.70106074	13.38898345	15.82571826
25	2.78233044	7.41750609	10.70102615	13.38834923	15.81924074
30	2.78233052	7.41750588	10.70102563	13.38832431	15.81888806
35	2.78233052	7.41750590	10.70102557	13.38832353	15.81887214
40		7.41750590	10.70102558	13.38832349	15.81887152
45			10.70102558	13.38832349	15.81887149
50					15.81887149
		$\lambda = 100$	$g = 1$		
10	9.35966852	26.70397902	41.44872496	53.83672948	64.45752724
20	9.35941813	26.70596477	41.44110330	53.83909110	64.18782502
25	9.35941803	26.70596566	41.44109963	53.83909383	64.18745791
30	9.35941803	26.70596563	41.44109976	53.83909326	64.18744198
35		26.70596563	41.44109975	53.83909327	64.18744105
40			41.44109975	53.83909326	64.18744100
45				53.83909326	64.18744100

Table 4.1: Convergence of the eigenvalues with $V(y) = y^2 + \frac{\lambda y^2}{1+gy^2}$. $w_1(y) = \exp(-\alpha y^2)$, where α is chosen for the fatest convergence.

N	λ_1	λ_2	λ_3	λ_4	λ_5
		$\lambda = 1$	$g = 10$		
10	1.11770702	3.54168906	6.69900727	11.03978681	16.69475171
30	1.05932983	3.08883073	5.09038673	7.13612019	9.26980877
50	1.05929698	3.08809133	5.08285715	7.09048160	9.08892124
60	1.05929690	<u>3.08809085</u>	5.08284796	7.09037430	9.08805809
70	1.05929689	3.08809085	5.08284769	7.09037053	9.08801960
80	<u>1.05929688</u>		<u>5.08284768</u>	<u>7.09037041</u>	9.08801815
90	1.05929688		5.08284768	7.09037041	<u>9.08801810</u>
100					9.08801810
		$\lambda = 10$	$g = 10$		
10	1.65877686	4.53929108	8.04585051	13.12551490	19.66357857
30	1.58013523	3.88195452	5.85711306	8.03082593	10.30455803
50	1.58002278	3.87904292	5.83286153	7.90413992	9.88876928
70	1.58002235	3.87903684	5.83276776	7.90315755	9.88233330
80	<u>1.58002233</u>	<u>3.87903683</u>	5.83276755	7.90315433	9.88230079
90	1.58002233	3.87903683	<u>5.83276753</u>	7.90315417	9.88229884
100			5.83276753	<u>7.90315416</u>	<u>9.88229873</u>
110				7.90315416	9.88229873
		$\lambda = 100$	$g = 10$		
10	5.82541635	12.16555870	15.97213490	22.13479362	29.83816388
50	5.79394465	11.57221790	13.62913696	15.99309324	17.99876164
70	5.79394241	11.57219684	13.62877371	15.98848089	17.97250413
90	5.79394231	11.57219677	13.62877143	15.98843454	17.97208972
100	<u>5.79394230</u>	<u>11.57219678</u>	<u>13.62877142</u>	15.98843423	17.97208598
110	5.79394230	11.57219678	13.62877142	<u>15.98843421</u>	17.97208565
120				15.98843421	<u>17.97208562</u>
130					17.97208562

Table 4.2: Convergence of the eigenvalues with $V(y) = y^2 + \frac{\lambda y^2}{1+gy^2}$. $w_1(y) = \exp(-\alpha y^2)$, where α is chosen for the fatest convergence.

N	λ_1	λ_2	λ_3	λ_4	λ_5
		$\lambda = 1$	$g = 100$		
10	1.74034331	6.61289499	14.45434406	25.73416848	40.57425497
30	1.04840358	3.33049421	6.20396393	9.96961039	14.75340147
50	1.01083691	3.04192292	5.19309999	7.64468189	10.57282857
100	1.00841233	3.00987806	5.00989049	7.01481472	9.03654508
150	1.00841061	3.00983181	5.00927636	7.00985617	9.00959190
170	1.00841060	3.00983177	5.00927557	7.00984578	9.00949511
180	1.00841060	3.00983177	5.00927553	7.00984517	9.00948856
		$\lambda = 10$	$g = 100$		
10	2.12557689	8.03895659	17.66231586	31.55531547	49.82378424
50	1.09321568	3.19606870	5.54663516	8.42645412	11.98070336
100	1.08408954	3.09891916	5.09892856	7.13621223	9.24759634
150	1.08406343	3.09831922	5.09279892	7.09883559	9.09763231
170	1.08406335	3.09831722	5.09276616	7.09850083	9.09530236
180	1.08406335	3.09831706	5.09276332	7.09846755	9.09503285
		$\lambda = 100$	$g = 100$		
10	2.92175390	9.34160581	19.45189904	34.28680807	53.64778578
50	1.84742726	4.11049745	6.47955464	9.57139193	13.28590654
100	1.83638157	3.98422018	5.93857806	8.04492347	10.17201242
150	1.83633621	3.98310435	5.92841712	7.98535022	9.95499695
170	1.83633594	3.98309903	5.92834037	7.98458485	9.95023642
180	1.83633590	3.98309857	5.92833282	7.98449794	9.94960676

Table 4.3: Convergence of the eigenvalues with $V(y) = y^2 + \frac{\lambda y^2}{1+gy^2}$. $w_1(y) = \exp(-\alpha y^2)$, where α is chosen for the fatest convergence.

N	λ_1	λ_2	λ_3	λ_4	λ_5
		$\lambda = 1$	$g = 1$		
10	1.23272180	3.50666367	5.59128149	7.64562064	9.69097632
30	1.23235100	3.50738781	5.58978006	7.64819920	9.68404558
40	1.23235074	3.50738831	5.58977901	7.64820110	9.68404226
50	1.23235073	3.50738835	5.58977894	7.64820123	9.68404204
60	1.23235072	3.50738835	5.58977893	7.64820124	9.68404202
70	1.23235072		5.58977893	7.64820124	9.68404202
		$\lambda = 10$	$g = 1$		
10	2.78258502	7.41837822	10.73118613	13.60393371	16.67001724
20	2.78233137	7.41750412	10.70105591	13.38888589	15.82484591
30	2.78233053	7.41750587	10.70102563	13.38832411	15.81888465
40	2.78233052	7.41750590	10.70102558	13.38832349	15.81887151
45	2.78233052	7.41750590	10.70102558	13.38832349	15.81887149
50					15.81887149
		$\lambda = 100$	$g = 1$		
10	9.35945915	26.70572641	41.44628014	53.91385775	64.86511926
15	9.35941761	26.70596964	41.44114465	53.84147035	64.23043100
20	9.35941803	26.70596558	41.44110119	53.83917850	64.19022920
25	9.35941803	26.70596563	41.44109978	53.83909702	64.18763807
30		26.70596563	41.44109975	53.83909346	64.18745616
35			41.44109975	53.83909328	64.18744228
40				53.83909327	64.18744111
45				53.83909326	64.18744101
50				53.83909326	64.18744100
55					64.18744100

Table 4.4: Convergence of the eigenvalues with $V(y) = y^2 + \frac{\lambda y^2}{1+gy^2}$. Weight function $w_1(y) = \exp(-y^2\sqrt{1 + \frac{\lambda}{1+0.5g}})$.

N	λ_1	λ_2	λ_3	λ_4	λ_5
		$\lambda = 1$	$g = 10$		
10	1.06515662	3.08692234	5.08700592	7.08838586	9.09234744
30	1.06003407	3.08794408	5.08337022	7.09012096	9.08856179
50	1.05946708	3.08805698	5.08296831	7.09031284	9.08814362
100	1.05930820	3.08808859	5.08285570	7.09036658	9.08802645
150	1.05929829	3.08809057	5.08284868	7.09036993	9.08801914
170	1.05929756	3.08809071	5.08284816	7.09037018	9.08801860
180	1.05929736	3.08809075	5.08284802	7.09037025	9.08801845
		$\lambda = 10$	$g = 10$		
10	1.61407526	3.87252286	5.85545056	7.90700483	9.98909626
30	1.58268033	3.87852707	5.83441119	7.90231956	9.88401555
50	1.58046212	3.87895272	5.83303946	7.90301643	9.88258285
100	1.58003812	3.87903382	5.83277730	7.90314922	9.88230893
150	1.58002355	3.87903660	5.83276829	7.90315378	9.88229952
170	1.58002282	3.87903674	5.83276784	7.90315400	9.88229905
180	1.58002265	3.87903677	5.83276773	7.90315406	9.88229894
		$\lambda = 100$	$g = 10$		
10	5.89164179	11.65464995	14.22630311	17.92322840	22.47689280
30	5.79569188	11.57183960	13.62953798	15.99205694	17.99649871
50	5.79404301	11.57217532	13.62879829	15.98841237	17.97213192
100	5.79394280	11.57219667	13.62877155	15.98843409	17.97208577
130	5.79394234	11.57219677	13.62877143	15.98843420	17.97208563
140	5.79394232	11.57219677	13.62877142	15.98843420	17.97208562
150	5.79394231	11.57219677	13.62877142	15.98843421	17.97208562
160	5.79394230	11.57219678		15.98843421	
170	5.79394230	11.57219678			

Table 4.5: Convergence of the eigenvalues with $V(y) = y^2 + \frac{\lambda y^2}{1+gy^2}$. Weight function $w_1(y) = \exp(-y^2\sqrt{1 + \frac{\lambda}{1+0.5g}})$.

N	λ_1	λ_2	λ_3	λ_4	λ_5
		$\lambda = 1$	g = 100		
10	1.00943021	3.00981139	5.00980562	7.00981397	9.00989938
30	1.00902768	3.00981943	5.00959630	7.00982620	9.00973614
50	1.00883028	3.00982338	5.00949367	7.00983220	9.00965609
100	1.00860665	3.00982785	5.00937742	7.00983900	9.00956543
150	1.00851699	3.00982964	5.00933081	7.00984172	9.00952908
170	1.00849611	3.00983006	5.00931996	7.00984236	9.00952062
180	1.00848760	3.00983023	5.00931554	7.00984261	9.00951717
		$\lambda = 10$	g = 100		
10	1.09402833	3.09811836	5.09791649	7.09814755	9.09889054
30	1.08994543	3.09819977	5.09580087	7.09827100	9.09723424
50	1.08798805	3.09823881	5.09478843	7.09833030	9.09644473
100	1.08583151	3.09828179	5.09367433	7.09839559	9.09557603
150	1.08499665	3.09829842	5.09324340	7.09842085	9.09524005
170	1.08480631	3.09830221	5.09314518	7.09842660	9.09516348
180	1.08472929	3.09830374	5.09310544	7.09842893	9.09513250
		$\lambda = 100$	g = 100		
10	1.92323022	3.98167955	5.97436235	8.01099094	10.12548823
30	1.87989757	3.98225971	5.94937345	7.98317686	9.96554325
50	1.86200758	3.98260632	5.94066820	7.98370029	9.95876339
100	1.84549528	3.98292370	5.93271091	7.98417970	9.95257021
150	1.84038615	3.98302127	5.93026369	7.98432709	9.95066627
170	1.83936741	3.98304068	5.92977655	7.98435641	9.95028732
180	1.83897462	3.98304816	5.92958881	7.98436771	9.95014127

Table 4.6: Convergence of the eigenvalues with $V(y) = y^2 + \frac{\lambda y^2}{1+g y^2}$. Weight function $w_1(y) = \exp(-y^2 \sqrt{1 + \frac{\lambda}{1+0.5g}})$.

N	λ_1	λ_2	λ_3	λ_4	λ_5
		$\lambda = 1$	$g = 1$		
5	1.39754248	6.00256900	11.66691170	27.12138709	52.46889173
10	1.23347542	3.50334632	5.91911961	7.73245910	13.42453838
15	1.23235072	3.50738845	5.58977876	7.64821025	9.68403519
20	1.23235072	3.50738835	5.58977894	7.64820124	9.68404205
25		3.50738835	5.58977893	7.64820124	9.68404202
30			5.58977893		9.68404202
(b)	1.23235072	3.50738835	5.58977892	7.64820121	9.68404195
(c)	1.23235353	3.50739706	5.58983355	7.64906899	
		$\lambda = 10$	$g = 1$		
5	2.78138892	8.72184392	14.67163572	29.92249451	55.15913549
10	2.78233156	7.41816173	10.81174060	13.48916964	18.62437460
15	2.78233052	7.41750593	10.70102881	13.38872711	15.82253275
20	2.78233052	7.41750590	10.70102558	13.38832349	15.81887215
25		7.41750590	10.70102558	13.38832349	15.81887149
30					15.81887149
(c)	2.78233054	7.41767206	10.70448059	13.39000325	
		$\lambda = 100$	$g = 1$		
5	9.35957820	26.76092127	41.56662303	60.49260798	91.26562732
10	9.35941835	26.70595968	41.44117242	53.84491548	64.45670875
15	9.35941803	26.70596563	41.44109980	53.83909597	64.18766807
20	9.35941803	26.70596563	41.44109975	53.83909326	64.18744157
25			41.44109975	53.83909326	64.18744100
30					64.18744100
(c)	9.35941803	26.70596563	41.44109975	53.83909296	

Table 4.7: Convergence of the eigenvalues with $V(y) = y^2 + \frac{\lambda y^2}{1+gy^2}$. Weight function $w_1(y) = \exp(-\alpha_1 y^2)/(1 + gy^2)^{\alpha_2}$, where α_1 and α_2 are given in Table 10. Results from (b) Fack and Vanden Berghe (1985) [124]; (c) Lai and Lin (1982) [118].

N	λ_1	λ_2	λ_3	λ_4	λ_5
		$\lambda = 1$	$g = 10$		
10	1.06078000	3.10750137	5.34002953	7.84826441	12.39506550
12	1.05934121	3.08925905	5.10521689	7.20306392	9.76442476
15	1.05929700	3.08810693	5.08309896	7.09455928	9.11338782
20	1.05929690	3.08809085	5.08284789	7.09037308	9.08806709
25	1.05929688	3.08809085	5.08284767	7.09037041	9.08801812
30	1.05929688		5.08284768	7.09037041	9.08801810
35			5.08284768		9.08801810
		$\lambda = 10$	$g = 10$		
10	1.67530513	4.31996615	9.75230993	10.43741586	29.54884661
20	1.58002638	3.87916818	5.83491979	7.91869454	9.97591517
25	1.58002232	3.87903807	5.83278723	7.90346720	9.88457979
30	1.58002233	3.87903684	5.83276775	7.90315728	9.88233966
35	1.58002233	3.87903683	5.83276753	7.90315420	9.88229915
40		3.87903683	5.83276753	7.90315416	9.88229873
45				7.90315416	9.88229873
(b)	1.58002233	3.87903683	5.83276752	7.90315413	9.88229866
		$\lambda = 100$	$g = 10$		
10	7.48981433	8.03655640	44.09323078	49.71269815	149.70360371
20	5.79394731	11.57682425	13.70481854	16.27467472	19.37491150
25	5.79394193	11.57225713	13.62958358	16.00289112	18.03283044
30	5.79394232	11.57219704	13.62878139	15.98861076	17.97411182
35	5.79394230	11.57219678	13.62877147	15.98843650	17.97211015
40	5.79394230	11.57219678	13.62877142	15.98843422	17.97208593
45	.		13.62877142	15.98843421	17.97208562
50				15.98843421	17.97208562

Table 4.8: Convergence of the eigenvalues with $V(y) = y^2 + \frac{\lambda y^2}{1+gy^2}$. Weight function $w_1(y) = \exp(-\alpha_1 y^2)/(1 + gy^2)^{\alpha_2}$, where α_1 and α_2 are given in Table 10. (b) results from Fack and Vanden Berghe (1985) [124].

N	λ_1	λ_2	λ_3	λ_4	λ_5
		$\lambda = 1$	$g = 100$		
10	1.04129101	3.29082677	6.43712676	10.95519923	55.86316463
20	1.00841165	3.00986701	5.00988241	7.01509885	9.04372955
25	1.00841060	3.00983203	5.00928092	7.00992522	9.01020204
30	1.00841060	3.00983177	5.00927556	7.00984573	9.00949652
35		3.00983177	5.00927551	7.00984496	9.00948602
40			5.00927551	7.00984495	9.00948596
45				7.00984495	9.00948596
		$\lambda = 10$	$g = 100$		
10	1.45426410	5.01654653	29.97472996	72.98922478	243.24844347
20	1.08416996	3.10035001	5.11504606	5.81559287	7.21912972
30	1.08406336	3.09831782	5.09277943	7.09864757	9.09661478
40	1.08406334	3.09831700	5.09276191	7.09844919	9.09486638
45	1.08406334	3.09831700	5.09276189	7.09844907	9.09486470
50			5.09276190	7.09844907	9.09486466
55			5.09276190		9.09486466
		$\lambda = 100$	$g = 100$		
10	.25273328	58.55206092	526.35484897	565.24148666	1785.60704400
20	1.89936536	4.43121455	8.05177942	12.63918879	27.70284628
30	1.83635795	3.98374475	5.93607533	8.03086862	10.15714058
40	1.83633587	3.98309869	5.92833557	7.98453363	9.95000108
50	1.83633584	3.98309834	5.92832858	7.98444358	9.94916197
60	1.83633583	3.98309834	5.92832857	7.98444352	9.94916096
65	1.83633583		5.92832857	7.98444352	9.94916096
(b)	1.83633444	3.98309836	5.92832790	7.90315413	9.88229866

Table 4.9: Convergence of the eigenvalues with $V(y) = y^2 + \frac{\lambda y^2}{1+gy^2}$. Weight function $w_1(y) = \exp(-\alpha_1 y^2)/(1 + gy^2)^{\alpha_2}$, where α_1 and α_2 are given in Table 10. (b) Results from Fack and Vanden Berghe (1985) [124].

g/λ	1	10	100
1	(1,10)	(1.2,10)	(3,12)
10	(1.4,6)	(2,8)	(2,14)
10	(1.4,6)	(2,8)	(2,14)
100	(2,6)	(2.4,8)	(2.5,16)

Table 4.10: (α_1, α_2) used for Tables 4.7-4.9.

has suggested that a useful choice of weight function would be derived from the "super-potential" associated with the potential. This would require the solution of the Riccati equation [120] which is as difficult if not more so than the solution of the Schrödinger equation. However, we have also shown that this choice of weight function is not always the best choice. Nevertheless, we have used an empirical weight function of the form,

$$w_1(y) = \exp(-\alpha_1 y^2)/(1 + gy^2)^{\alpha_2}. \tag{4.4.1}$$

The results obtained with this weight function are shown in Tables 4.7-4.9. In Table 4.10, we list the values of α_1 and α_2 in the weight function. For all pairs of λ and g, we obtain convergence of the eigenvalues to 9-10 significant figures with no more than 60 quadrature points. It is useful to compare the convergence of λ_5 for $\lambda = 100$ and $g = 100$ in Table 4.9 and Table 4.3. In Table 4.3, λ_5 is converged to 9.950 with 180 quadrature points whereas it is converged to 9.94916096 with 50 points in Table 4.9. This demonstrates the usefulness of the QDM and the use of arbitrary weight functions to accelerate the convergence. This could mean a great decrease in computational times for two and three dimensional problems.

In Table 4.11, we compare the present results for λ_1 with the results reported in the literature by other workers. The methods used by others have been summarized in the introduction to the thesis. The weight function used is of the form given by Eq. (4.4.1)

λ	1	10	100	500
			g = 1	
QDM	1.232350723406	2.782330515932	9.359418026324	21.65874769959
a	1.23235072	2.78233052	9.35941803	
b	1.23235072			
c	1.24213			
d	1.23235353	2.78233054	9.35941803	
e	1.23237205	2.782330	9.35941803	21.6587477
f	1.23235	2.78233	9.3594	
			g = 10	
QDM	1.059296880862	1.580022327392	5.793942300193	16.73274738223
a	1.05929688	1.58002233	5.79394230	
b		1.58002233		
e	1.05929700	1.5800249	5.793947	16.73919
f	1.05929	1.58002	5.794	
			g = 100	
QDM	1.008410597947	1.084063335494	1.836335833449	5.083683913501
a	1.00841060	1.08406334	1.83633583	
b			1.83633444	
c		1.08411	1.8411	
e	1.0084106	1.0840543	1.8363850	5.0840857
f	1.00841	1.08406	1.8364	
			g = 500	
QDM	1.001849154630	1.084063335494	1.18486023962	1.92317625551
a				
c			1.18451	1.92255
e	1.0018491	1.0184910	1.1848632	1.9232260

Table 4.11: Comparison of the results of λ_1 with $V(y) = y^2 + \frac{\lambda y^2}{1+gy^2}$. a. Scherrer, Risken and Leiber (1988) [129], b. Fack and Vanden Berghe (1985) [124], c. Chaudhuri and Mukherjee (1983) [107], d. Lai and Lin (1982) [118], e. Bessis and Bessis (1980) [104], f. Mitra (1978) [101].

with values of α_1 and α_2 which are chosen empirically for different values of λ and g. The QDM results shown in this table are converged to the significant figures shown; either 12 or 13. These converged results are considered to be accurate based on our experience in the calculation for analytic models. The most difficult parameter region is for $g = 500$ and as can be seen from the results in the table, we have achieved remarkable convergence with $g = 500$. The only other work to compare with are the results by Bessis and Bessis [104] and by Chaudhuri and Mukherjee [107]. The QDM results are far superior to the previous results.

Figure 4.2 shows the variation of the error in λ_1 for the NPO model ($g = \lambda = 10$) versus the number of quadrature points, n, for four different weight functions. λ_1^{exact} is defined as the eigenvalue converged to 14 significant figures calculated with the QDM. The fourth weight function (d) gives the most rapid convergence. The significant improvement with weight function (d) over the scaled Gaussian weight function can be explained with the variation of the eigenfunction shown in Figures 4.3 and 4.4. The convergence of the eigenvalue depends on the accurate determination of the eigenfunction near the origin. Figures 4.3 and 4.4 show the details of the ground state eigenfunction near the origin. The solid curves are determined with the new weight function, Eq. (4.4.1), and N = 140. This is considered to be very close to the exact result. The other results are obtained with N = 25. Figure 4.3 is for $g = \lambda = 100$ for three different weight functions; Hermite polynomials (*), scaled Hermite polynomials (+) and the new weight function (o). Figure 4.3B shows the eigenfunction on a small scale near the origin.

From the figure, we see that the points generated from the scaled Gaussian weight function can not describe the rapid variation of the eigenfunction near the origin. However, the new weight function, with a denser grid of quadrature points near the origin where the potential (Fig. 4.1) and the eigenfunction vary rapidly, is better. It is clear that the results with the new weight function, Eq. (4.4.1), gives the best convergence.
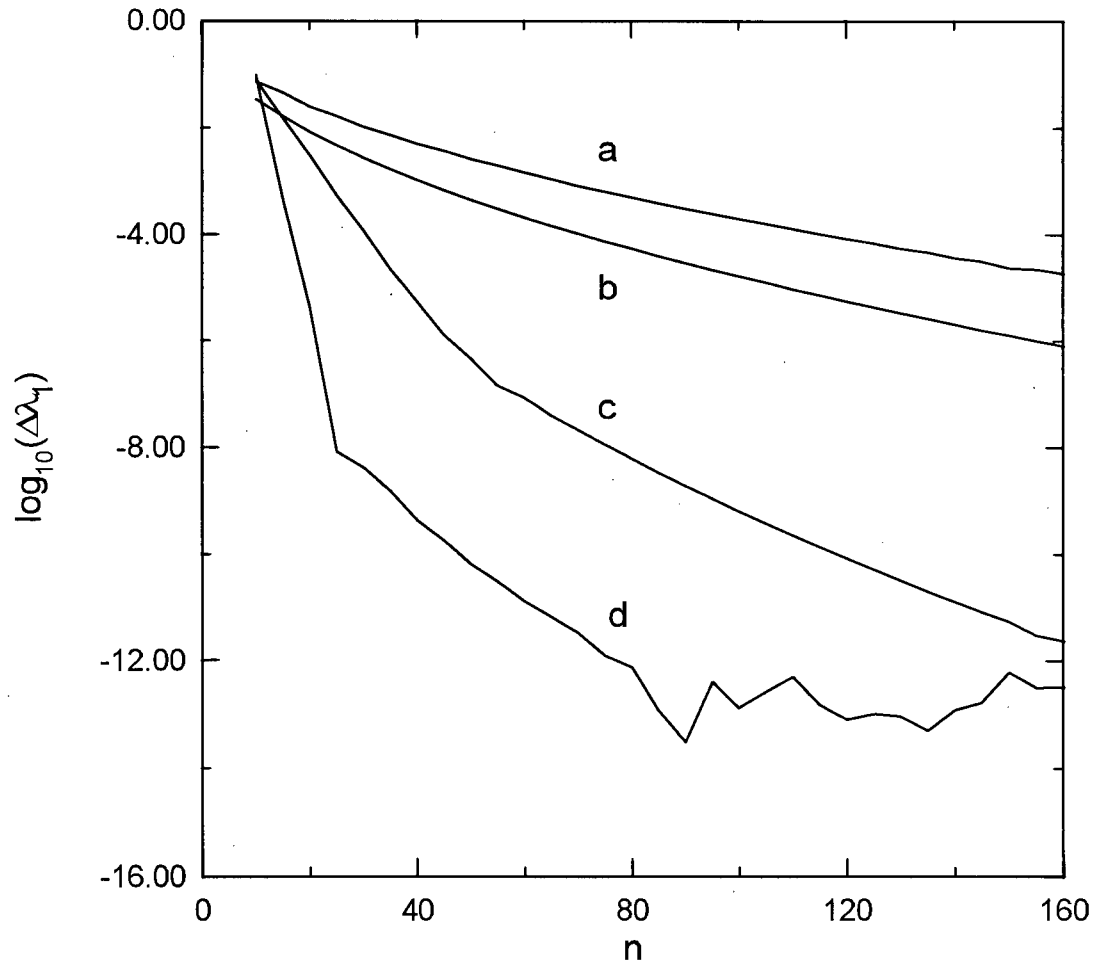
Figure 4.2: Variation of the error in λ_1, $\Delta\lambda_1 = |\lambda_1 - \lambda_1^{exact}|$ for the NPO potential versus the number of grid points n for different weight functions. (a) $w(y) = \exp(-y^2)$, (b) $w(y) = \exp(-y^2\sqrt{1 + \frac{\lambda}{1+0.5g}})$, (c) $w(y) = \exp(-5.8y^2)$, (d) $w(y) = \frac{\exp(-2y^2)}{(1+gy^2)^8}$; $\lambda = g = 10$
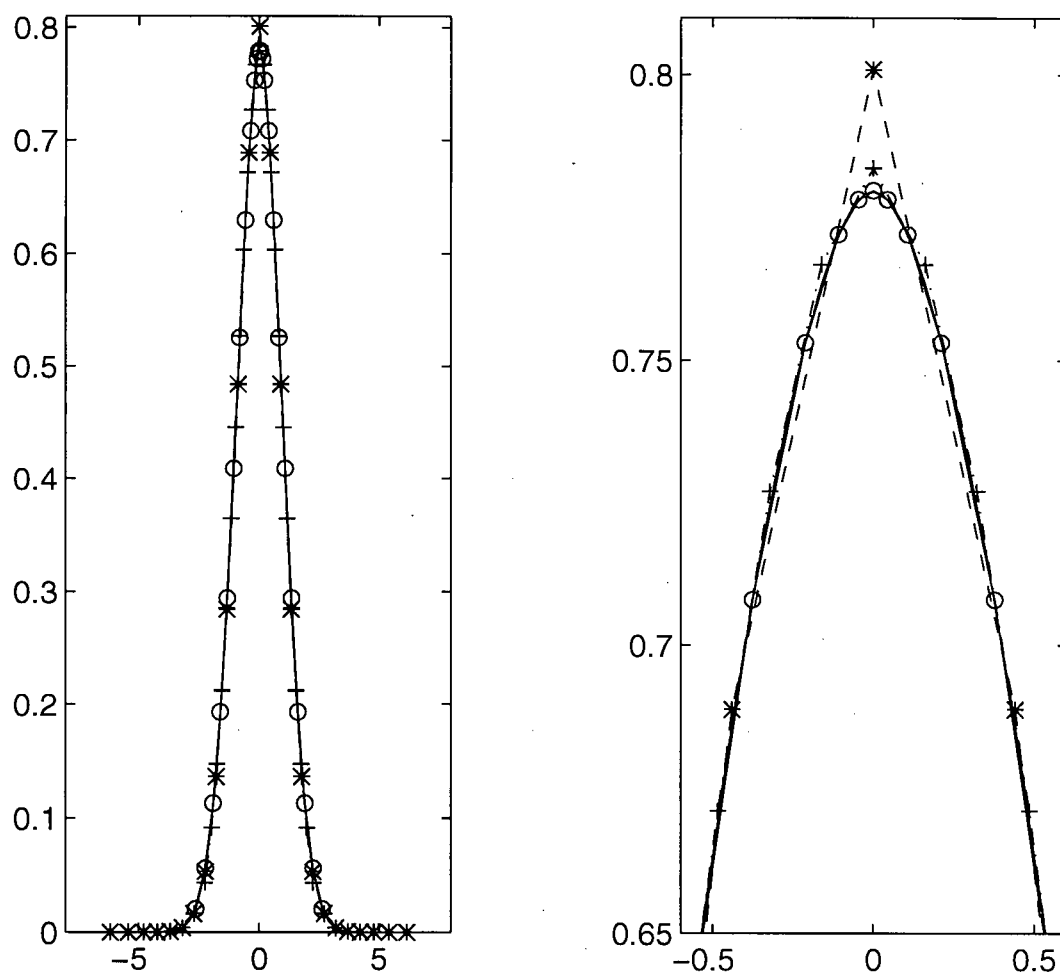
Figure 4.3: Ground state eigenfunction for the NPO potential with $g = \lambda = 100$, $N = 25$, with different weight functions. ($*$) $w(y) = \exp(-y^2)$, ($+$) $w(y) = \exp(-17y^2)$ and (o) $w(y) = \frac{\exp(-3y^2)}{(1+gy^2)^8}$. The solid curve is for the last weight function with N=140; (A) full scale; (B) small scale near the origin.
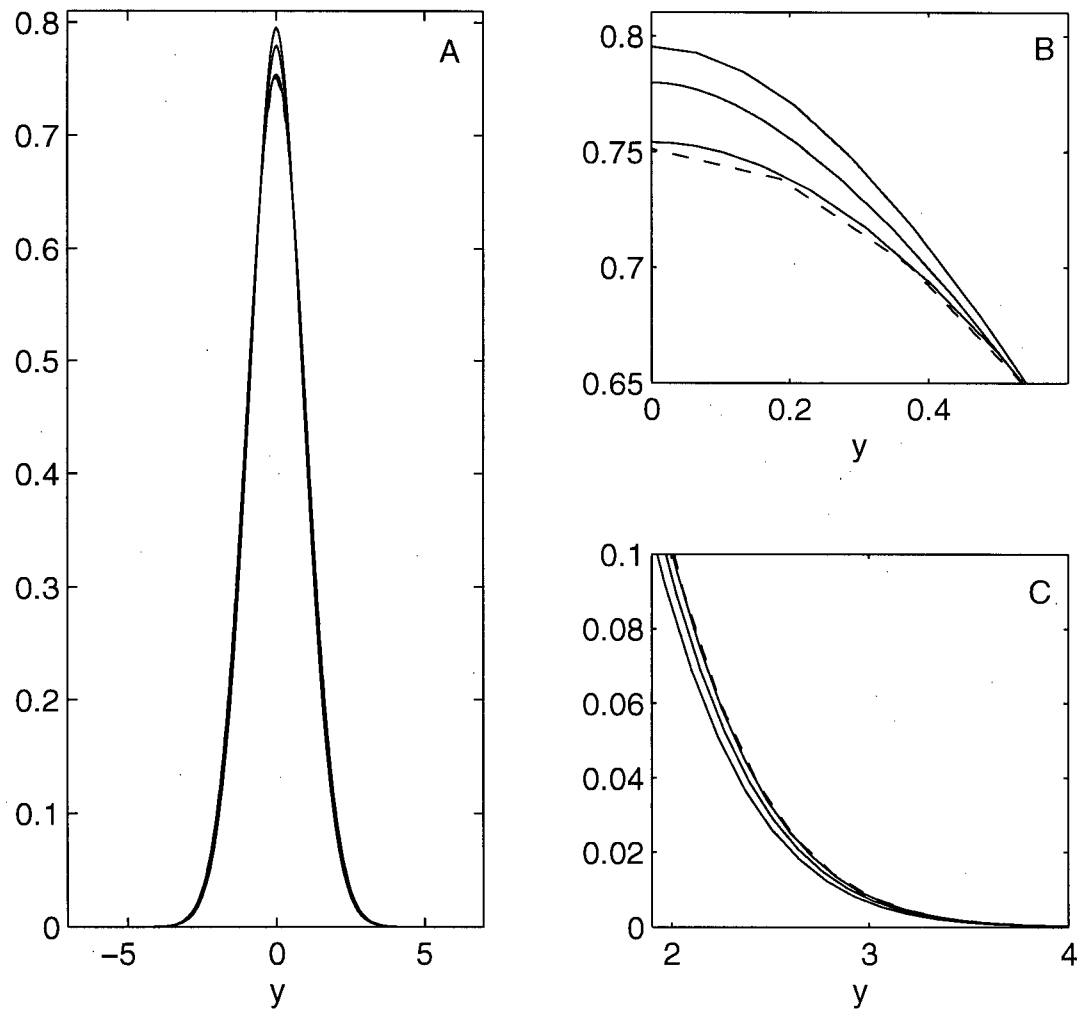
Figure 4.4: Ground state eigenfunction for the NPO potential. λ and g are equal to (a) 10, 10 (b) 100, 100 (c) 10, 100 and (- - -) 0, 0. (A) full scale; (B) small scale near the origin; (C) small scale at large positions from the origin.

Figure 4.4 shows the behavior near the origin for three different pairs of values of g and λ. Figure 4.4B shows the small scale behavior near the origin whereas Fig. 4.4C shows the small scale behavior at large positions from the origin. The dashed curve is the result with the Gaussian weight function.

If the potential belongs to the class of potentials in supersymmetric quantum mechanics [114,115], then the ground state eigenfunction is known with the eigenvalue equal to zero. This is the case for the potential given by Eq. (4.1.3), considered by Sinha et al [131]. The weight function that corresponds to the superpotential is of the form,

$$w_2(y) = \exp(-y^4/4) \tag{4.4.2}$$

The basis set was determined following the prescription by Gautschi [134] and the quadrature points as described in the earlier papers. For this choice of weight function, $V(y) \equiv \tilde{V}(y)$ and the representative of the Hamiltonian in the QDM representation is from Eq. (4.3.8) given by $H_{ij} = \sum_k D_{ki}D_{kj}$. We have studied the convergence of the eigenvalues for this potential with three different weight functions one of which corresponds to the Hermite polynomials, $w_2(y)$ defined earlier with $\alpha = 5$, and another given by,

$$w_2(y) = \exp(-y^4/4 - 5y^2) \tag{4.4.3}$$

The results with the three weight functions are shown in Table 4.12. The overall convergence is very similar with all three weight functions, although the second weight function Eq. (4.4.2) appears to give marginally faster convergence, in particular for the first eigenvalue. Our results are consistent with the results of Sinha et al [131] to the precision that they report in their paper.

The third potential (Eq. (4.1.4)) chosen was studied by Braun *et al* [125] and Kaluza [130] and also belongs to the class of potentials in supersymmetric quantum mechanics. Kaluza chose basis functions such that the matrix representative of the Hamiltonian is

N	λ_1	λ_3	λ_5	λ_{10}
		$w_2(y) = \exp(-5y^2)$		
5	3.20578381	19.34421619		
10	1.92166391	11.48428663	24.44773756	
15	1.93541230	11.67877474	25.22960745	72.68872477
20	1.93548442	11.68098869	25.25435384	71.64137641
25	1.93548209	11.68097117	25.25461676	71.57368183
30	1.93548210	11.68097087	25.25460450	71.57923539
35		11.68097089	25.25460490	71.57902800
40			25.25460488	71.57903698
45				71.57903668
50				71.57903669
		$w_2(y) = \exp(-y^4/4)$		
5	1.95003306	13.51720225		
10	1.93549705	11.68815652	25.58769695	
15	1.93548226	11.68108903	25.26571988	75.81549114
20	1.93548210	11.68097109	25.25463882	72.04071624
25		11.68097089	25.25460546	71.58445530
30			25.25460488	71.57920993
35				71.57903737
40				71.57903670
45				71.57903669
		$w_2(y) = \exp(-y^4/4 - 5y^2)$		
5	4.54466778	23.73100470		
10	2.23089971	13.39054786	31.59035642	
15	1.94701006	11.78606709	25.89623300	83.65936104
20	1.93570651	11.68371077	25.28051990	73.07062002
25	1.93548392	11.68099725	25.25493023	71.64923337
30	1.93548212	11.68097108	25.25460771	71.57992969
35	1.93548210	11.68097089	25.25460489	71.57904422
40		11.68097089	25.25460488	71.57903671
45				71.57903669

Table 4.12: Convergence of the eigenvalues for SE with $V(y) = y^6 - 3y^2$.

tridiagonal. The generation of the basis set is essentially a Gram-Schmidt orthogonalization which is subject to considerable round-off errors [75,143]. Kaluza avoids these numerical difficulties by using symbolic algebraic techniques in mathematics. For arbitrary weight functions, this analytic approach is not feasible, whereas the Gautschi algorithm is generally convergent. Braun *et al* [125] employed a spectral method of solution based on Chebyshev polynomials on a finite interval where the cutoff at y = 8 is an additional parameter. They used up to 512 grid points and report the first 48 eigenvalues up to 18 significant figures. We have chosen the weight function,

$$w_3(y) = \exp(-2y^2 - y^4/2) \tag{4.4.4}$$

and determined the matrix representative of the Hamiltonian in the "polynomial basis" representation, Eq. (4.3.5) with $V_{nm} - \tilde{V}_{nm} = 2$. The matrix elements of the Hamiltonian are determined with the quadrature define by the weight function, Eq. (4.4.4). Because of the symmetry of the potential, the eigenfunctions are of either even or odd parity. The matrix H_{nm} of dimension $N \times N$ can be decomposed into two matrices for the odd and even eigenfunctions each of dimension $\frac{N}{2} \times \frac{N}{2}$. Since the matrix H_{nm} is pentadiagonal, the submatrices of even and odd parity are tridiagonal. The convergence of the eigenvalues from the numerical diagonalization of these tridiagonal matrices is rapid. The first 48 eigenvalues converge to 13 significant figures with less than 100 grid points and agree with the results by Braun *et al.*

The fourth potential studied is given by Eq. (4.1.5). This potential is not in the class of potentials in supersymmetric quantum mechanics. We have in the first instance used scaled Hermite polynomials and the associated quadrature points to determine the eigenvalues with Eq. (4.3.8). The convergence of the lower order eigenvalues is shown in Table 4.14 for three values of ϵ. The scaling is very important in order that the grid points are distributed over the region of y where the eigenfunctions are concentrated.

N	λ_1	λ_3	λ_5	λ_7
1	1.00000000000000000			
3	1.00000000000000000	15.832389169799		
5		15.124216267224	40.6232236023546	
8		15.118931530866	36.367167641896	66.261603950851
10		15.118929992544	36.343021051640	62.648395926012
15		15.118929986242	36.342716214160	62.356049424923
20		15.118929986242	36.342716212413	62.356028944861
25			36.342716212413	62.356028944603
30				62.356028944604
35				62.356028944604

N	λ_{20}	λ_{30}	λ_{40}	λ_{48}
30	310.4920471524	848.8060217068		
40	309.4993497820	588.5806628599	1346.579274312	
50	309.4993484837	566.4282265701	947.4614543288	1597.421054106
55	309.4993484837	566.4026817440	893.9968790569	1364.247596709
60		566.4026355012	872.0907745529	1248.445773964
65		566.4026354734	868.2562193165	1183.544197185
70		566.4026354734	868.1457422322	1149.943901457
75			868.1452015357	1138.668487703
80			868.1452006773	1137.541785229
85			868.1452006767	1137.522672203
90			868.1452006767	1137.522588690
95				1137.522588541
100				1137.522588541

Table 4.13: Convergence of the eigenvalues of even parity with $V(y) = \frac{1}{2}y^2 + 2y^4 + \frac{1}{2}y^6$. $w_3(y) = \exp(-2y^2 - y^4/2)$.

With the notion that the optimal weight function should be the square of the ground state eigenfunction, we have fitted, to polynomials, the ground state eigenfunction determined previously with Hermite quadrature points. This is an alternative to solving the Riccati equation for the superpotential [106]. The fit is reasonably accurate but $V(y)$ is not exactly equal to $\tilde{V}(y)$. In Table 4.15, we show the convergence of the eigenvalues with this alternate weight function. The results with this weight function show a moderate improvement in the rate of convergence. We find for example that with the new weight function for $\epsilon = 100$, λ_1 is converged to 9 significant figures with 15 points whereas 20 points are required with scaled Hermite polynomials. Similarly, λ_3 is converged to 8 significant figures with 20 points whereas 25 are required with scaled Hermite polynomials. The choice of weight function is clearly important for the rapid convergence of the eigenvalues.

The QDM is also applied to a two-dimensional Schrödinger equation with Henon-Heiles potential, given by

$$\left[-\frac{1}{2}\frac{\partial^2}{\partial^2 x} - \frac{1}{2}\frac{\partial^2}{\partial^2 y} + V(x,y) \right] \psi_{nl}(x,y) = \lambda_{nl}\psi_{nl}(x,y), \qquad (4.4.5)$$

where $V(x,y) = \frac{1}{2}(x^2 + y^2) + \lambda x(y^2 - \frac{1}{3}x^2)$ and $\lambda = \sqrt{0.0125}$, consistent with the choice of previous workers. Since the parameter λ is not too large and the Hamiltonian is close to the two-dimensional harmonic oscillator, we choose, in the first instance, the discretization based on Hermite polynomials in both the x and the y directions. The QDM representation of the Hamiltonian given by Eq. (4.3.18) is easily constructed, with the potential function evaluated at the quadrature points in each dimension. The numerical diagonalization of the QDM matrix yields the eigenvalues and eigenfunctions.

The convergence of the two basis sets in each variable is shown in Table 4.16. N_x and N_y are the numbers of quadrature points in x and y dimension, respectively. In the tables, the eigenvalues are labeled with the principle quantum number n and angular

N	λ_1	λ_3	λ_5	λ_{10}
		$\epsilon = 10^{(a)}$		
12	2.44917485	16.63595545	35.88068953	94.30085478
15	2.44917408	16.63591955	35.88506209	95.81165911
20	2.44917407	16.63592150	35.88517148	96.15949348
25	2.44917407	16.63592149	35.88517122	96.15623411
30		16.63592149	35.88517122	96.15626312
35				96.15626298
40				96.15626298
		$\epsilon = 100^{(b)}$		
10	4.99945382	34.87447875	75.72914876	253.32604009
12	4.99941563	34.87402295	75.88739267	201.40793502
15	4.99941758	34.87398862	75.87689375	205.27637088
20	4.99941755	34.87398427	75.87700463	204.79428957
25	4.99941755	34.87398426	75.87700403	204.79476335
30		34.87398426	75.87700403	204.79477459
35				204.79477451
40				204.79477451
		$\epsilon = 10000^{(c)}$		
10	22.86146298	160.68335404	350.84170426	1022.19210882
12	22.86161867	160.68601691	350.38352262	924.84691394
15	22.86160889	160.68588347	350.43503532	944.02953926
20	22.86160887	160.68591272	350.43589703	947.71986787
25	22.86160887	160.68591261	350.43589621	947.68562278
30		160.68591261	350.43589622	947.68596392
35			350.43589622	947.68596166
40				947.68596167
45				947.68596167

Table 4.14: Convergence of the eigenvalues with $V(y) = y^2 + \epsilon y^4$. $^{(a)}w_4(y) = \exp(-6y^2)$; $^{(b)}w_4(y) = \exp(-10y^2)$; $^{(c)}w_4(y) = \exp(-60y^2)$.

N	λ_1	λ_3	λ_5	λ_{10}
$\epsilon = 10^{(a)}$				
10	2.44917318	16.63603391	35.86694240	107.31938413
12	2.44917406	16.63593038	35.88380588	98.84824260
15	2.44917407	16.63592170	35.88516632	96.71828902
20	2.44917407	16.63592149	35.88517122	96.16096863
25		16.63592149	35.88517122	96.15625913
30				96.15626298
35				96.15626298
$\epsilon = 100^{(b)}$				
12	4.99941762	34.87397375	75.87733275	210.04422203
15	4.99941755	34.87398436	75.87701004	205.20313119
20	4.99941755	34.87398426	75.87700401	204.79819433
25		34.87398426	75.87700403	204.79477654
30			75.87700403	204.79477452
35				204.79477451
40				204.79477451
$\epsilon = 10000^{(c)}$				
10	22.86160088	160.68728162	350.26068143	1055.94778633
12	22.86160897	160.68596913	350.42650209	973.50076873
15	22.86160887	160.68591446	350.43583997	952.12677503
20	22.86160887	160.68591261	350.43589612	947.72238259
25		160.68591261	350.43589622	947.68593841
30			350.43589622	947.68596166
35				947.68596167
40				947.68596167

Table 4.15: Convergence of the eigenvalues with $V(y) = y^2 + \epsilon y^4$ calculated by fitting weight function to ground state eigenfunction. $^{(a)}w_4(y) = \exp(-(y^4 + 5y^2)/2)$; $^{(b)}w_4(y) = \exp(-(2y^4 + 6y^2))$; $^{(c)}w_4(y) = \exp(-(50y^4 + 25y^2))$.

momentum quantum number l, as discussed by Noid and Marcus [174]. The convergence of the lower-order eigenvalues is very rapid. Although the higher eigenvalues converge slower, the convergence is evidently still rapid. Even for the 80th eigenvalue, $\lambda_{12,2}$, only 28 basis functions were required in each dimension. We cannot comment on the rate of convergence of other methods, since these are not reported by the earlier authors.

The contour plots of several eigenfunctions are shown in Fig. 4.5 . The C_{3v} symmetry of the eigenfunction is clearly evident and essentially converged with 32 new basis functions. It is surprising that this small number of basis functions can resolve the details of the eigenfunctions as shown in Fig. 4.5.

Since the basic idea of the QDM is to suggest nonclassical basis functions for which the rate of convergence is increased, we have also used the grid points based on the polynomials orthogonal with respect to the weight function,

$$u(x) = \left[-x^2 + \frac{2}{9}\lambda x^3 \right] \tag{4.4.6}$$

The grid points in y remain defined by the Hermite polynomials. We find some improvement in the rate of convergence, as shown in Table 4.17 for a selected number of eigenvalues. Since the potential is similar to a two-dimensional harmonic oscillator by virtue of the choice of the value λ, it is not surprising that the Hermite basis set works as well as it does. The rates of convergences of the eigenvalue in the x and y dimensions are similar for both weight functions we applied. In Table 4.18, we compare, with the results of Feit *et al* [164], where the eigenvalues occur in almost degenerate pairs. Their results were calculated with 128×128 Fourier basis functions. Our results in this table for Hermite quadrature points converge to the significant figures shown with $N_x = N_y = 50$. With the new quadrature defined by the weight function given by Eq. (4.4.6), this convergence is achieved with $N_x = N_y = 32$. This demonstrated a significant saving of computational time in comparison with other researchers. As can be seen from

N_y/N_x	4	6	8	10	12	16	20	24	28
			$\lambda_{2,0}$ (4th)						
4	2.9692	2.9605	2.9601	2.9601					
6	2.9632	2.9566	2.9563	2.9563					
8	2.9631	2.9566	2.9563	2.9562					
			$\lambda_{5,1}$ (16th)						
4	7.0182	5.9903	5.9126	5.9092	5.9089				
6	5.9505	5.8914	5.8677	5.8322	5.8256				
8	5.8784	5.8311	5.8279	5.8242	5.8192				
10	5.8716	5.8204	5.8179	5.8176	5.8176				
12	5.8713	5.8198	5.8174	5.8171	5.8170				
16	5.8712	5.8198	5.8174	5.8170	5.8170				
			$\lambda_{8,8}$ (44th)						
4					13.2657	12.6973	12.2964		
6			11.0336	10.1869	10.1688	10.1686	10.1686		
8		11.1240	9.6935	9.1708	9.1287	9.1284	9.1284		
10		10.0448	9.0536	9.0347	9.0264	9.0241	9.0240		
12	13.1807	9.9003	9.0499	9.0334	9.0247	9.0223	9.0222		
16	12.4574	9.8905	9.0497	9.0330	9.0243	9.0218	9.0217		
			$\lambda_{9,-9}$ (54th)						
4						15.4681	14.5918	14.5446	
6				12.2319	12.1574	11.6740	11.5832	11.5749	
8			11.2850	10.7096	10.6113	10.4985	10.4785	10.4774	
10		12.4479	10.6346	10.1248	10.0684	10.0643	10.0640	10.0639	
12		11.8715	10.5047	10.1240	10.0441	10.0379	10.0375	10.0375	
16	15.5873	11.4840	10.3447	10.1237	10.0425	10.0361	10.0356	10.0355	
20	14.9696	11.4788	10.3234	10.1237	10.0425	10.0360	10.0355	10.0354	
			$\lambda_{10,10}$ (65th)						
4							17.8647	17.2548	17.0406
6					14.1919	13.5202	13.2560	13.1758	13.1734
8				12.3695	12.1856	11.8637	11.8527	11.8502	11.8489
10			12.3214	11.5307	11.2580	11.1959	11.1959	11.1699	11.1609
12		14.4481	11.9189	11.1145	11.0690	11.0547	11.0532	11.0531	11.0531
16		13.4192	11.6239	11.1072	11.0642	11.0515	11.0506	11.0502	11.0501
20	18.1812	13.2653	11.6110	11.1055	11.0637	11.0512	11.0499	11.0498	11.0497
24	17.7635	13.2631	11.6095	11.1051	11.0636	11.0512	11.0498	11.0497	11.0497
			$\lambda_{12,2}$ (80th)						
4							26.0197	21.9893	21.0597
6						16.2730	16.0380	15.8520	15.5594
8				17.2961	14.4322	13.7976	13.4736	13.4400	13.4335
10			17.7483	13.5335	13.0533	12.8019	12.6324	12.6245	12.6207
12			14.3616	12.8665	12.5890	12.3091	12.2442	12.2176	12.2143
16		16.1730	13.4822	12.4343	12.3128	12.1503	12.1477	12.1465	12.1463
20	25.3965	15.9680	13.3034	12.3997	12.2177	12.0693	12.0666	12.0655	12.0651
24	21.9153	15.6562	13.2932	12.3940	12.2139	12.0689	12.0660	12.0652	12.0651
28	21.3602	15.5597	13.2926	12.3932	12.2138	12.0689	12.0660	12.0651	12.0650

Table 4.16: Convergence of the eigenvalues, $\lambda_{n,l}$, for the Henon-Heiles potential with Hermite points[a]. [a]Weight function, $u(x) = exp(-x^2)$ and $v(y) = exp(-y^2)$.
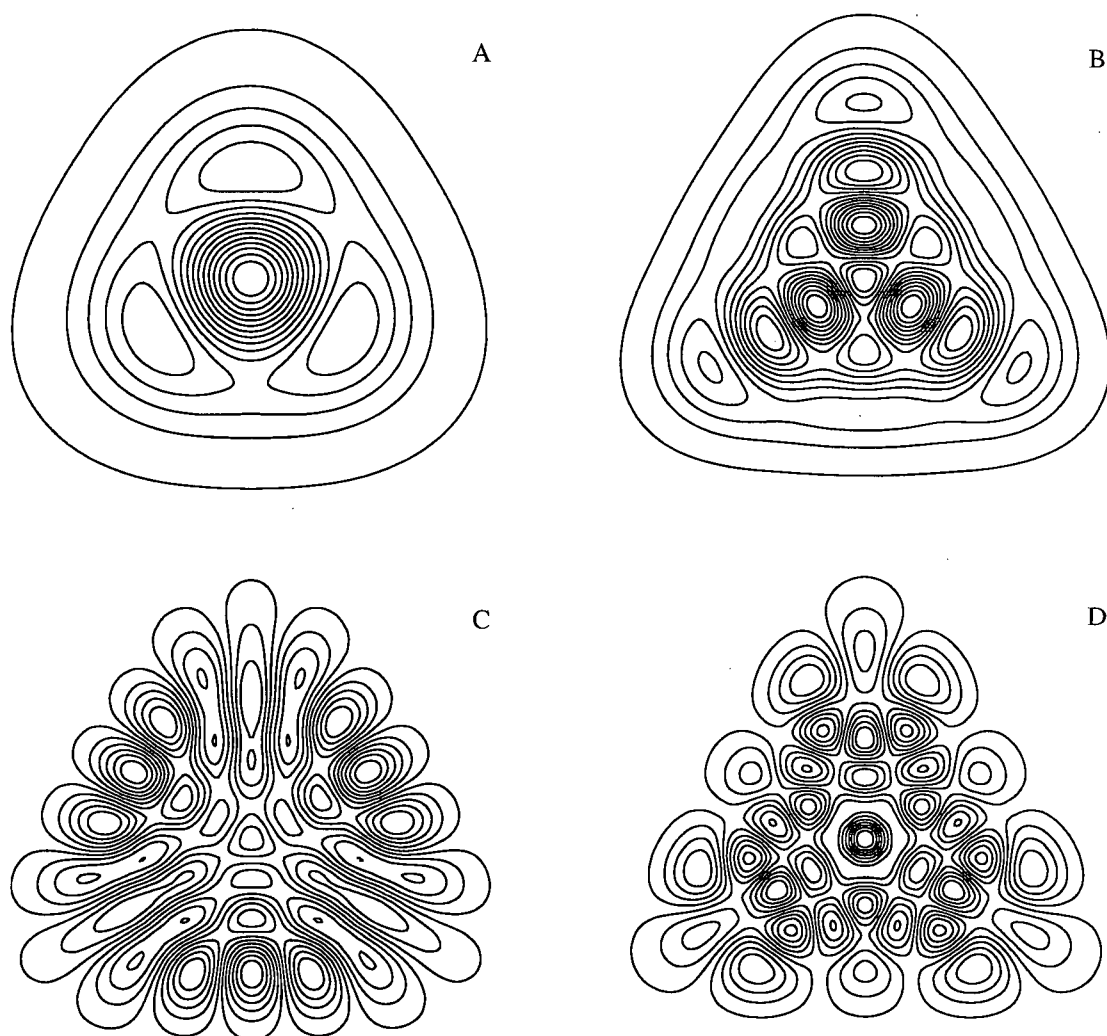
Figure 4.5: Contour plots of the eigenfunctions of the Schrödinger equation for the Henon-Heiles potential with n and l equal to (a) 2,0 (b) 6,0 (c) 9,-9 and (d) 10,6. new quadrature points were used with $N_x = N_y = 32$.

N_y/N_x	4	6	8	10	12	16	20	24
$\lambda_{2,0}$ (4th)								
4	2.9616	2.9601						
6	2.9575	2.9563						
8	2.9575	2.9562						
$\lambda_{5,1}$ (16th)								
4	7.0082	5.9439	5.9089	5.9089				
6	5.9531	5.8738	5.8283	5.8248				
8	5.8413	4.9878	4.9865	4.9865				
10	5.8764	5.8185	5.8176	5.8172				
12	5.8761	5.8179	5.8171	5.8170				
16	5.8761	5.8179	5.8170	5.8170				
$\lambda_{8,8}$ (44th)								
4					12.7920	12.2620		
6			11.1456	10.1687	10.1686	10.1686		
8		11.2597	9.7190	9.1286	9.1284	9.1284		
10		10.0603	9.0446	9.0250	9.0241	9.0240		
12	13.2729	10.0034	9.0436	9.0232	9.0222	9.0222		
16	12.5442	9.9984	9.0433	9.0227	9.0218	9.0217		
$\lambda_{9,-9}$ (54th)								
4						14.7114		
6				12.2173	11.7764	11.5794		
8			11.3010	10.6143	10.5439	10.4775		
10		12.5191	10.6767	10.0691	10.0644	10.0639		
12		11.9125	10.5473	10.0420	10.0379	10.0375		
16	15.6786	11.5413	10.3703	10.0403	10.0361	10.0355		
20	15.0393	11.5353	10.3499	10.0403	10.0360	10.0354		
$\lambda_{10,10}$ (65th)								
4							17.1066	
6					14.1440	13.2565	13.1733	
8				12.3709	11.9700	11.8518	11.8489	
10			12.3221	11.5196	11.1959	11.1959	11.1608	
12		14.4451	11.9199	11.0714	11.0553	11.0531	11.0531	
16		13.4728	11.7027	11.0702	11.0517	11.0504	11.0501	
20	18.2794	13.3615	11.6918	11.0697	11.0514	11.0498	11.0497	
$\lambda_{12,2}$ (80th)								
4							23.8554	20.5669
6						16.0422	15.6786	15.2330
8				17.2781	14.3895	13.4600	13.4334	13.4323
10			17.9498	13.6380	12.9474	12.6293	12.6209	12.6180
12			14.4303	12.8445	12.3391	12.2266	12.2142	12.2141
16		16.2757	13.5128	12.4913	12.1806	12.1469	12.1463	12.1462
20	25.6830	15.9901	13.3842	12.4590	12.1705	12.0660	12.0651	12.0651
24	21.9864	15.7582	13.3790	12.4532	12.1701	12.0654	12.0651	12.0650

Table 4.17: Convergence of eigenvalues, $\lambda_{n,l}$, for the Henon-Heiles potential with new points[b]. [b]Weight function, $u(x) = exp(-x^2 + \frac{2}{9}\lambda x^3)$ and $v(y) = exp(-y^2)$.

the results in Table 4.18, we have obtained excellent agreement with the previous results. For $n \leq 11$ our results are smaller than those of Feit *et al*, whereas for $n \geq 11$ our results are slight larger.

4.5 Summary

In this chapter, we have provided an extensive study of the use of the QDM in the solution of the Schrödinger equation for several one-dimensional and two-dimensional potential functions considered recently by several other researchers. The main theme of this work is to determine the optimal set of basis functions, equivalently the weight function, that provides rapid convergence of the eigenvalues versus the number of basis functions or grid points. Although this work is more restricted to one-dimensional problems, the extension to two and three dimensions is straightforward [51] as shown for the Henon-Heiles problem given in this chapter. The eigenvalues can be determined by the numerical diagonalization of the representative of the Hamiltonian in either the polynomial or the discrete basis. The work in this chapter generally employed the discretized version of the Hamiltonian at a set of points that correspond to the quadrature points associated with the chosen weight function. The distribution of grid points is determined by the weight function, which controls the convergence of the eigenvalues and eigenfunctions. We have demonstrated in this chapter the flexibility of the QDM in that arbitrary weight functions can be employed to improve the rate of convergence. In some cases, the improvement is remarkable such as for the nonpolynomial oscillator.

n	l	Feit *et al.*	QDM[a]	QDM[b]
3	3	3.9825	3.982 417	nc[c]
	-3	3.9859	3.985 761	nc
5	3	5.8672	5.867 015	nc
	-3	5.8816	5.881 446	nc
6	6	6.9991	6.998 932	nc
	-6	6.9996	6.999 387	nc
7	3	7.6979	7.697 721	nc
	-3	7.7371	7.736 885	nc
8	6	8.8116	8.811 327	nc
	-6	8.8154	8.815 188	nc
9	9	10.0356	10.035 413	nc
	-9	10.0359	10.035 592	nc
10	6	10.5727	10.572 480	nc
	-6	10.5907	10.590 470	nc
11	3	11.1603	11.160 258	11.160 259
	-3	11.3253	11.325 231	nc
11	9	11.7497	11.749 519	nc
	-9	11.7525	11.752 297	nc
12	6	12.3335	12.333 785	12.333 786
	-6	12.2771	12.277 192	nc
12	12	12.7474	12.748 445	12.748 520
	-12	13.0310	13.032 062	13.032 065
13	3	13.0868	13.086 873	nc
	-3	13.0800	13.081 196	13.081 199

Table 4.18: Eigenvalues for the Henon-Heiles potential. [a]Hermite qudrature points based on $u(x) = exp(-x^2)$ and $v(y) = exp(-y^2)$, with $N_x = N_y = 50$. [b]New quadrature points based on $u(x) = exp(-x^2 + \frac{2}{9}\lambda x^3)$ and $v(y) = exp(-y^2)$, with $N_x = N_y = 32$. [c]nc indicates no change from the QDM[a] results.

Chapter 5

Summary and future work

In previous chapters, we have presented the quadrature discretization method (QDM) and have applied it to some model problems as well as a large class of Fokker-Planck equations and Schrödinger equations. It has been shown that the QDM is easy to implement. The method provides high accuracy and rapid convergence, and is very efficient in solving high dimensional PDEs. Unlike most spectral methods and FD methods, it is possible for the QDM discretization to preserve the symmetry for the self-joint joint differential operator. Furthermore, by introducing Stieltjes's procedure, one can generate a set of nonclassical polynomials for any weight function, which is a significant improvment from previous work by Shizgal and Blackmore [71,72,74]. The flexibility of the QDM in choosing weight function provides one the opportunity to achieve the best solution with the least computing work.

The QDM is a discretization procedure based on a grid of points that coincide with the quadrature points defined by a weight function over some interval. The major advantage of the QDM over the classical spectral method is that the QDM allows one to use nonclassical polynomial basis set such that more choices are provided in the solution of differential equations. In the case that the basis functions are classical, the QDM is equivalent to the classical pseudospectral method. By introducing the Stieltjes's procedure, it is easy for one to construct a set of nonclassical polynomials defined by an arbitrary weight function accurately. For a specific problem, a specific weight function close to the solution, which is usually nonclassical, may be chosen to optimize the accuracy and

convergence of the solution. Therefore, the use of nonclassical basis sets may provide not only more choices but also superior accuracy and convergence than the classical spectral method for the solution of a given problem.

The modified QDM (MQDM) derivative matrix is also introduced in the thesis. It is the Galerkin matrix of the derivative operator based on the nonclassical polynomial basis set. The MQDM has similar properties as the QDM. Furthermore, the MQDM matrix representative of a second order self-joint differential operator is symmetric.

In the application to the model problems, such as the one-dimensional and three-dimensional Poisson equations, the QDM works remarkable well and competes favorably with the classical spectral method in both accuracy and the rate of convergence of the solution. In comparison with the finite difference method, the numerical solution of the QDM is more accurate and converges at a much faster rate. In the solution of the three dimensional Poisson problem, the QDM requires much smaller number of grid points and less CPU time than the FD method to converge to a given accuracy.

In the solution of the model problem, an analytic time-dependent Fokker-Planck equations, the QDM with the equilibrium solution as weight function converges faster than the classical Hermite and Legendre methods. All the eigenvalues of the Fokker-Planck discretization matrix calculated by the QDM (and MQDM) are real. By contrast, spurious imaginary eigenvalues occur for the classical Hermite and Legendre methods. The condition number of the FP operator is less than or equal to $O(N^2)$ for the QDM and classical methods.

The main objective of the QDM is to determine the weight function that defines the polynomial basis sets and hence the grid points which provide optimum convergence in a given application. In the applications to the Fokker-Planck and Schrödinger equations, the matrix representative of the differential operator is very easy to construct and the

matrix is symmetric. All the eigenvalues, except the zero eigenvalue, are real and negative. Spurious imaginary eigenvalues do not occur. The convergence of the eigenvalues and eigenfunctions is extremely rapid with a judicious choice of the weight function.

The QDM is applied to three one-dimensional Fokker-Planck equations referred to as the optical bistable potential, the quartic potential and the climate potential, respectively. Comparisons have been made to investigate the influence of the choice of weight function or basis set on the rate of convergence of the eigenvalues with several weight functions. The result indicates that the choice of weight function (or the polynomial basis set) is important with respect to the rate of convergence of the eigenvalues and eigenfunctions. In general, to achieve fast convergence of the eigenvalues and eigenfunctions of the Fokker-Planck operator, the equilibrium solution can be chosen as weight function if the potential barriers are small. If the potential is symmetric, the weight function chosen as a Gaussian function centered on some symmetry axis with an appropriate width can be used. In the case that the potential barriers are very large, the weight function should be chosen such that the quadrature points that are generated are concentrated near the minima and maxima of the potential, or in the wells of the equivalent Schrödinger potential.

The time dependent solution of the Fokker-Planck equation has been calculated for the climate model by both explicit and implicit time discretization. For implicit time discretization, since the eigenvalues of the differential matrix are negative, the solution is always stable and the selections of the time step is only controlled by the accuracy requirement. For explicit time discretization, the time step is decided by both stability and accuracy requirements. For a stable solution, one need to consider the condition number of the differential matrix. The larger the condition number, the smaller the time step can be chosen. We find that for all three Fokker-Planck equations we have studied, the condition number of the differential matrix constructed with equilibrium solution as weight function, grows as $O(N^p)$, with $1 \leq p \leq 2$, as $N \to \infty$.

In the Fokker-Planck equation for the climate model, the drift coefficient function is piecewise linear but not smooth. By applying the QDM, we obtain very good convergence of the eigenvalues and eigenfunctions. This indicates that the QDM can work well for nonsmooth functions.

The QDM is also applied to the one-dimensional Schrödinger equations with several potentials. The QDM in the solution of the Schrödinger equation is closely related to the methods for the solution of the Fokker-Planck equation. The matrix representative of the Hamiltonian is symmetric and all the eigenvalues are real. Different choices of weight functions in the QDM solution of the Schrödinger equations are compared and studied. The ground state wave function (if it is known) or some approximate form is chosen as weight function in the QDM to solve the problem. The convergence is very rapid in comparison with the classical Hermite method. For the Schrödinger equation with the nonpolynomial oscillator potential, the Hermite method converges very slowly in some cases, while the QDM with appropriate weight function converges extremely rapidly.

In the application to the two dimensional Schrödinger equation with the Henon-Heiles potential, very rapid convergence of the eigenvalues and eigenfunctions is obtained with selected weight functions. The basis sets are constructed with different weight functions in each dimension, so as to optimaize the convergence of the eigenvalues and the resolution of the eigenfunctions. The results are in very good agreement with previous results by others.

In general, the QDM is very efficient to the solution of the differential equations discussed in this thesis. The QDM also includes most classical spectral methods when one choose to use classical weight function (or basis set). Ability to use nonclassical basis set in the QDM gives one more flexibility in the solution of differential equations. With the QDM, it is possible to obtain the superior convergence and accuracy of the solution of some problems, for which any classical spectral method fails to deliver. The QDM can

be easily extended to the solution of high dimensional differential equations.

The present work has concentrated on the basic development of the QDM and its application to some model problems as well as Fokker-Planck and Schrödinger equations. For a complete understanding, improvement and broader applications of the QDM, some future work will be considered.

(i) Adaptive selection of the weight function to optimize the solution. In general we may consider a function close to the solution as a weight function. In the case that no clue about the solution is given, one may choose an arbitrary weight function to generate a solution and then use this solution as a new weight function to solve the solution again.

(ii) The nonclassical polynomials are generated by the Stieltjes's procedure. The accuracy of polynomials and hence the points and weights as well as the derivative matrix depends on the accuracy of numerical calculation of the recurrence coefficients by the Stieltjes's procedure. In some cases, the Stieltjes's procedure may not be accurate. Therefore other possibilities may be considered and studied to improve the accuracy of calculation of the nonclassical polynomials.

(iii) The current QDM is based on the nonclassical polynomial basis set. To extend the class of the nonclassical basis set, a possibility of other nonpolynomial basis sets, for example the rational polynomial basis set, etc. may be considered.

(iv) Both Fokker-Planck and Schrödinger equations are parabolic type in the infinite interval. They have similar forms and properties as advection-diffusion equations used extensively for the fluid dynamic problems. The techniques used in solving Fokker-Planck and Schrödinger equations may apply to this class of problems. Therefore studies of the QDM in the solution of the advection-diffusion equation is our main task in the near future.

(v) All the problems we discussed in this thesis are linear differential equations. Some studies in spectral method in the solution of nonlinear problem (for example, the Burger's

equation) has been carried out. Our interest in the future is to study how to apply the QDM to the solution of the nonlinear differential equations.

(vi) When compared with the FD method, the spectral method is superior in accuracy and convergence of rate. However finite difference is the most popular numerical schemes used by scientists and engineers. One of the reasons is that it is easy to use and standard software routines are usually available and ready to use. In the future, we may consider to provide a general guideline for the choice of the weight function for a given class of problems and to develop standard software routines in order that one can apply the QDM easily.

Bibliography

[1] C.W. Gear, *Numerical Initial value problems in ordinary differential equations.* (Prentice-Hall, New Jersy, 1971).

[2] J.D. Lambert, *Computational methods in ordinary differential equations.* (John Wiley & Sons, New York, 1973).

[3] L.F. Shampine and M.K. Gordon, *Computer solution of ordinary differential equations: the initial value problem.* (Freeman, San Francisco, 1976).

[4] K. Dekker, *Stability of Runge-Kutta methods for stiff nonlinear differential equations.* (Elsevier Science, New York, 1984).

[5] J.C. Butcher, *The numerical analysis of ordinary differential equations: Runge-Kutta and general linear methods.* (John Wiley & Sons, New York, 1987).

[6] E. Hairer, *The numerical solution of differential-algebraic systems by Runge-Kutta methods.* (Springer-Verlag, 1989).

[7] D. Gottlieb, M. Gunzburger, and E. Turkel, SIAM J. Numer. Anal. **19(4)**, 671 (1982).

[8] R.E. Ewing, Comput. Meth. in Appl. Mech. Engrg. **47**, 74 (1984).

[9] R.E. Ewing and R.F. Heinemann, Comput. Meth. in Appl. Mech. Engrg. **47**, 161 (1984).

[10] V. Girailt and O. Raviart, *Finite element methods for Navior-Stokes equations.* (Springer, Berlin, 1896)

[11] T. Peterson, SIAM J. numer. Anal. **28(1)**, 133 (1991).

[12] R. Rannacher, Aamm Z. angew. Math. Mech. **73(9)**, 203 (1993).

[13] P.P. Chavez, *A two-dimensional finite element analysis of the stationary semiconductor device equations.* [microform]. Thesis. University of British Columbia. (1997)

[14] M.A. Crisfield, *Non-linear finite element analysis of solids and structures.* (Wiley, New York, 1997)

[15] J. Bonet, *Nonlinear continuum mechanics for finite element analysis.* (Cambridge, New York, 1997).

[16] V. Thomee, *Galerkin finite element methods for parabolic problems.* (Springer, Berlin, 1997)

[17] L.T. Tenek, *Finite element analysis for composite structures. Solid mechanics and its applications; v. 59.* (Kluwer Academic Publishers, Boston, 1998).

[18] C. Canuto, M.Y. Hussaini, A. Quarteroni and T.A. Zang, *Spectral methods in fluid dynamics.* (Spring-Verlag, Berlin, 1987).

[19] B. Fornberg, *A practical guide to pseudospectral methods.* (Cambridge University Press, Cambridge, 1996).

[20] M.Y. Hussaini, M.D. Salas and T.A. Zang, *Advances in computational transonics.* (Pineridge Press, Swansea, 1983).

[21] E. Tadmor, SIAM J. Numer. Anal. **26(1)**, 30 (1989).

[22] J.M. Augenbaum, Appl. Numer. Math. **5**, 459 (1989).

[23] A. Noullez and M. Vergassola, J. Sci. Comput. **9(3)**, 259-281 (1994).

[24] B. Fornberg, SIAM J. Numer. Anal. **27(4)**, 904 (1990).

[25] A. Orszag, J. Comput. Phys. **37**, 70 (1980).

[26] K.Z. Korczak and A.T. Pattera, J. Comput. Phys. **62**, 361 (1980).

[27] M.G. Macaraeg and C.L. Streett, Appl. Numer. Math. **2**, 95 (1986).

[28] D. Funaro, Numer. Math. **52**, 329 (1988).

[29] J.P. Boyd, *Chebychev and Fourier Spectral Methods. Lecture Notes in engineering.* (Springer, Berlin, 1989).

[30] W. Heinrichs, Appl. Math. **37(6)**, 401 (1992).

[31] M.O. Deville and E. H. Mund, J. Comp. Phys. **95**, 359 (1991).

[32] E.T. Olsen, and J. Douglas, Numer. Math. **69**, 333 (1995).

[33] T.D. Taylor, R.B. Myers and J.H. Albert, Comput. Fluids **9(4)**, 469 (1981).

[34] C. L. Streett, AIAA-83-1949-CP: Proceedings of the sixth AIAA computational Fluid Dynamics conference, Danvers, Massachusatts, USA (1983).

[35] A. Orszag and L.C. Kell, J. Fluid. Mech. **96**, 159 (1980).

[36] D. Gottlieb and S. Orszag, *Numerical analysis of spectral methods: theory and applications.* (SIAM, Philadephia, 1977).

[37] A. Zebib, J. Comput. Phys. **53**, 443 (1984).

[38] R.G. Voigt, D. Gottlieb, and M.Y. Hussaini, *Spectral method for partial differential equations.* (SIAM, Philadelphia, 1984).

[39] N. Funaro, *Polynomial approximation of differential equations. Lecture notes in physics.* (Springer-Verlag, New York, 1992).

[40] G. Mansell, W. Merryfield, B. Shizgal and U. Weinert, Comput. Meth. Appl. Mech. Engrg. **104**, 295 (1993); H. H. Yang, B. R. Seymour and B. D. Shizgal, Comp. Fluids **23**, 829 (1994); H. H. Yang and B. Shizgal, Comput. Meth. Appl. Mech. Engrg. **118**, 47 (1994).

[41] I.M. Kuria and P.E. Raad, Comput. Meth. Appl. Mech. Engrg. **120**, 163 (1995).

[42] B. Machenhauer, *Spectral method in Numerical Methods on Atmospheric Models*, 1 (seminar proceeding), European Center for Medium Range Weather Forecast, Reading, UK (1991).

[43] B.D. Shizgal and H. Chen, J. Chem. Phys. **107(19)**, 8051 (1997).

[44] R.E. Robson, Aust. J. Phys. **46**, 465 (1993).

[45] H. Chen, K. Leung and B. D. Shizgal, Proceeding of the 20th international Symposium on Rarefied Gas Dynamics, 273 (1996).

[46] K. Leung, *Electron and Ion relaxation in atomic and molecular moderators.* PhD. thesis. (University of British Columbia, Vancouver, 1997).

[47] K. Leung, B.D. Shizgal and H. Chen, J. Math. Chem. In press.

[48] R. Kosloff and H. Tal-Ezer, J. Chem. Phys. **81**, 3967 (1984).

[49] M. Berman, R. Kosloff and H. Tal-Ezer, J. Phys. A **25**, 1283 (1992).

[50] W. Zhu, Y. Huang and D.J. Kouri, Chem. Phys. lett. **217(1)**, 73 (1994).

[51] B.D. Shizgal and H. Chen, J. Chem. Phys. **104(11)**, 4137 (1996).

[52] K.S. Breuer and R.M. Everson, J. Comput. Physics **99**, 56 (1992).

[53] L.N. Trefethen and M.R. Trummer, SIAM J. Numer. Anal. **24(5)**, 1008 (1987).

[54] J.A.C. Weideman and L.N. Trefethen, SIAM J. Numer. Anal. **25(6)**, 1279 (1988).

[55] W.S. Don and A. Solomonoff, SIAM J. Sci. Comput. **16(6)**, 1253 (1995).

[56] A. Bayliss, A. Class and B.J. Matkowsky, J. Compt. Phys. **116**, 380 (1994).

[57] W. Heinrichs, Math. Comput. **53**, 103 (1989).

[58] W. Heinrichs, Numer. Math. **56**, 25 (1989).

[59] E. Rothman, Proc. 2nd symposium on high-performance computing (Durand and Dabaghi, eds), Montpellier, France, 7 (1991).

[60] D. Kosloff and H. Tal-Ezer, J. Comput Phys. **104**, 457 (1993).

[61] T.A. Zang, Y.S. Wong and M.Y. Hussaini, J. Compt. Phys. **54**, 489 (1984).

[62] D. Funaro and W. Heinrichs, Numer. Math. **58**, 399 (1990).

[63] M.O. Deville and E.H. Mund, SIAM J. Stat. Comput. **13(2)**, 596 (1992).

[64] C. Canuto and A. Quarteroni, J. Comput. Phys. **60**, 315 (1985).

[65] T. Phillips, T. Zang and M.Y. Hussaini, IAM J. Numer. Analysis **6**, 273 (1986).

[66] D. Funaro, SIAM J. Numer. Anal. **24(5)**, 1024 (1987).

[67] T. Tang, SIAM J. Sci. Comput. **14(3)**, 594 (1993).

[68] D. Funaro and O. Kavian, Math. Comput. **57(196)**, 597 (1991).

[69] V. Iranzo and A. Falques, Comput. Meth. in Appl. Mech. Engrg. **98**, 105 (1992).

[70] R. Blackmore, U. Weinert and B. Shizgal, Trans. Theory and Stat. Phys. **15**, 181 (1986).

[71] R. Blackmore and B.D. Shizgal, Phys. Rev. **A31(3)**, 1855 (1985).

[72] B. Shizgal and R. Blackmore, J. Comput. Phys. **55**, 313 (1984).

[73] J.A.C. Weideman, Numer. Math. **61**, 409 (1992).

[74] B. Shizgal, J. Chem. Phys. **70(4)**, 1948 (1978).

[75] B. Shizgal, J. Computat. Phys. **41**, 309 (1981)

[76] A.D. Fokker, Ann. Physik **43**, 810 (1914).

[77] M. Planck. Sitzber. Akad. Wiss. 324 (1917).

[78] A. N. Malakhov and A. L. Pankratov, Physica A **229**, 109 (1996).

[79] T. Blum and A. J. McKane, J. Phys. A: Math. Gen. **29**, 1859 (1996).

[80] H. Risken and T. Leiber, Phys. Rev. A **40**, 1582 (1989).

[81] J. B. Avalos and I. Pagonabarraga, Phys. Rev. E **52**, 5881 (1995).

[82] Y. Jia and J. Li, Phys. Rev. E **53**, 5764 (1996).

[83] B. Nowakowski, Phys. Rev. A **53**, 2964 (1996).

[84] S. Stepanow, Phys. Rev. E **54**, 2209 (1996). A. Perico, R. Pratolongo, K. F. Freed and A. Szabo, J. Chem. Phys. **101**, 2554 (1994); R. Pratolongo, A. Perico, K. F. Freed and A. Szabo, J. Chem. Phys. **102**, 4683 (1995); G. J. Moro, J. Chem. Phys. **103**, 7514 (1995)

[85] A. P. Blokhin and M. F. Gelin, Mol. Phys. **87**, 455 (1966); Physica A **229**, 501 (1996).

[86] T. Theuns, Month. Not. R. Astron. Soc. **279**, 827 (1996).

[87] O. Lies-Svendsen and M. H. Rees, J. Geophys. Res. **101**, 2415 (1996).

[88] H. G. Jhang and C. S. Chang, Phys. Plasmas **2**, 3917 (1995).

[89] P. Wilmott, S. Howison and J. Dewynne *The Mathematics of Financial Derivatives* (Cambridge University Press, Cambridge, 1995).

[90] Y. Abe, S. Ayik, P.-G. Reinhard and E. Suraud, Phys. Reports **275**, 49 (1996).

[91] M. Schulz, Physica Scripta **37**, 632 (1988).

[92] N. G. van Kampen, *Stochastic Processes in Chemistry and Physics* (North Holland, Amsterdam, 1981).

[93] H. Risken, *The Fokker-Planck Equation*, 2nd ed. (Springer, Berlin, 1984).

[94] C. W. Gardiner, *Stochastic Methods*, (Springer, Berlin, 1983)

[95] J. J. Duderstadt and W. R. Martin, *Transport Theory* (Wiley, New York, 1979); K. M. Case and P. F. Zweifel, *Linear Transport Theory* (Addison-Wesley, Reading, Mass., 1967); B. Davison, *Neutron Transport* (Oxford University Press, Oxford, 1957).

[96] V. Kourganov, *Basic Methods in Transfer Problems* (Oxford University Press, Oxford, 1963).

[97] J. S. Chang and G. Cooper, J. Computat. Phys. **6**, 1 (1970).

[98] E. W. Larsen, C. D. Levermore, G. C. Pomraning and J. G. Sanderson, J. Computat. Phys. **61**, 359 (1985).

[99] E. M. Epperlein, J. Computat. Phys. **112**, 291 (1994); Laser and Particle Beams **12**, 257 (1994).

[100] B. T. Park and V. Petrosian, Astrophys. J. Suppl. Series **103**, 255 (1996); Astrophys. J. **446**, 699 (1995).

[101] A. K. Mitra, J. Math. Phys. **19**, 2018 (1978).

[102] K. Banerjee, S.P. Bhatnagar, V.Choudhry and S.S.Kanwal, Proc. R. Soc. Lond. A **360**, 575 (1978).

[103] K. Banerjee, Proc. R. Soc. Lond. A **364** (1978) 265

[104] N. Bessis and G. Bessis, J. Math. Phys. **21**, 2760, (1980).

[105] A. Hautot, J. Computat. Phys. **39**, 72 (1981).

[106] F. M. Fernandez, G. A. Arteca and E. A. Castro, Physica A **122**, 37 (1983).

[107] R. N. Chaudhuri and B. Mukherjee, J. Phys. A: Math. Gen. **16**, 4031 (1983).

[108] G. A. Arteca, F. M. Fernandez and E. A. Castro, J. Math. Phys. **25**, 932, 1984.

[109] M. R. M. Witwit, Pramana, J. Phys. **43**, 279 (1994).

[110] M. R. M. Witwit, J. Computat. Phys. **129**, 220 (1996).

[111] M. R. M. Witwit, J. Math. Chem. **19**, 75 (1996).

[112] R. S. Kaushal, J. Phys. A: Math. Gen. **12**, 253 (1979).

[113] N. Bessis, G. Bessis and G. Hadinger, J. Phys. A: Math. Gen. **16**, 497 (1983).

[114] R. Dutt, A. Khare and U. P. Sukhatme, Am. J. Phys. **56**, 163 (1988).

[115] A. Comtet, A. D. Bandrauk and D. K. Campbell, Phys. Letters B **150**, 159 (1985).

[116] R. Dutt, A. Mukherjee and Y. P. Varshni, Phys. Rev. A **52**, 1750 (1995).

[117] M. R. M. Witwit, J. Math. Chem. **20**, 273 (1996).

[118] C. S. Lai and H. E. Lin, J. Phys. A: Math. Gen. **15** 495 (1982).

[119] C. R. Handy, J. Phys. A: Math. Gen. **18**, 3593 (1985).

[120] F. M. Fernandez and E. A. Castro, J.Phys. A: Math. Gen. **20**, 5541 (1987)

[121] M. R. M. Witwit, J. Phys. A: Math. Gen. **24**, 5291 (1991).

[122] F. M. Fernandez and R. H. Tipping, Can. J. Phys. **74**, 697 (1996).

[123] S. Galicia and J.P. Killingbeck, Phys. Lett. A **71**, 17 (1979).

[124] V. Fack and G. Vanden Berghe, J. Phys. A: Math. Gen. **18** 3355 (1985).

[125] M. Braun, S. A. Sofianos, D. G. Papageorgiou and I. E. Lagaris, J. Computat. Phys. **126** 315 (1996).

[126] G. P. Flessas, Phys. Let. A **83** (1981) 121; *ibid.* **100**, 383 (1984).

[127] D. Singh and Y. P. Varshni, Phys. Rev. A **28**, 2606 (1983).

[128] Y. P. Varshni, Phys. Rev. **36** 3009 (1987).

[129] H. Scherrer, H. Risken and T. Leiber, Phys. Rev. A **38**, 3949 (1988).

[130] M. Kaluza, Comp. Phys. Comm. **79**, 425 (1994).

[131] A. Sinha, R. Roychoudhury and Y. P. Varshni, Can. J. Phys. **74**, 39 (1996).

[132] J.C. Light, I.P. Hamilton and J.V. Lill, J. Chem. Phys. **82(3)** 1400 (1985); R.M. Whitnell and J.C. Light, *ibid.* **89(6)**, 3674 (1989); S.E. Choi and J.C. Light, *ibid.* **92(4)**, 2129 (1990); *ibid.* **97(10)**, 7031-7054 (1992); Z. Bacic and J.C. Light, Annu. Rev. Phys. Chem. **40**, 469 (1989)

[133] H. Wei and T.J. Carrington, Chem. Phys. **101**, 1343 (1994); K. Sakimoto and K. Onda, *ibid.* **100**, 1171 (1994); S. M. Auerbach and W.H. Miller, *ibid.* **100**, 1103 (1994); J.K.G. Watson, Can. J. Phys. **72**, 238 (1994); J. Szalay, J. Chem. Phys. **99**, 1978 (1993); J. Tennyson and J.R. Henderson, *ibid.* **91**, 3815 (1989).

[134] W.J. Gautschi, Computat. Appl. Math. **12**, 61 (1985).

[135] P. Nevai, editor *Orthogonal Polynomials: Theory and Practice* (Kluwer Academic, Norwell, MA, 1990); G.Freud, *Orthogonal Polynomials* (Pergamon, New York, 1971); T. S. Chihara, *An Introduction of Orthogonal Polynomials*, (Gordon and Breach, New York, 1978).

[136] P. Davis and P. Rabinowitz, *Method of Numerical Integration*. Academic, New York (1975).

[137] R. Peyret and T.D. Taylor, *Computational methods for fluid flow* (Springer-Verlag, New York, 1983).

[138] R. Peyret, *Handbook of computational fluid mechanics*. (Academic Press, London, 1996).

[139] D.J. Evans, *Preconditioning methods : analysis and applications*. (Gordon and Breach Science, New York, 1983).

[140] I. Gohberg, M. Hanke and I. Koltracht, SIAM J. Numer. Anal. **31(2)**, 429 (1994).

[141] B. Koren and B. van Leer, Adv. Comput. Math **4**, 127 (1995).

[142] H. Chen and B.D. Shizgal, J. Math. Chem. In press. (1998)

[143] A. S. Clarke and B. Shizgal, J. Computat. Phys. **104**, 140 (1993).

[144] J.D. Jackson, *Mathematics for Quantum Mechanics*. 93-94, (Academic Press, New York 1975).

[145] C. Indira, M. C. Valsakumar, K. P. N. Murthy and G. Ananthakrisna, J. Stat. Phys. **33**, 181 (1983).

[146] K. Voigtlaender and H. Risken, Chem. Phys. Lett. **105**, 506 (1984); H. F. Ouyang, Z. Q. Huang, and E. J. Ding, Phys. Rev. E **50**, 2491 (1994); A. Debosscher, Phys. Rev. A **42**, 4485 (1990); A. Debosscher, Phys. Rev. A **44**, 908 (1991); G. Hu and Q. Zheng, Phys. Lett. A **110**, 68 (1985); G. Hu, Phys. Lett. A **110**, 253 (1985); H. Dekker and N. G. Van Kampen, Phys. Lett A **73**, 374 (1979).

[147] B. Shizgal and D. R. A. McMahon, Phys. Rev. A **32**, 3669 (1985).

[148] X. G. Wu and R. Kapral, J. Chem. Phys. **91**, 5528 (1989)

[149] I. L'Heureux, Phys. Rev. E **51**, 2787 (1995); V. I. Melnikov, Phys. Rep. **209**, 1 (1991); P. Hanggi, P. Talkner, and M. Borkovec, Rev. Mod. Phys. **62**, 251 (1990); P. Talkner, Chem. Phys. **180**, 199 (1994).

[150] R. Bonifacio and L. A. Lugiato, in *Disspative Systems in Quantum Optics*, edited by R. Bonifacio (Springer Verlag, Berlin, 1982); C. M. Bowden, M. Ciftan and H. R. Robl, editors *Optical Bistability* (Plenum Press, New York, 1981).

[151] J. C. Englund, W. C. Schieve, W. Zurek and R. F. Gragg, in *Optical Bistability* edited by C. M. Bowden, M. Ciftan and H. R. Robl (Plenum Press, New York, 1981); A. R. Bulsara, W. C. Cheive and R. F. Gragg, Phys. Lett. A **68**, 294 (1978); P. Hanggi, A. R. Bulsara and R, Janda, Phys. Rev. A **22**, 671 (1980); A. Schenzle and H. Brand, Phys. Rev. A **20**, 1628 (1979).

[152] V. A. Shneidman, Phys. Rev. A **44**, 8441 (1991); D. T. Wu, J. Chem. Phys. **97**, 1922, 2644 (1992); I. Edrei and M. Gitterman, J. Chem. Phys. **85** 190, (1986); G. Shi, H. Seinfeld, and K. Okuyama, Phys. Rev. A **41**, 2101 (1990); B. Shizgal and J. C. Barrett, J. Chem. Phys. **91**, 6505 (1989); L. Demeio and B. Shizgal, J. Chem. Phys. **98**, 5713 (1993).

[153] W. T. Coffey and D. S. F. Crothers, Phys. Rev. A **54**, 4768 (1996); W. T. Coffey, D. S. F. Crothers, Yu. P. Kalmykov, E. S. Massawe and J. T. Waldron, Phys. Rev. E **49**, 1869 (1994).

[154] C. Nicolis and G. Nicolis, Tellus **33**, 225 (1981); C. Nicolis, Solar Physics **70**, 473 (1981).

[155] D. R. Chialvo and A. V. Apkaran, J. Stat. Phys. **70**, 375 (1993); T. Heskes, J. Phys. A: Math. Gen. **27**, 5145 (1994).

[156] K. R. Yawn, B. N. Miller and A. Maier, Phys. Rev. E **52**, 3390 (1995); L. Spitzer, Jr., *Dynamical Evolution of Globular Clusters*, (Princeton University Press, Princeton, N.J., 1987); J. Binney and S. Tremaine, *Galactic Dynamics*, (Princeton University Press, Princeton, N.J., 1987)

[157] A. N. Drozdov and M. Morillo, Phys. Rev. E **54**, 3304 (1996).

[158] P. Hanggi and P. Jung, Adv. Chem. Phys. **89**, 239 (1995); J. Kuczka, P. Hanggi and A. Gadomski, Phys. Rev. E **51**, 2933 (1995); A. J. Bray, A. J. McKane and T. J. Newman, Phys. Rev. A **41**, 657 (1990); M. M. Dygas, B. J. Matkowsky and Z. Schuss, J. Chem. Phys. **83**, 597 (1985); J. Masoliver, B. J. West and K.Lindenberg, Phys. Rev. A **35**, 3086 (1987); R. F. Fox, Phys. Rev. A **37**, 911 (1988); S. A. Adelman, J. Chem. Phys. **64**, 124 (1976);

[159] H. A. Kramers, Physica **7**, 284 (1940).

[160] M. J. Englefield, Physica A **167**, 877 (1990); H. Okamoto, J. Phys. A: Math. Gen. **23**, 5535 (1990), T. Miyazawa, Phys. Rev. A **39**, 1447 (1989); M. J. Englefield, J. Stat. Phys. **52**, 369 (1988); H. Risken and K. Voigtlander, Z. Phys. B **54** 253, (1984).

[161] D.W.Noid and R.A.Marcus, J. Chem. Phys. **67(2)**, 559 (1977).

[162] D.W.Noid, M. L. Koszykowski, M. Tabor, and R.A.Marcus, J. Chem. Phys. **72(2)**, 6169 (1980).

[163] M.J. Davis and E. J. Heller, J. chem. Phys. **71(8)**, 3383 (1979).

[164] M.D.Feit, J.A.Fleck, Jr., and A.Steiger, J. comput. Phys. **47**, 412 (1982).

[165] R. Kosloff and H. Val-Ezer. Chem. Phys. Letter **223**, 127 (1986).

[166] G. C. Groenboom and H. M. Buck, J. Chem. Phys. **92(7)**, 4374 (1990).

[167] R.Q. Chen and H. Guo, J. chem. Phys. **105(4)**, 1311 (1996).

[168] O.A. Sharafeddin, Chem. Phys. Lett. **247**, 470 (1995).

[169] B.I. Henry and J. Grindlay, Can. J. Phys. **75(8)**, 517 (1997).

[170] P.K. Chattaraj96 and S. Sengupta, Indian J. Pure Appl. Phys. **34(8)** 518 (1996).

[171] S. Sengupta and P.K. Chattaraj96, Phys. Lett. A **215**, 119 (1996).

[172] W.M. Vieira and P.S. Letelier, Phys. Rev. Lett. **76**, 1409 (1996).

[173] P. Hatchison and R.E. Wyatt, Phys. Rev. A **23**, 1567 (1981).

[174] Noid, D.W. and Marcus, R.A. J Chem. Phys. **62(6)**, 2119 (1975).